Radioactivity, nuclear structure, chemists, and the abundances of the elements.

William B. Walters

Department of Chemistry and Biochemistry
University of Maryland
College Park MD 20742 USA

This work has been supported by the US Department of Energy under grant DE-FG02-94-ER40834.

The University of Maryland is located inside the Capital Beltway around Washington, DC.

This is a short memorial tribute to our late daughter Kathy (1966-2013) who died after a four-year battle with ovarian cancer, a year ago in March, just prior to this meeting. She was a "gamer" and also an adult "mixed-gender" ice hockey player. Here, she is holding one of the trophies earned by the team which qualified for an international tournament in Toronto on one occasion.

Topics on my agenda

Chemists and Elemental abundances

^{68}Ni and neighbors for the structure people, along with a discussion of experimental methods

The coming end of the “big dip”.

The “myth” of important experimental measurements

Who is eating Rh?

[CONTRIBUTION FROM THE KENT CHEMICAL LABORATORY OF THE UNIVERSITY OF CHICAGO.]

THE EVOLUTION OF THE ELEMENTS AND THE STABILITY OF COMPLEX ATOMS.

I. A NEW PERIODIC SYSTEM WHICH SHOWS A RELATION BETWEEN THE ABUNDANCE OF THE ELEMENTS AND THE STRUCTURE OF THE NUCLEI OF ATOMS.

BY WILLIAM D. HARKINS.

Received November 6, 1916.

The Hydrogen-Helium Structure of Complex Atoms.

It has been shown in previous papers[1] that the elements are very probably intra-atomic compounds of hydrogen. The hydrogen first forms helium, and this becomes a secondary unit of fundamental importance in the formation of all of the elements with atomic weights higher than its own.

TABLE III.—AVERAGE COMPOSITION OF METEORITES ARRANGED ACCORDING TO THE PERIODIC SYSTEM.

Series.	Group 1. Odd.	Group 2. Even.	Group 3. Odd.	Group 4. Even.	Group 5. Odd.	Group 6. Even.	Group 7. Odd.	Group 8. Even.	Group 8. Odd.	Group 8. Even.
2				6C 0.04%		8O 10.10				
3	11Na 0.17%	12Mg 3.80	13Al 0.39	14Si 5.20	15P 0.14	16S 0.49				
4	19K 0.04%	20Ca 0.46		22Ti 0.01		24Cr 0.09	25Mn 0.03	26Fe 72.06	27Co 0.44	28Ni 6.50
	29Cu 0.01%									

Table III gives the average composition of iron and stone meteorites, arranged according to the periodic system. The numbers before the symbols represent the atomic numbers, and the numbers underneath give the percentage of the element. It will be noted that *the even-numbered elements are in every case more abundant than the adjacent odd-numbered elements*. The helium group elements form no chemical compounds,

Journal of the American Chemical Society **39**, 856 (1917).

Chemists have long recognized the relationship between elemental abundances……measured by analytical chemists and by geochemists, and the structure of the nucleus, even before the neutron was discovered.

The centennial of this paper in the Journal of the American Chemical Society **39**, 856 (1917) is fast approaching. Perhaps an ACS symposium should be held to mark the occasion and celebrate the work of William Harkin.

As this is a “school” I would like to spend a bit of time describing some of the modern methods for studying the structure of nuclei.

Gammasphere and Gretina are modern detector systems.

Deep Inelastic reactions and fast fragmentation are methods for production

Gammasphere is 20 years old and consisted of ONE HUNDRED COMPTON SUPPRESSED DETECTORS

A lot of solid angle is lost to the BGO.

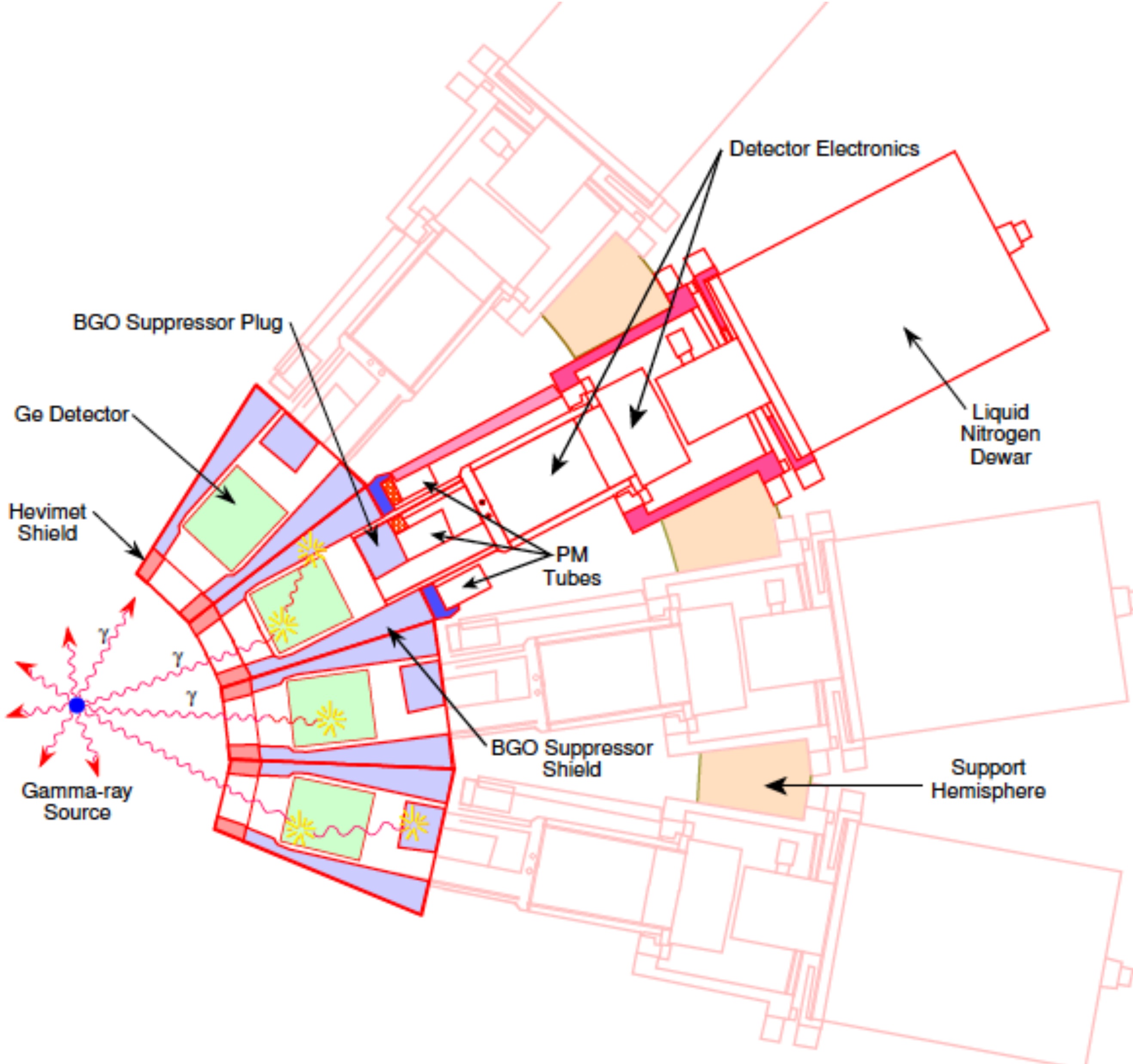

Figure 2.5: Schematic depiction of the layout of Gammasphere detector mod and of the types of interactions between γ rays and the detector material.

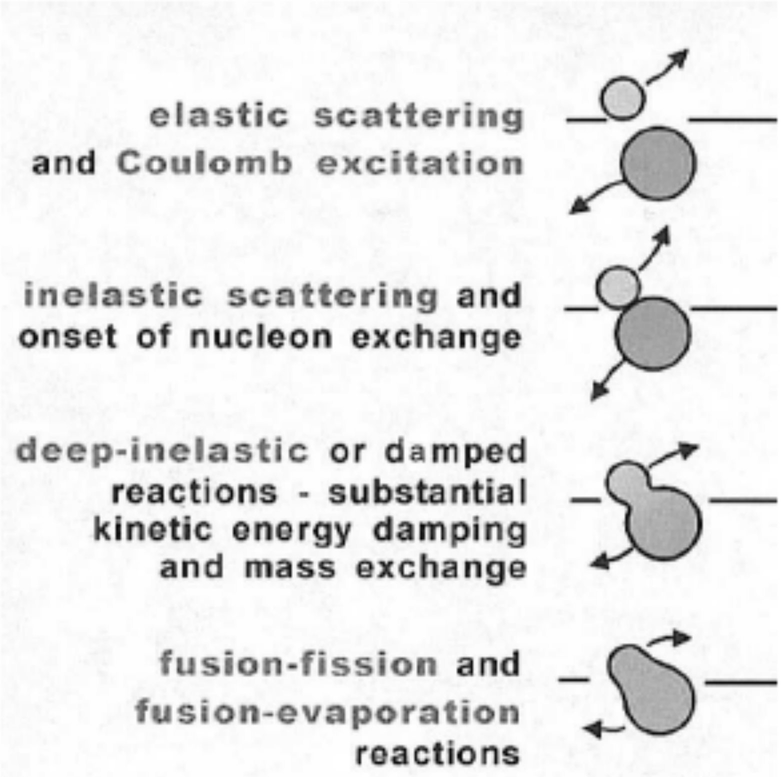
elastic scattering
and Coulomb excitation
inelastic scattering and
onset of nucleon exchange
deep-inelastic or damped
reactions - substantial
kinetic energy damping
and mass exchange
fusion-fission and
fusion-evaporation
reactions

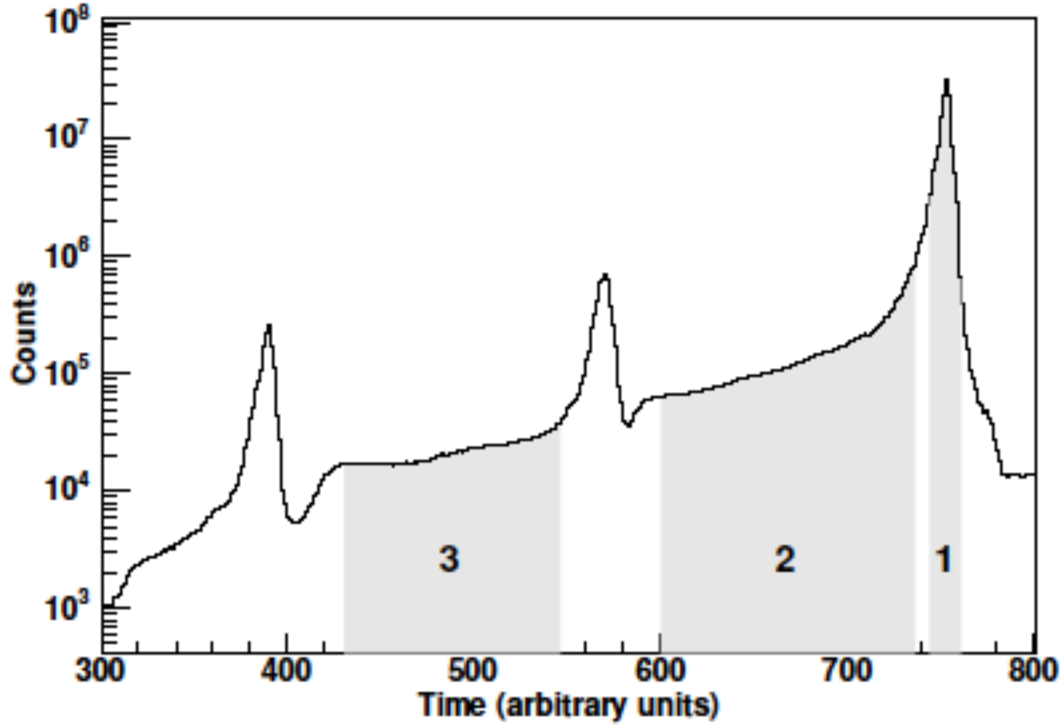

Figure 2.7: The time with respect to an RF pulse for a selected group of γ-ray signals. Shaded region 1 depicts the "prompt" flash of radiation arriving with the beam pulse. Regions 2 and 3 indicate "delayed" transitions which arrive between beam pulses. Note that time increments backwards in this spectrum.

Prompt gamma rays, window 1, delayed gamma rays, isomers, beta decay in window 2.

Hard wired triple coincidences…..old Gammasphere

Digital Gammasphere, all data are written and then events reconstructed with whatever is needed. MUCH MORE SOFTWARE INTENSIVE.

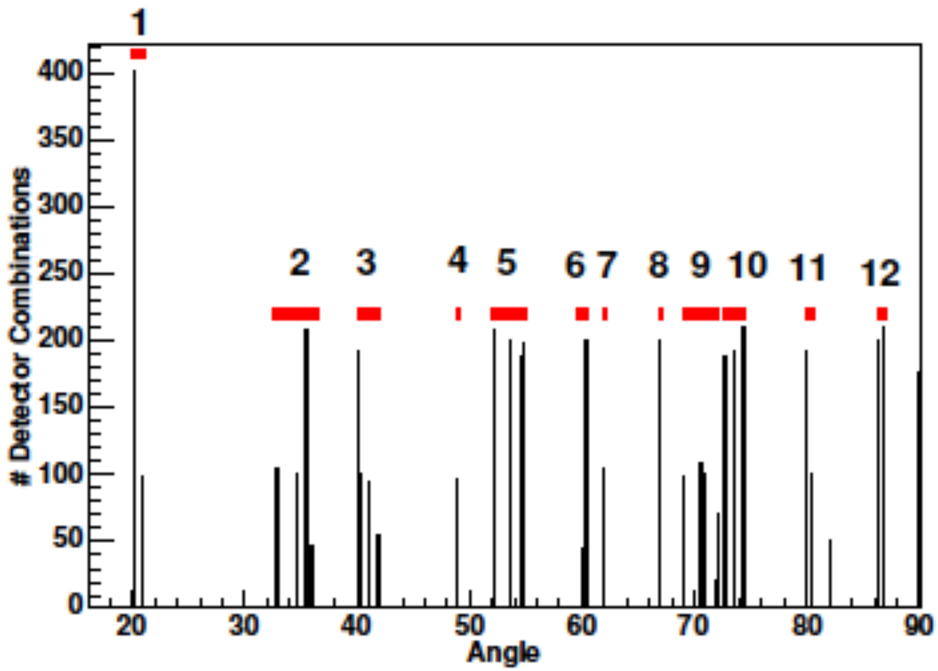

Figure 2.10: The distribution of possible angles between detectors with the 100-detector setup used for this experiment. Horizontal lines depict the angular bins used for the construction of correlation curves. Bins 4 and 7 exhibited very low statistics and were omitted from the analysis reported in this work.

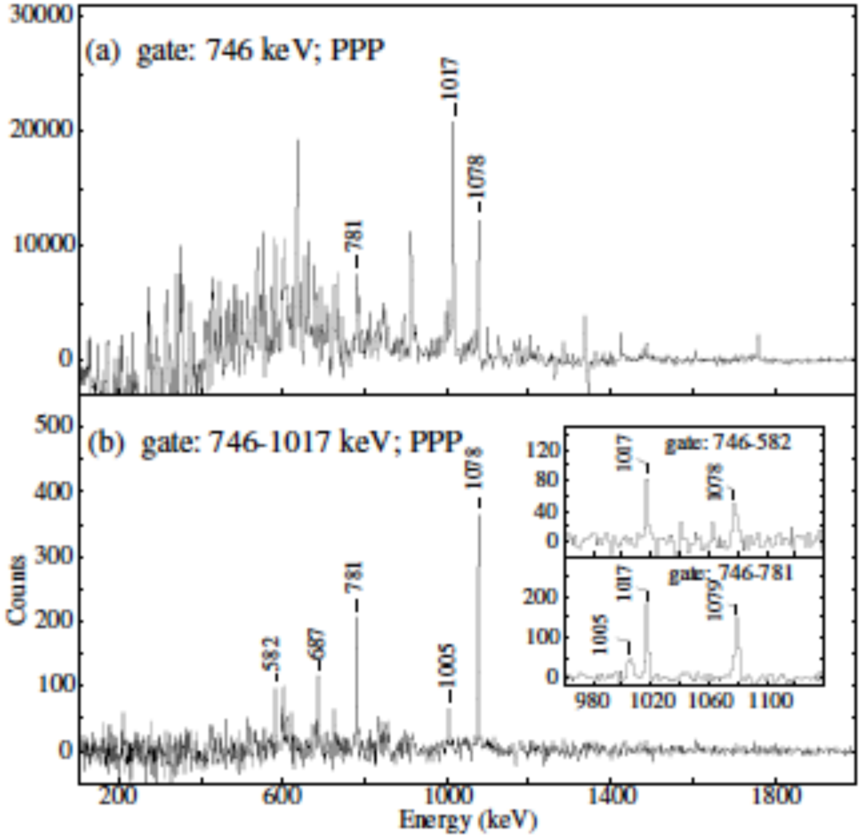

At the start of this work, the one sure gamma ray in ^{64}Fe was at 746 keV, discovered at ISOLDE in the decay of ^{64}Mn in 1997, the experiment that STARTED the whole ^{68}Ni craze. The reaction was $^{64}Ni + ^{238}U$.

Figure 3.15: Representative spectra from coincidence gates on $2^+ \rightarrow 0^+$ and $4^+ \rightarrow 2^+$ transitions in ^{64}Fe in prompt cube. The insets illustrate a systematic shift in the centroid position of the 1078-keV peak.

VOLUME 82, NUMBER 7 PHYSICAL REVIEW LETTERS 15 FEBRUARY 1999

Decay of Neutron-Rich Mn Nuclides and Deformation of Heavy Fe Isotopes

M. Hannawald,[1] T. Kautzsch,[1] A. Wöhr,[2] W.B. Walters,[3] K.-L. Kratz,[1] V.N. Fedoseyev,[4] V.I. Mishin,[4] W. Böhmer,[1] B. Pfeiffer,[1] V. Sebastian,[5] Y. Jading,[6] U. Köster,[7] J. Lettry,[6] H.L. Ravn,[6] and the ISOLDE Collaboration[6]

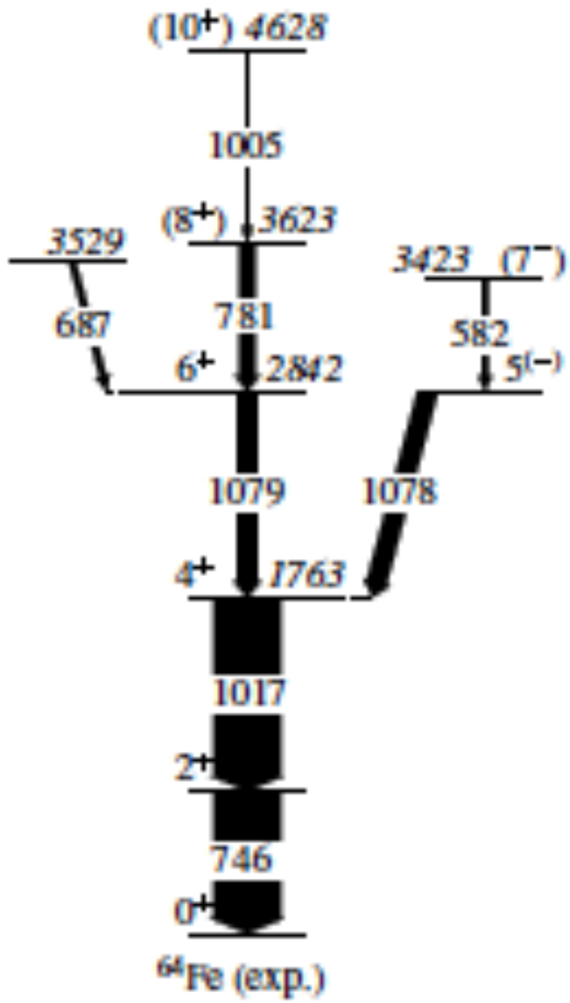

Why GRETINA. In Gammasphere a lot of data are thrown away via the Compton Suppression. Each detector is surrounded by a BiGeO low-resolution detector system that detects Compton scattering and cancels that event.

PHYSICAL REVIEW C **74**, 064313 (2006)

Yrast structure of ^{64}Fe

N. Hoteling,[1,2] W. B. Walters,[1] R. V. F. Janssens,[2] R. Broda,[3] M. P. Carpenter,[2] B. Fornal,[3] A. A. Hecht,[1,2] M. Hjorth-Jensen,[4] W. Królas,[3,5] T. Lauritsen,[2] T. Pawłat,[3] D. Seweryniak,[2] X. Wang,[2,6] A. Wöhr,[6] J. Wrzesiński,[3] and S. Zhu[2]

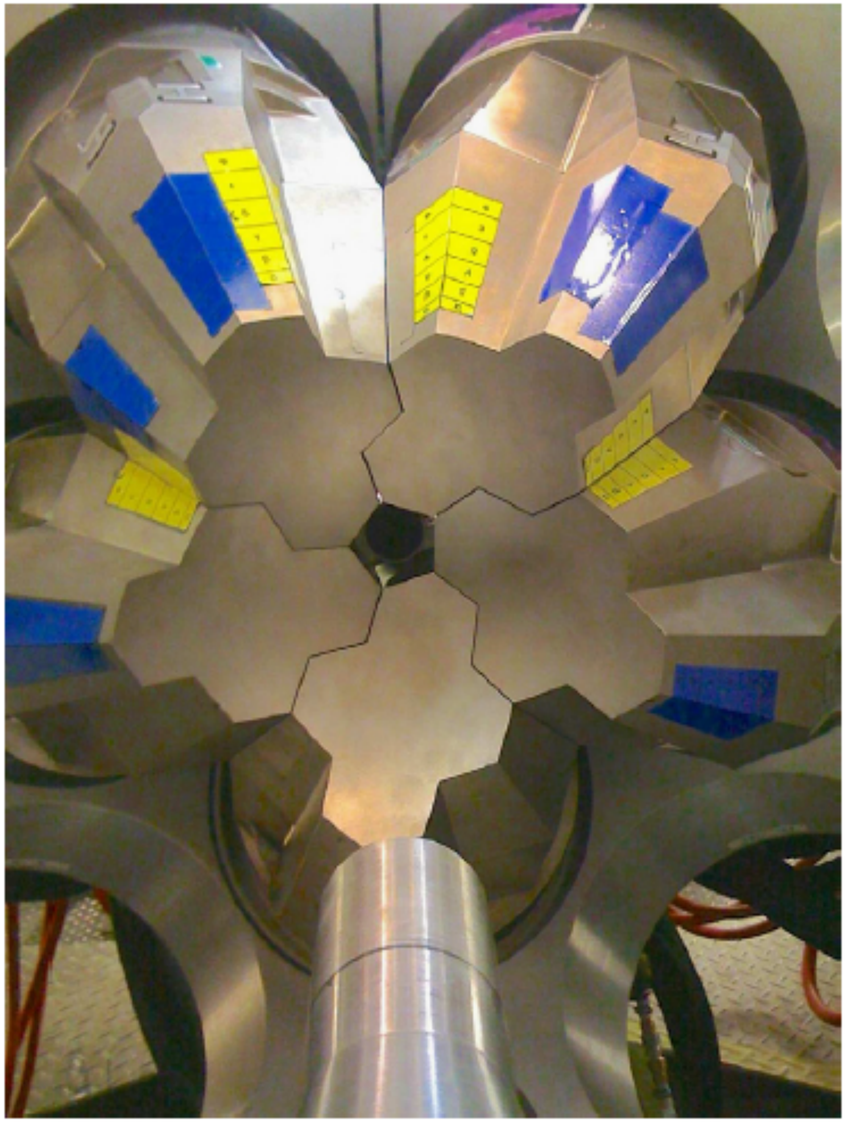

Fig. 2. A photograph of the actual array showing five GRETINA detector modules (20 crystals) mounted in a close-packed configuration.

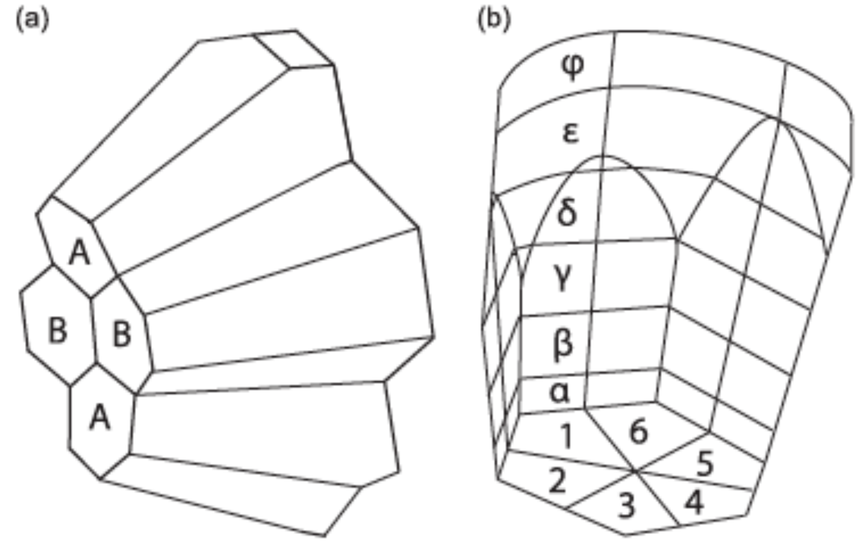

Fig. 3. Schematic drawing of (a) four crystals packed in one module, two A-type crystals and two B-type crystals and (b) an individual crystal showing the electrical segmentation of its outer contact.

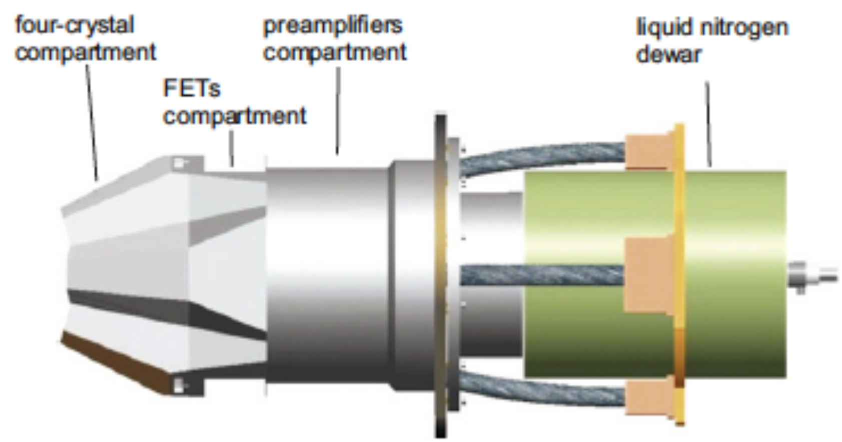

Fig. 4. A side-view drawing of the GRETINA detector module.

Each module is broken into 36 segments, 6 x 6. The Compton events are detected and added back to produce full-energy events.

VERY SOFTWARE INTENSIVE.

Nuclear Instruments and Methods in Physics Research A 709 (2013) 44–55

Contents lists available at SciVerse ScienceDirect

Nuclear Instruments and Methods in Physics Research A

journal homepage: www.elsevier.com/locate/nima

ELSEVIER

The performance of the Gamma-Ray Energy Tracking In-beam Nuclear Array GRETINA

S. Paschalis [a,*], I.Y. Lee [a,**], A.O. Macchiavelli [a], C.M. Campbell [a], M. Cromaz [a], S. Gros [a], J. Pavan [a], J. Qian [a], R.M. Clark [a], H.L. Crawford [a], D. Doering [a], P. Fallon [a], C. Lionberger [a], T. Loew [a], M. Petri [a], T. Stezelberger [a], S. Zimmermann [a], D.C. Radford [b], K. Lagergren [b], D. Weisshaar [c], R. Winkler [c], T. Glasmacher [c], J.T. Anderson [d], C.W. Beausang [e]

PHYSICAL REVIEW C **88**, 041302(R) (2013)

Configuration mixing and relative transition rates between low-spin states in ^{68}Ni

F. Recchia,[1,*] C. J. Chiara,[2,3] R. V. F. Janssens,[3] D. Weisshaar,[1] A. Gade,[1,4] W. B. Walters,[2] M. Albers,[3] M. Alcorta,[3] V. M. Bader,[1,4] T. Baugher,[1,4] D. Bazin,[1] J. S. Berryman,[1] P. F. Bertone,[3,†] B. A. Brown,[1,4] C. M. Campbell,[5] M. P. Carpenter,[3] J. Chen,[6] H. L. Crawford,[5] H. M. David,[3,7] D. T. Doherty,[3,7] C. R. Hoffman,[3] F. G. Kondev,[6] A. Korichi,[3,8] C. Langer,[1] N. Larson,[1,9] T. Lauritsen,[3] S. N. Liddick,[1,9] E. Lunderberg,[1,4] A. O. Macchiavelli,[5] S. Noji,[1] C. Prokop,[1,9] A. M. Rogers,[3,‡] D. Seweryniak,[3] S. R. Stroberg,[1,4] S. Suchyta,[1,9] S. Williams,[1] K. Wimmer,[1,10] and S. Zhu[3]

First Gretina paper in print from MSU, winner of the Macchiavelli prize

Here are spectra from DIS at Gammasphere
See the gamma at 1139 keV.

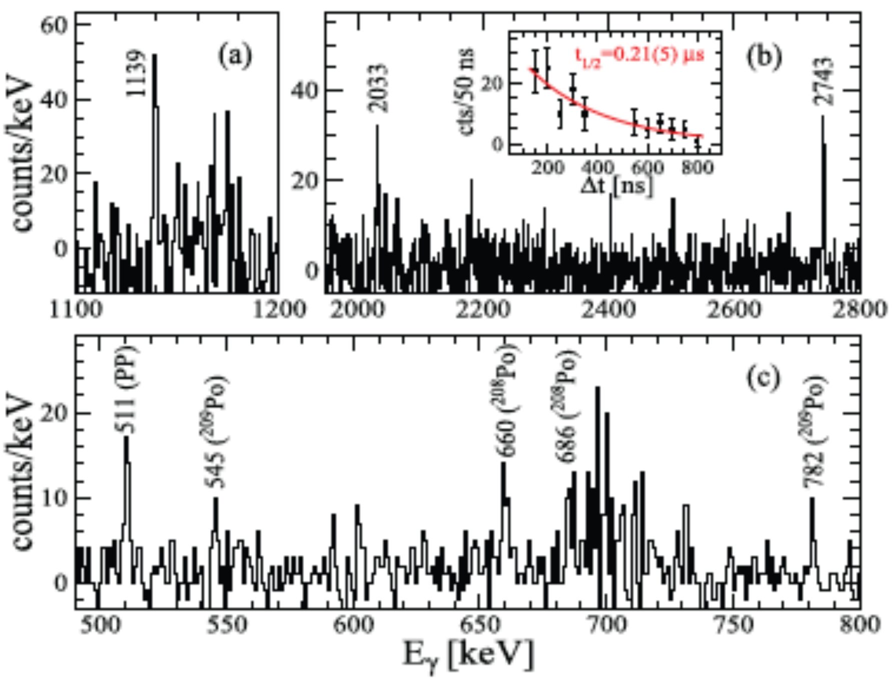

FIG. 3. (Color online) Spectra from the DIS data. (a), (b) Prompt γ rays coincident with the 662-keV γ ray and delayed ^{208,209}Po lines. (c) Delayed γ rays coincident with prompt 662- and 1139-keV transitions. Inset to (b): decay curve for the 511-keV line; random events associated with the next beam burst at ~400 ns are excluded from the fit.

TABLE I. Intensities I_γ and $B(E2)$ ratios $R(E_\gamma)$ (see text) for transitions from the 2_2^+ state in ^{68}Ni. The bottom row provides weighted averages of the values from the two data sets presented here (DIS and 2nKO) and the earlier β-decay work [4].

Reaction	$I_\gamma(2743)$, $2_2^+ \to 0_1^+$	$I_\gamma(1139)$, $2_2^+ \to 0_2^+$	$I_\gamma(710)$, $2_2^+ \to 2_1^+$	$R(1139)$	$R(710)$
DIS	100(11)	47(10)	58(10)	38(9)	346^{+117}_{-225}
2nKO	100(3)	50(6)	52(9)	41(5)	310^{+100}_{-199}
β [4]	100(5)	42(3)	41(3)	34(3)	244^{+69}_{-152}
Average	100(3)	44(3)	43(3)	36(2)	259^{+73}_{-161}

2743-keV $E2$ transition directly to the ground state. The presence of several branches offers an opportunity to explore the nature of the 0^+ and 2^+ states further by examining the properties of these transitions. Although an absolute determination of the $B(E2)$ strengths would require knowledge of the half-life of the 2_2^+ state, or a direct measurement of the $B(E2)$ value for one of the transitions, the *relative* strengths can be compared to those predicted by different calculations.

In the DIS data, the spectrum in Figs. 3(a) and 3(b) was

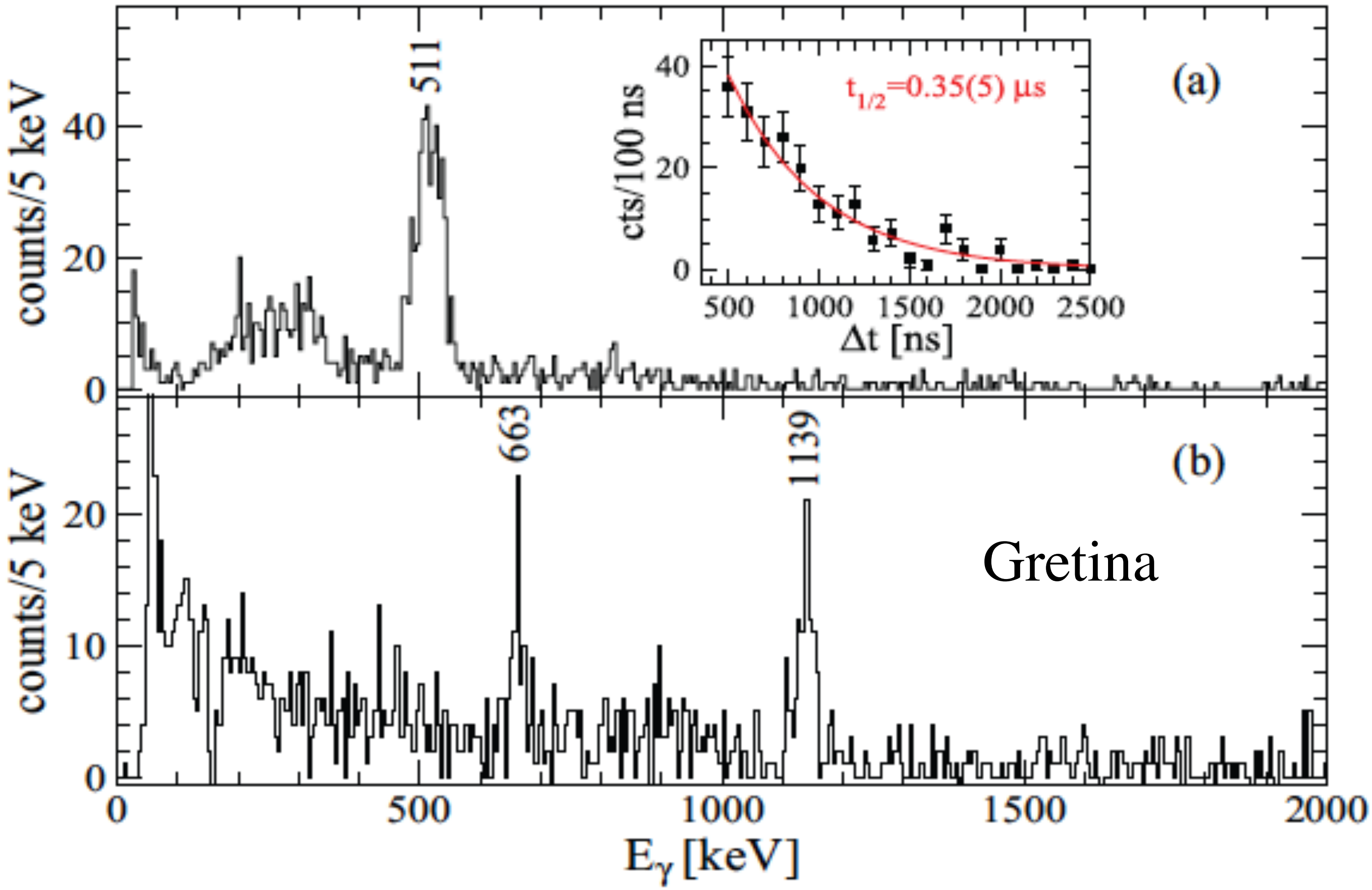

FIG. 2. (Color online) Spectra from the 2nKO data. (a) Delayed γ-ray spectrum recorded in the CsI(Na) scintillators in coincidence with implanted ^{68}Ni ions. Inset: decay curve for the 511-keV line. (b) Prompt GRETINA spectrum coincident with the identification of a ^{68}Ni recoil and the detection of a delayed 511-keV γ ray in the CsI(Na) detectors.

^{68}Ni was also produced in two-neutron knockout (2nKO) reactions at the Coupled Cyclotron Facility of the National Superconducting Cyclotron Laboratory (NSCL). A secondary cocktail beam containing ^{70}Ni, ^{69}Co, and ^{71}Cu ions was produced in the projectile fragmentation of a 140-MeV/u ^{82}Se beam on a 423-mg/cm^2 ^{9}Be production target located at the entrance of the A1900 fragment separator [18]. The momentum acceptance of the separator was set to 1%. Secondary beams with typical intensities of 10^5 ions/s were delivered

Knocking out 2 neutrons leaves an excited ^{68}Ni nucleus，whose gamma rays can be studied in coincidence with the ^{68}Ni fragment

^{82}Se VERY FAST + ^{9}Be ……. ^{70}Ni

^{70}Ni FAST + ^{9}Be………….^{68}Ni + 2n

Nuclear Structure Physics

- Complementary degrees of freedom are accessible
  - Single-particle properties
    - » Nucleon knockout
    - » Transfer reactions
  - Collective degrees of freedom

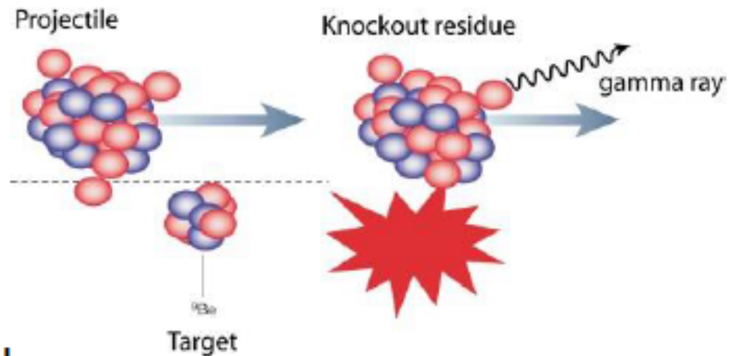

Direct reactions:

- nucleon-removing reactions (knockout)
- Nucleon-adding transfer reactions (light-ion and heavy-ion induced)

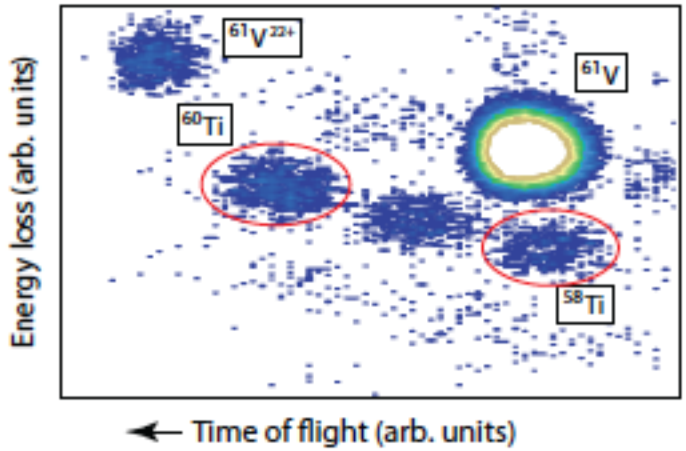

FIG. 1: (Color online) Identification spectrum for the reaction residues produced in $^{9}Be(^{61}V,^{A}Ti)X$ at a 90-MeV/u mid-target energy. All reaction residues are unambiguously identified by their energy loss, measured in the S800 ionization chamber, and their time of flight.

^{82}Se VERY FAST + ^{9}Be ……. ^{61}V

^{61}V FAST + ^{9}Be………..^{58}Ti + 2n+ 1p

^{61}V FAST + ^{9}Be………..^{60}Ti + 1p

^{70}Ni gammas, 5kev/bin, top from 2n KO from incoming ^{72}Ni, bottom ^{70}Ni made from incoming ^{73}Cu.

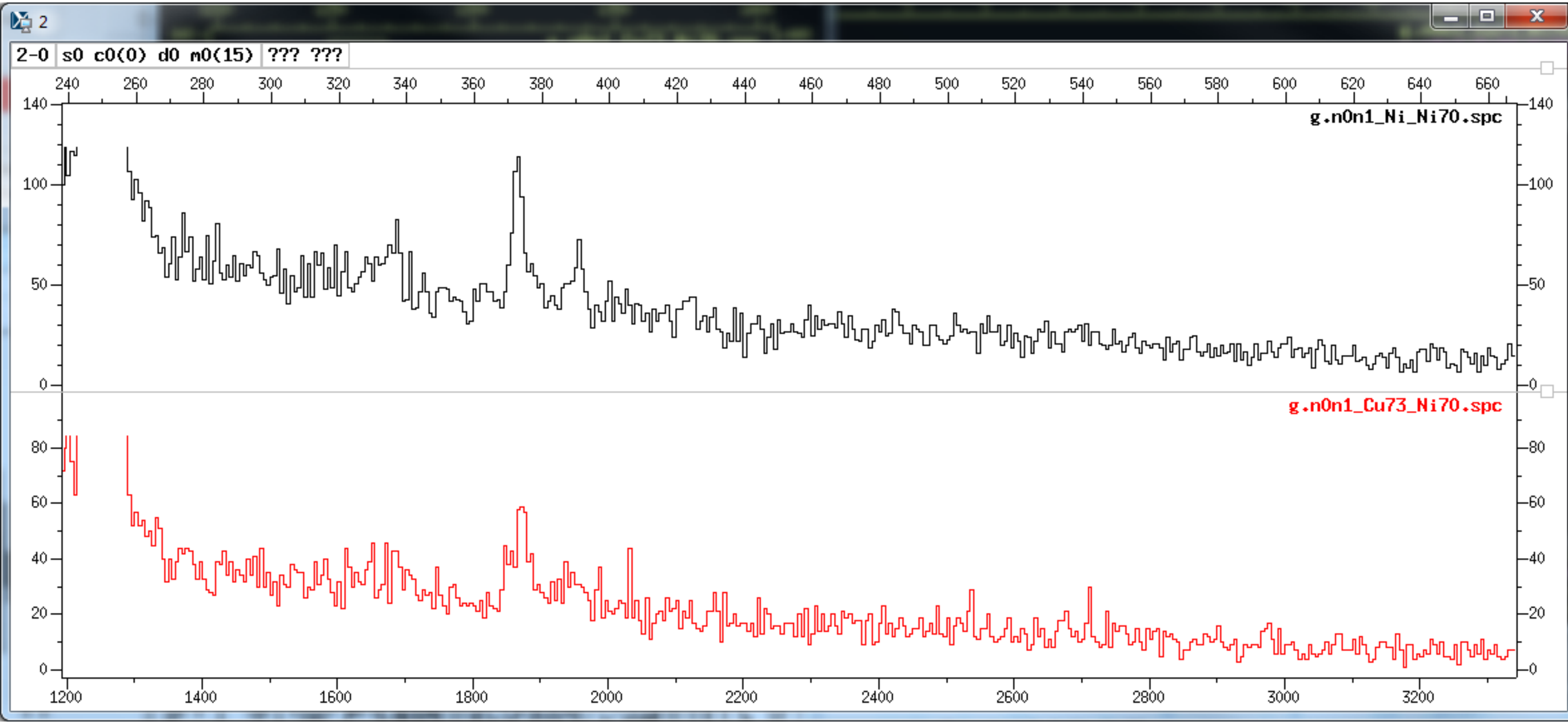

1866-keV gamma ray was identified in one decay study, but not in another decay paper. The other high-energy gamma rays were not previously seen.

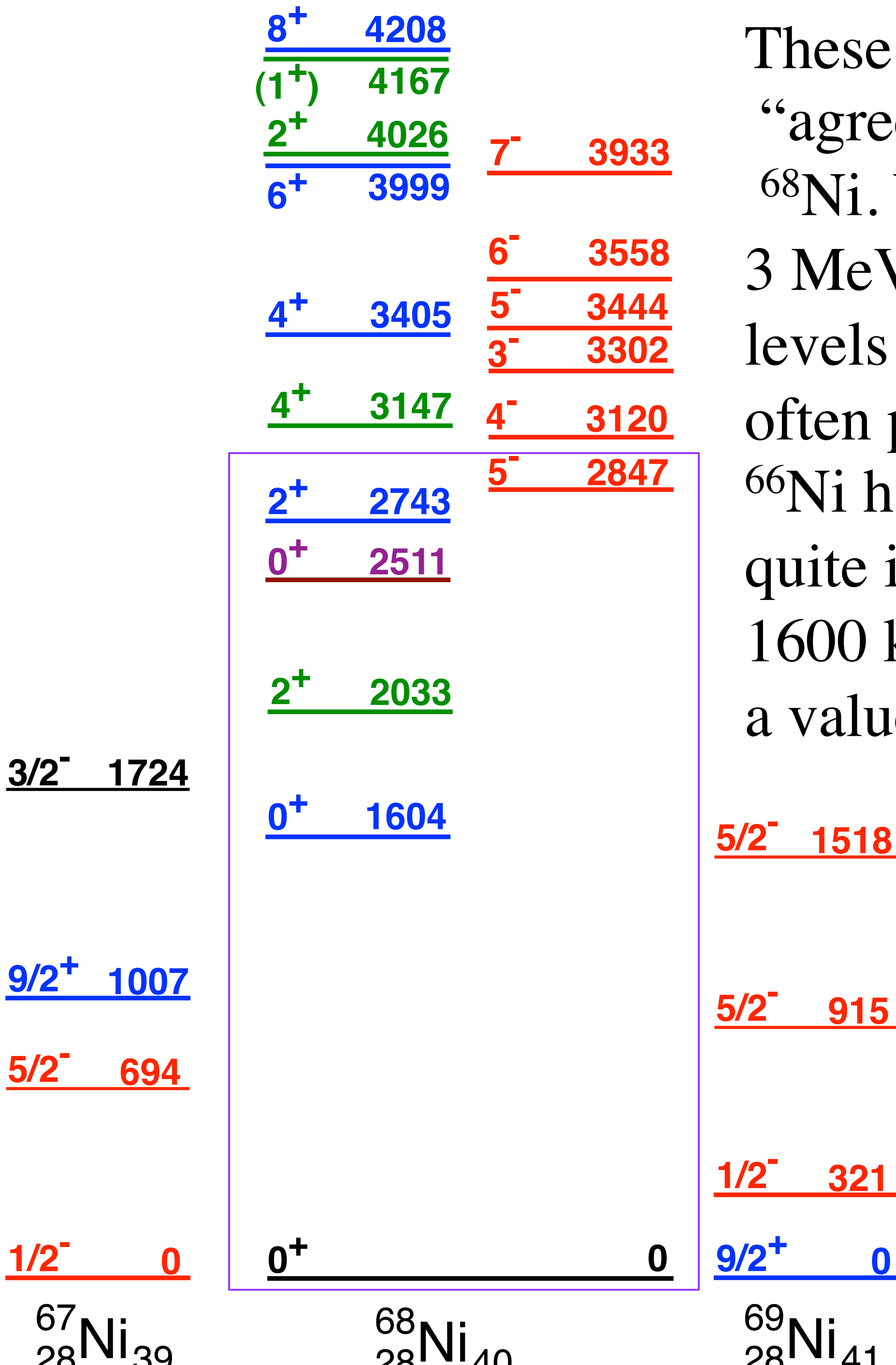

These seem to be the "agreed-on levels in magic ^{68}Ni. What is the fuss? Mainly that below 3 MeV, there are three 0^+ levels and two 2^+ levels and a single 5^- level. Although this often portrayed as "unique" the fact is that ^{66}Ni has a similar structure. This region is quite interesting owing to the "$p_{1/2}$ gap" of 1600 keV between the 9/2+ and 5/2- levels, a value comparable to the pairing energy.

A second major feature of the N = 40 oscillator shell gap is that 1-neutron-particle-1-hole states have negative parity, whereas, similar 1-proton-particle-1-hole states have positive parity. Hence they don't mix.

These are the five ^{68}Ni low-energy levels from Tsunoda et al., that will serve as a basis for an analysis of the level structure of ^{69}Cu. These graphs show the deformation from wavefunction components from Monte Carlo Shell Model calculations.

Novel shape evolution in exotic Ni isotopes and Type II shell evolution

Yusuke Tsunoda,[1] Takaharu Otsuka,[1,2,3] Noritaka Shimizu,[2] Michio Honma,[4] and Yutaka Utsuno[5]

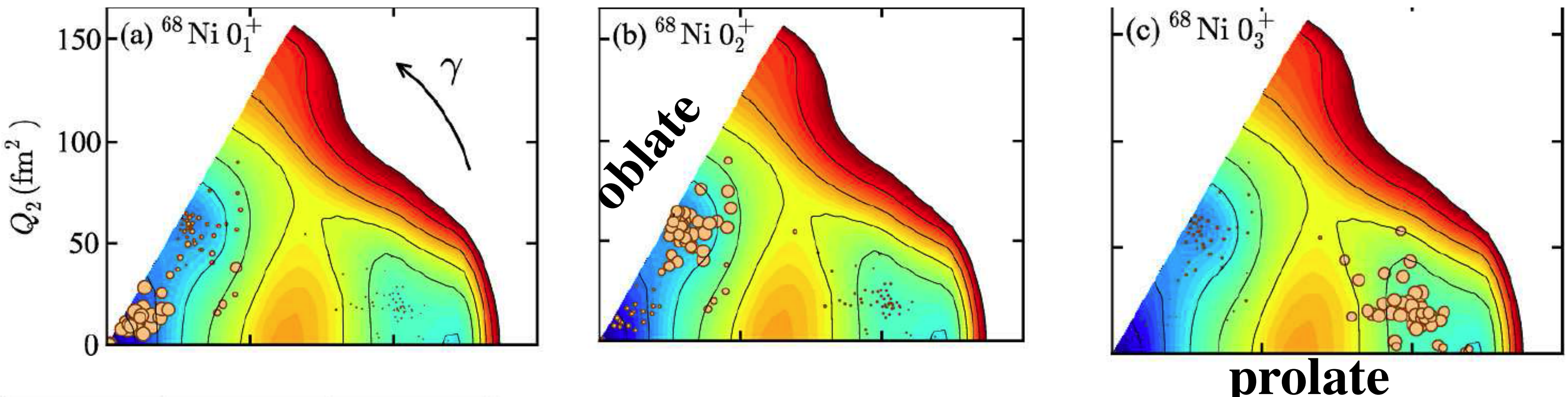

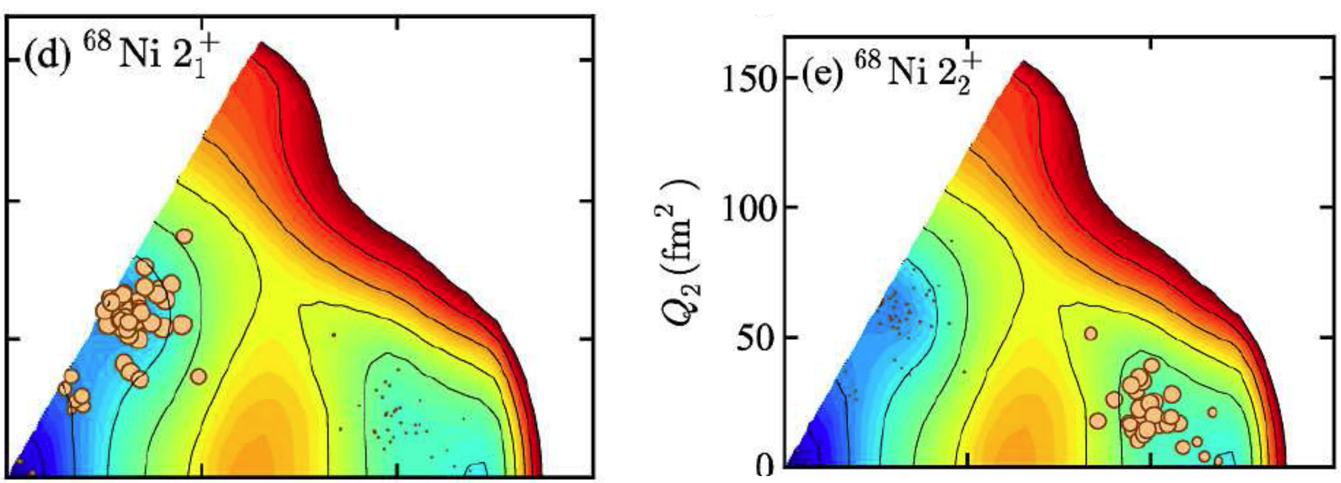

arXiv:1309.5851v1

Accepted PRC?

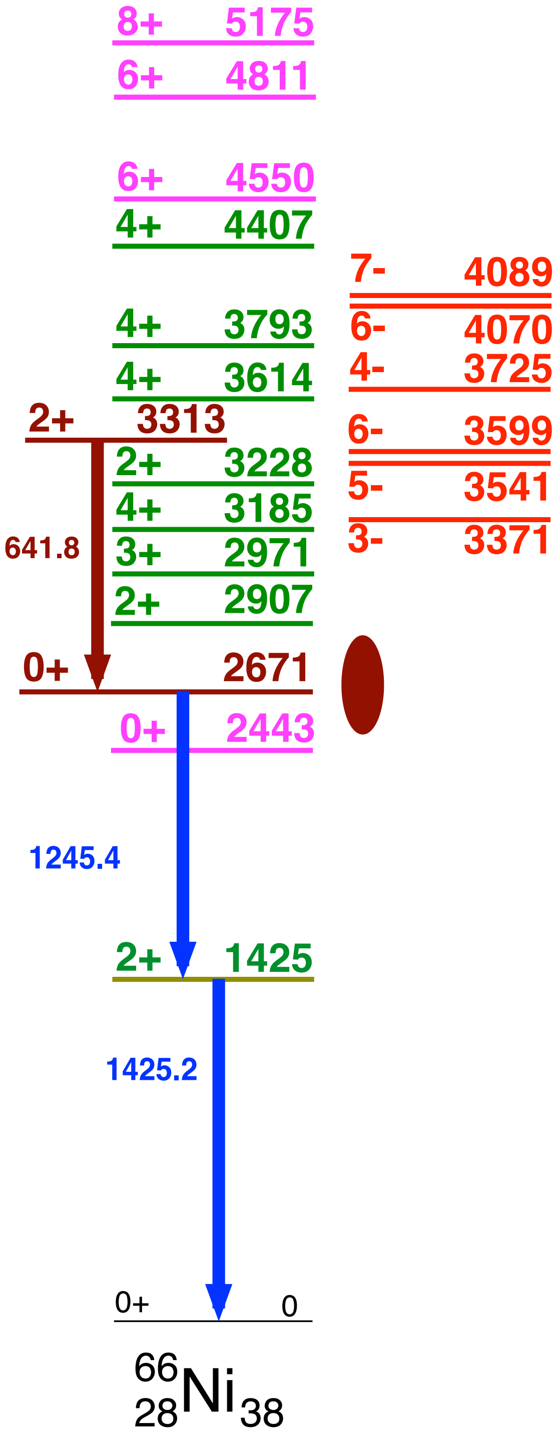

These seem to be the "agreed-on levels in magic ^{66}Ni. Guess what??? Below 3 MeV, there are three 0^+ levels and two 2^+ levels and a single 3^+ level.

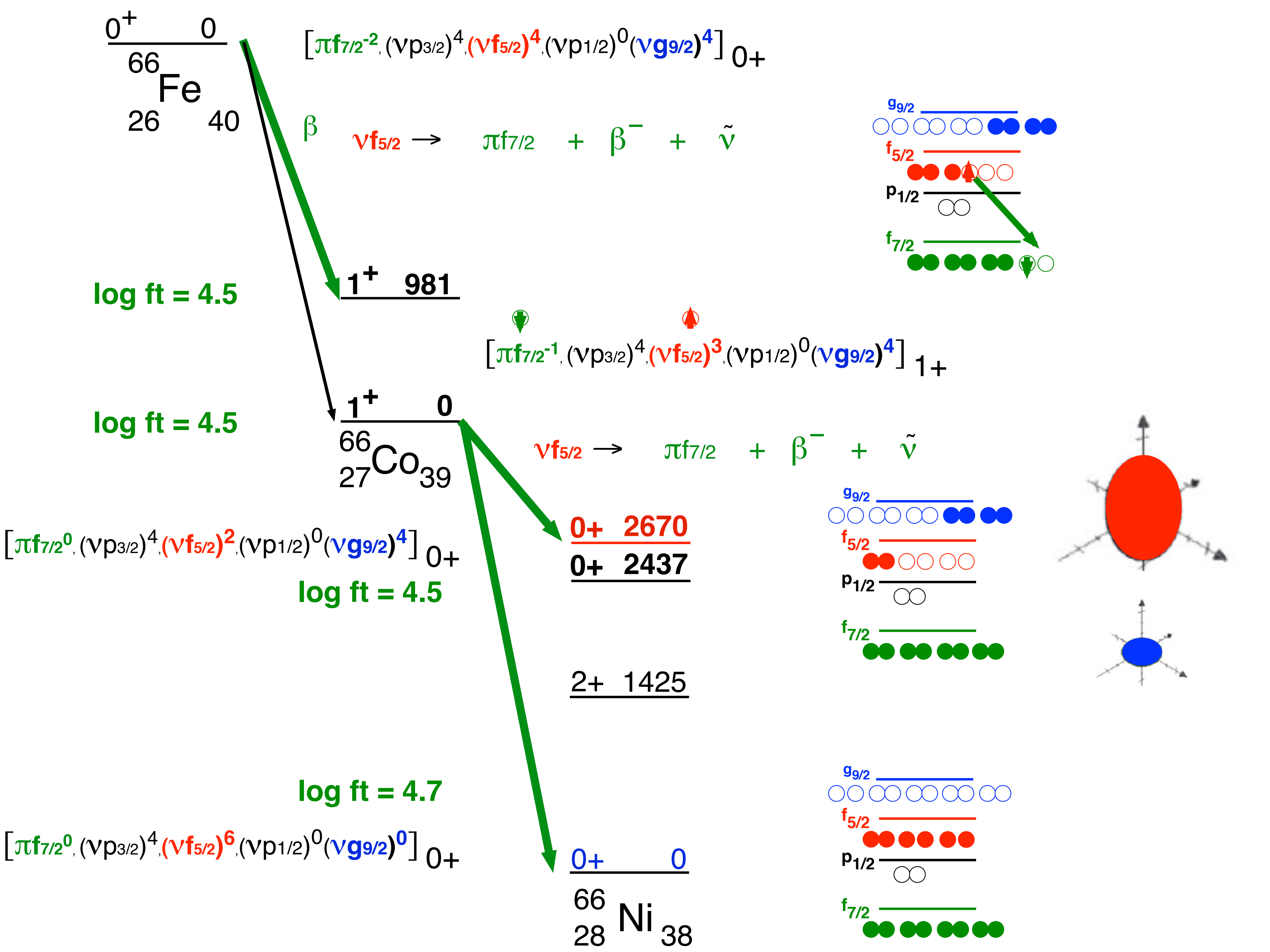

0+ 0
66 Fe 26 40
[πf7/2-2, (νp3/2)4, (νf5/2)4, (νp1/2)0 (νg9/2)4] 0+
β
νf5/2 → πf7/2 + β− + ν̃
g9/2
f5/2
p1/2
f7/2
log ft = 4.5
1+ 981
[πf7/2-1, (νp3/2)4, (νf5/2)3, (νp1/2)0 (νg9/2)4] 1+
log ft = 4.5
1+ 0
66 27 Co 39
νf5/2 → πf7/2 + β− + ν̃
[πf7/2 0, (νp3/2)4, (νf5/2)2, (νp1/2)0 (νg9/2)4] 0+
0+ 2670
0+ 2437
log ft = 4.5
2+ 1425
log ft = 4.7
[πf7/2 0, (νp3/2)4, (νf5/2)6, (νp1/2)0 (νg9/2)0] 0+
0+ 0
66 28 Ni 38

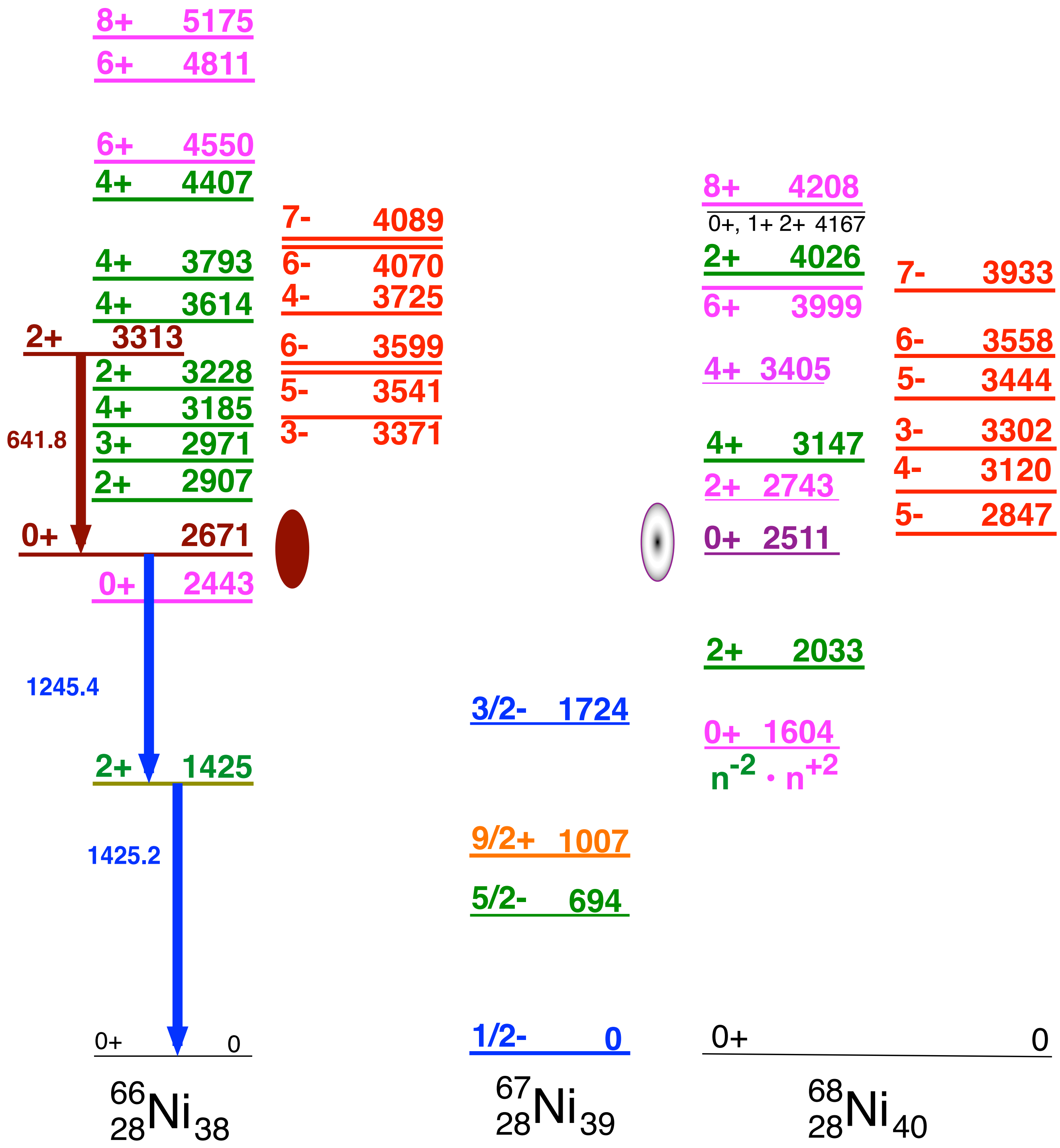

8+ 5175
6+ 4811
6+ 4550
4+ 4407
4+ 3793
4+ 3614
2+ 3313
2+ 3228
4+ 3185
3+ 2971
2+ 2907
641.8
0+ 2671
0+ 2443
1245.4
2+ 1425
1425.2
0+ 0
7- 4089
6- 4070
4- 3725
6- 3599
5- 3541
3- 3371
3/2- 1724
9/2+ 1007
5/2- 694
1/2- 0
8+ 4208
0+, 1+ 2+ 4167
2+ 4026
6+ 3999
4+ 3405
4+ 3147
2+ 2743
0+ 2511
2+ 2033
0+ 1604
$n^{-2} \cdot n^{+2}$
0+ 0
7- 3933
6- 3558
5- 3444
3- 3302
4- 3120
5- 2847
$^{66}_{28}Ni_{38}$
$^{67}_{28}Ni_{39}$
$^{68}_{28}Ni_{40}$

Two more points, first magnetic moment for the $p_{1/2}$ ground state has been measured and found to lie close to the Schmidt single-particle limit.

Second, Spin orbit splitting is restored in ^{67}Ni to nearly the same value as it was in ^{49}Ca…….before EIGHT J – L + 1 $f_{7/2}$ protons were added.

So, the tensor interaction is not the whole story in nuclear structure.

TABLE I. Experimental magnetic moments μ_{expt} and single-particle values μ_{sp} and their difference $\Delta\mu$ for odd-proton (π) and odd-neutron (ν) nuclei in the Pb region.

		μ_{expt}	μ_{sp}	$\Delta\mu$
^{209}Bi	$\pi h_{9/2}$	4.11	2.62	1.49
^{209}Bi	$\pi i_{13/2}$	2.78(10)[a]	3.56	−0.78
^{207}Tl	$\pi s_{1/2}^{-1}$	1.87	2.79	−0.92
^{207}Tl	$\pi d_{3/2}^{-1}$	0.76(19)[b]	0.12	0.64
^{209}Pb	$\nu g_{9/2}$	−1.47	−1.91	0.44
^{207}Pb	$\nu p_{1/2}^{-1}$	0.59	0.64	−0.05
^{207}Pb	$\nu f_{5/2}^{-1}$	0.79(3)	1.37	−0.58
^{207}Pb	$\nu i_{13/2}^{-1}$	−1.01(3)[c]	−1.91	0.90

All corrections have been collated in Table II. For the $p_{3/2}$ proton in ^{69}Cu, the calculated correction to the single-particle magnetic moment is large, $-0.94\mu_N$, while for the $p_{1/2}$ neutron in ^{67}Ni it is small, $-0.18\mu_N$. For the former, the result is in good agreement with experiment, while for the latter, the correction, although small, is a factor of 4 larger than required by experiment. The same phenomenon is found in the Pb region, where for the neutron $p_{1/2}$ state the calculated [12,14,15] correction is of order $\sim 0.2\mu_N$, compared with the experimental value of $0.05\mu_N$. The small changes observed for $p_{1/2}$ nuclei are related to the absence of nearby low angular momentum negative parity orbitals. The fact that, in ^{67}Ni, even this small correction is overestimated, provides evidence for the strength of the subshell closure at $N = 40$ in ^{68}Ni.

The first fully on-line use of the angular distribution of beta emission in detection of NMR of nuclei oriented at low temperatures is reported. The magnetic moments of the single valence particle, intermediate mass, isotopes ^{67}Ni($\nu p_{1/2}^{-1}$;1/2$^-$) and ^{69}Cu($\pi p_{3/2}^{1}$;3/2$^-$) are measured to be $+0.601(5)\ \mu_N$ and $+2.84(1)\ \mu_N$, respectively, revealing only a small deviation from the neutron $p_{1/2}$ single-particle value in the former and a large deviation from the proton $p_{3/2}$ single-particle value in the latter. Quantitative interpretation is given in terms of core polarization and meson-exchange currents.

VOLUME 85, NUMBER 7 PHYSICAL REVIEW LETTERS 14 AUGUST 2000

First On-Line Beta-NMR on Oriented Nuclei: Magnetic Dipole Moments of the $(\nu p_{1/2})^{-1}$ 1/2$^-$ Ground State in ^{67}Ni and $(\pi p_{3/2})^{+1}$ 3/2$^-$ Ground State in ^{69}Cu

J. Rikovska,* T. Giles, N. J. Stone, K. van Esbroeck,† G. White, and A. Wöhr
Department of Physics, Oxford University, Parks Road, OX1 3PU Oxford, United Kingdom

M. Veskovic
Department of Physics, University of Novi Sad, Novi Sad, Yugoslavia

I. S. Towner
Physics Department, Queen's University, Kingston, Ontario, K7L 3N6, Canada

P. F. Mantica, J. I. Prisciandaro, and D. J. Morrissey
Department of Chemistry, Michigan State University, East Lansing, Michigan 48824

V. N. Fedoseyev and V. I. Mishin
Institute of Spectroscopy, Russian Academy of Sciences, 142092 Troitsk, Russia

U. Köster
EP Division, CERN, CH 1211 Geneva 23, Switzerland

W. B. Walters
Department of Chemistry and Biochemistry, University of Maryland, College Park, Maryland 20742

and the NICOLE and ISOLDE Collaboration
(Received 17 April 2000)

Measured moment 0.60 (5)
Single-particle 0.64

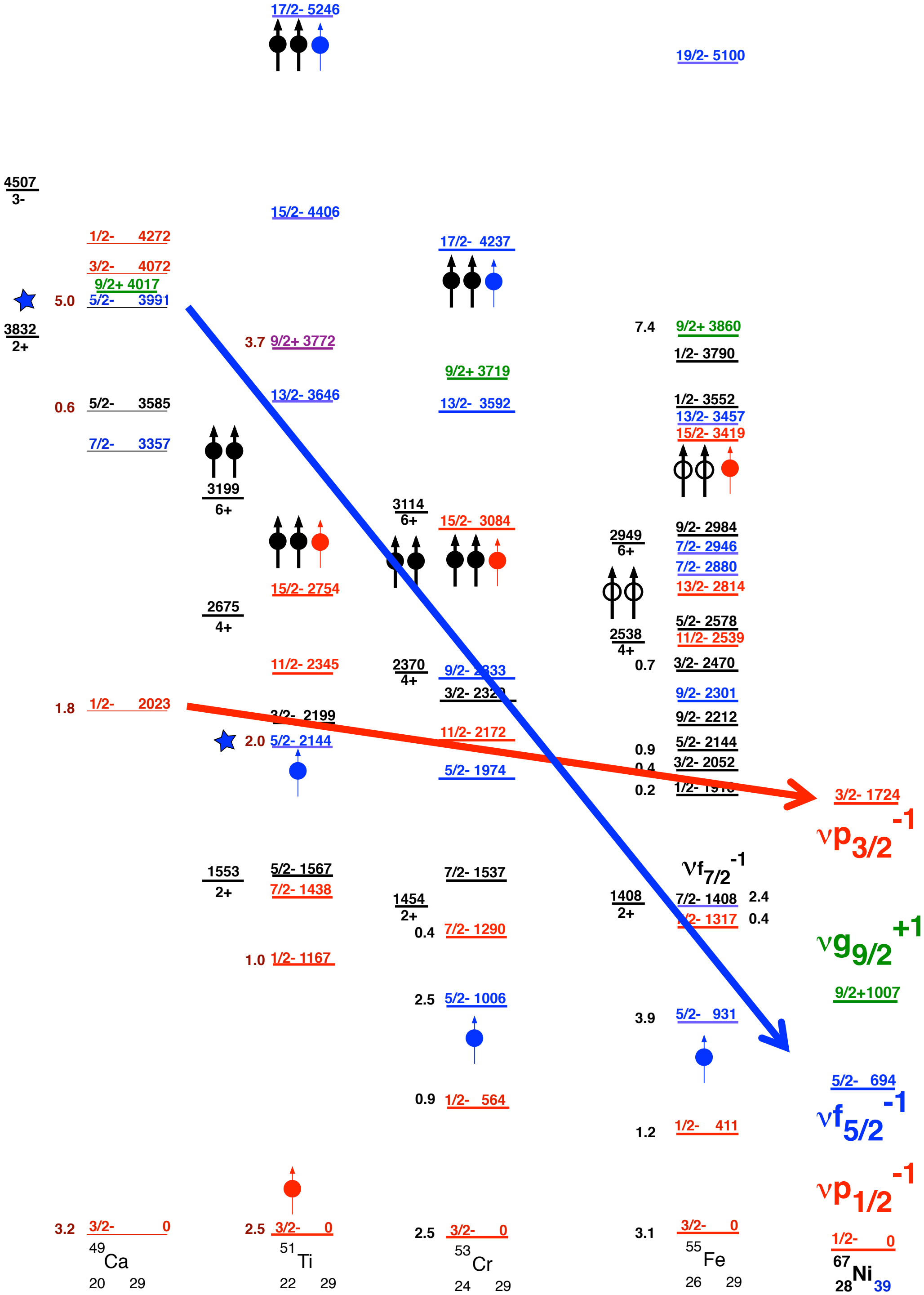

Here, I want to make an observation about spin-orbit splitting. Much comment has been made about the Tensor interaction and the lowering of the J – ½ state. BUT, look here, when the nucleus is returned to a largely spherical state in ^{67}Ni, lo and behold, **the total change is from <u>2020 to 1724 keV only 300 keV</u> relative to the splitting observed in ^{49}Ca for the $p_{3/2}$ to $p_{1/2}$ split!!!** **Compared to the high-j $f_{5/2}$ orbital, the change for the lower-J L = 1 orbitals is much smaller.**

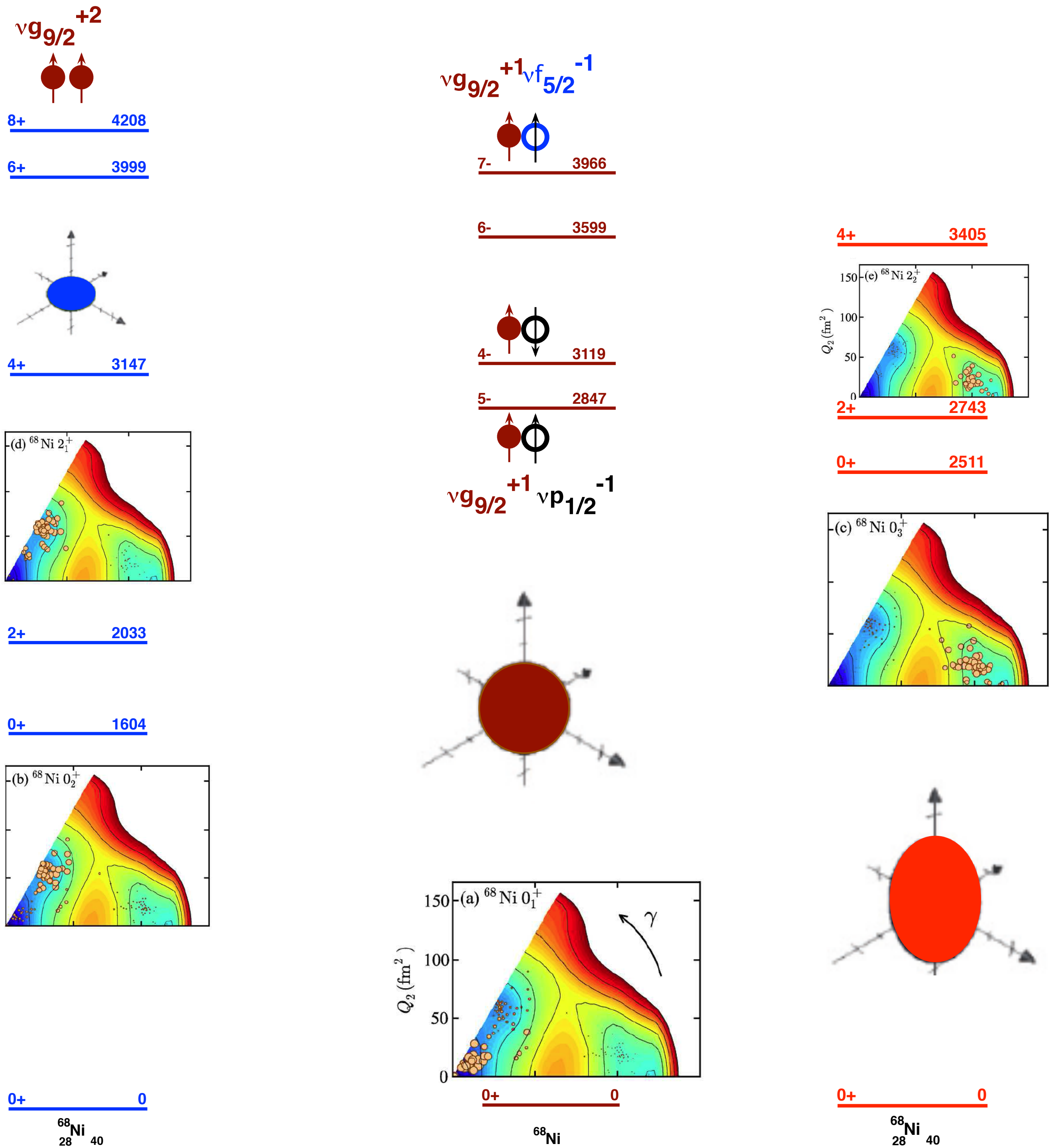

νg9/2+2
8+ 4208
6+ 3999
4+ 3147
(d) 68Ni 2+1
2+ 2033
0+ 1604
(b) 68Ni 0+2
0+ 0
68Ni 28 40
νg9/2+1 νf5/2-1
7- 3966
6- 3599
4- 3119
5- 2847
νg9/2+1 νp1/2-1
(a) 68Ni 0+1
γ
Q2 (fm2)
150
100
50
0
0+ 0
68Ni
4+ 3405
(e) 68Ni 2+2
2+ 2743
0+ 2511
(c) 68Ni 0+3
0+ 0
68Ni 28 40

PHYSICAL REVIEW C **89**, 021301(R) (2014)

Shape coexistence in ^{68}Ni

S. Suchyta,[1,2] S. N. Liddick,[1,2] Y. Tsunoda,[3] T. Otsuka,[1,3,4,5] M. B. Bennett,[1,4] A. Chemey,[1] M. Honma,[6] N. Larson,[1,2] C. J. Prokop,[1,2] S. J. Quinn,[1,4] N. Shimizu,[5] A. Simon,[1] A. Spyrou,[1,4] V. Tripathi,[7] Y. Utsuno,[8] and J. M. VonMoss[7]
[1]*National Superconducting Cyclotron Laboratory (NSCL), Michigan State University, East Lansing, Michigan 48824, USA*

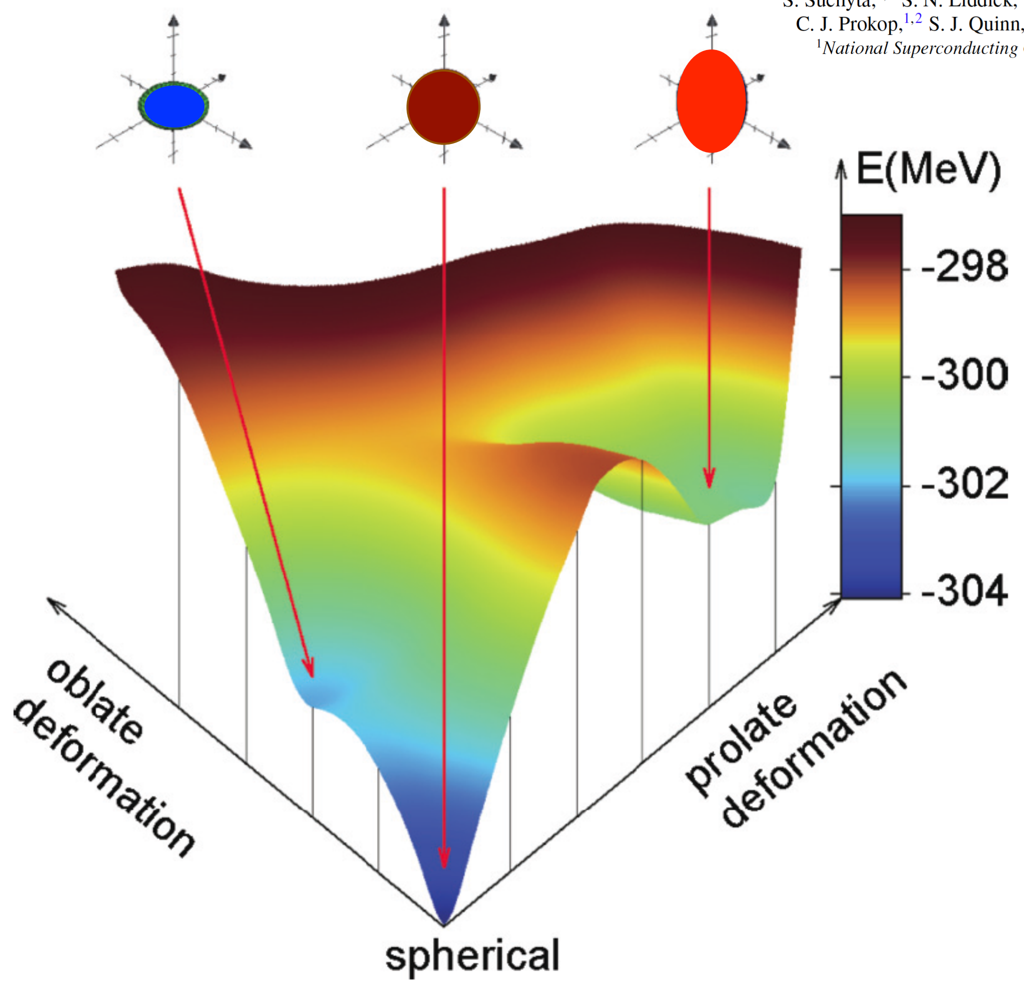

FIG. 3. (Color online) The energy of ^{68}Ni as a function of a given ellipsoidal shape. The energy was obtained by a Hartree-Fock calculation constrained by the quadrupole moment for the Hamiltonian being used. Each tick along the axis corresponds to an increment of 50 e fm^2 in the magnitude of the quadrupole moment.

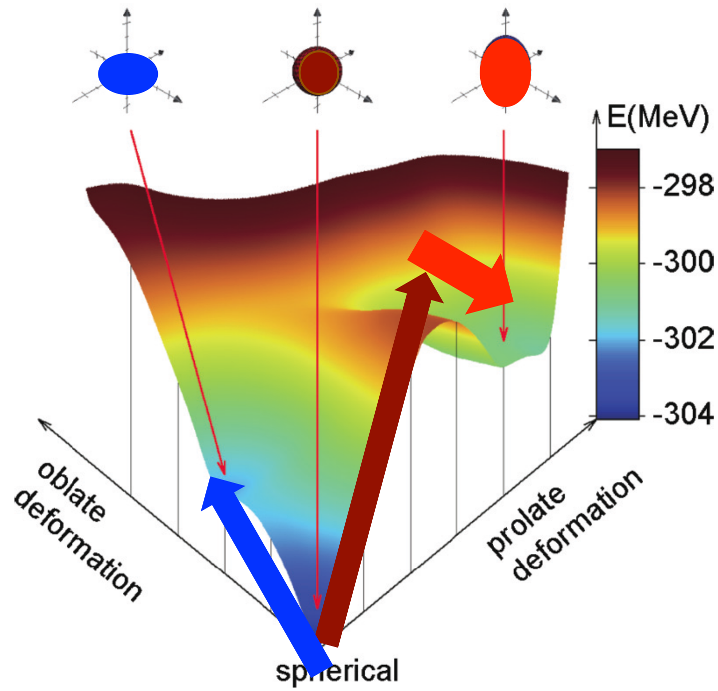

FIG. 3. (Color online) The energy of ^{68}Ni as a function of a given ellipsoidal shape. The energy was obtained by a Hartree-Fock calculation constrained by the quadrupole moment for the Hamiltonian being used. Each tick along the axis corresponds to an increment of 50 e fm^2 in the magnitude of the quadrupole moment.

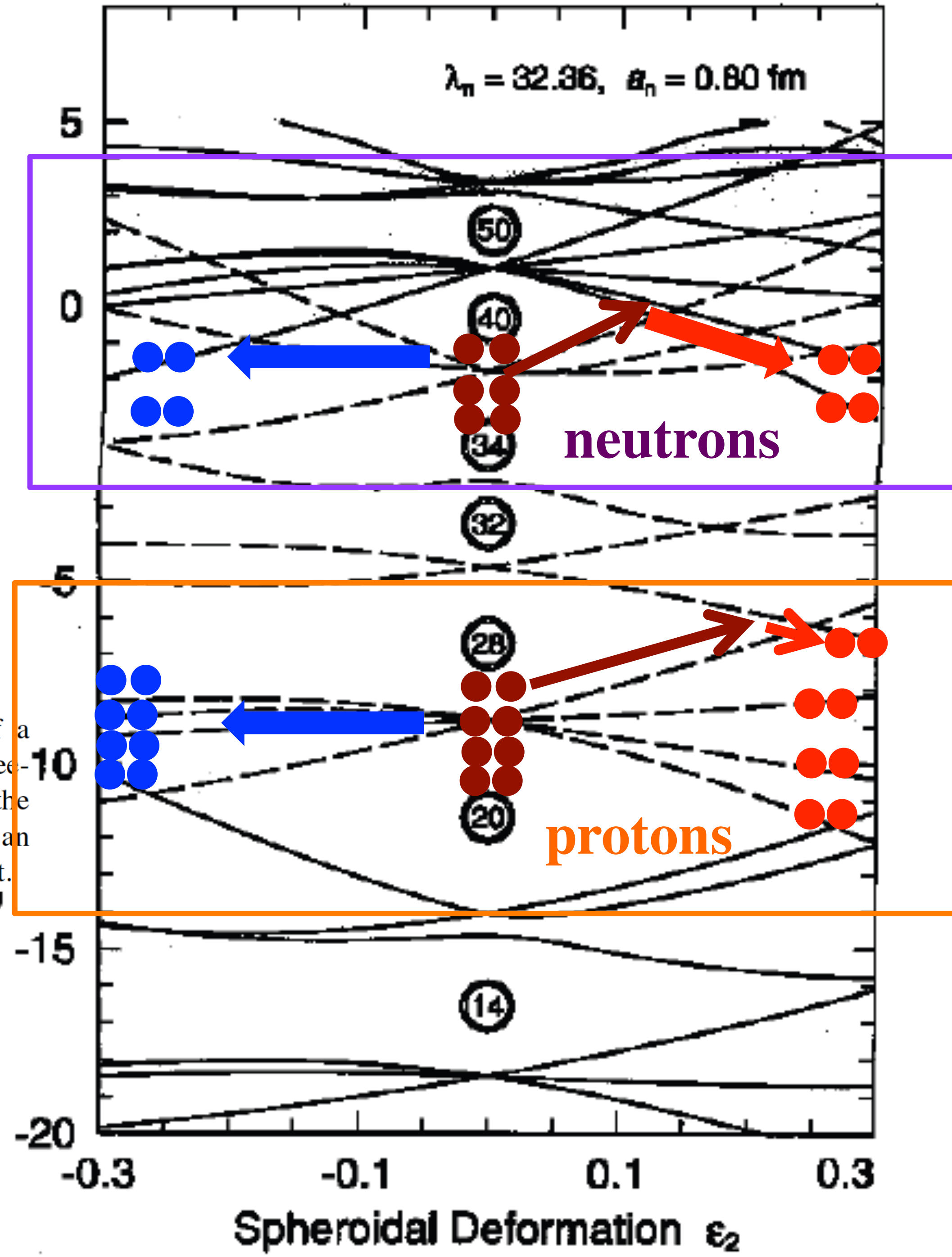

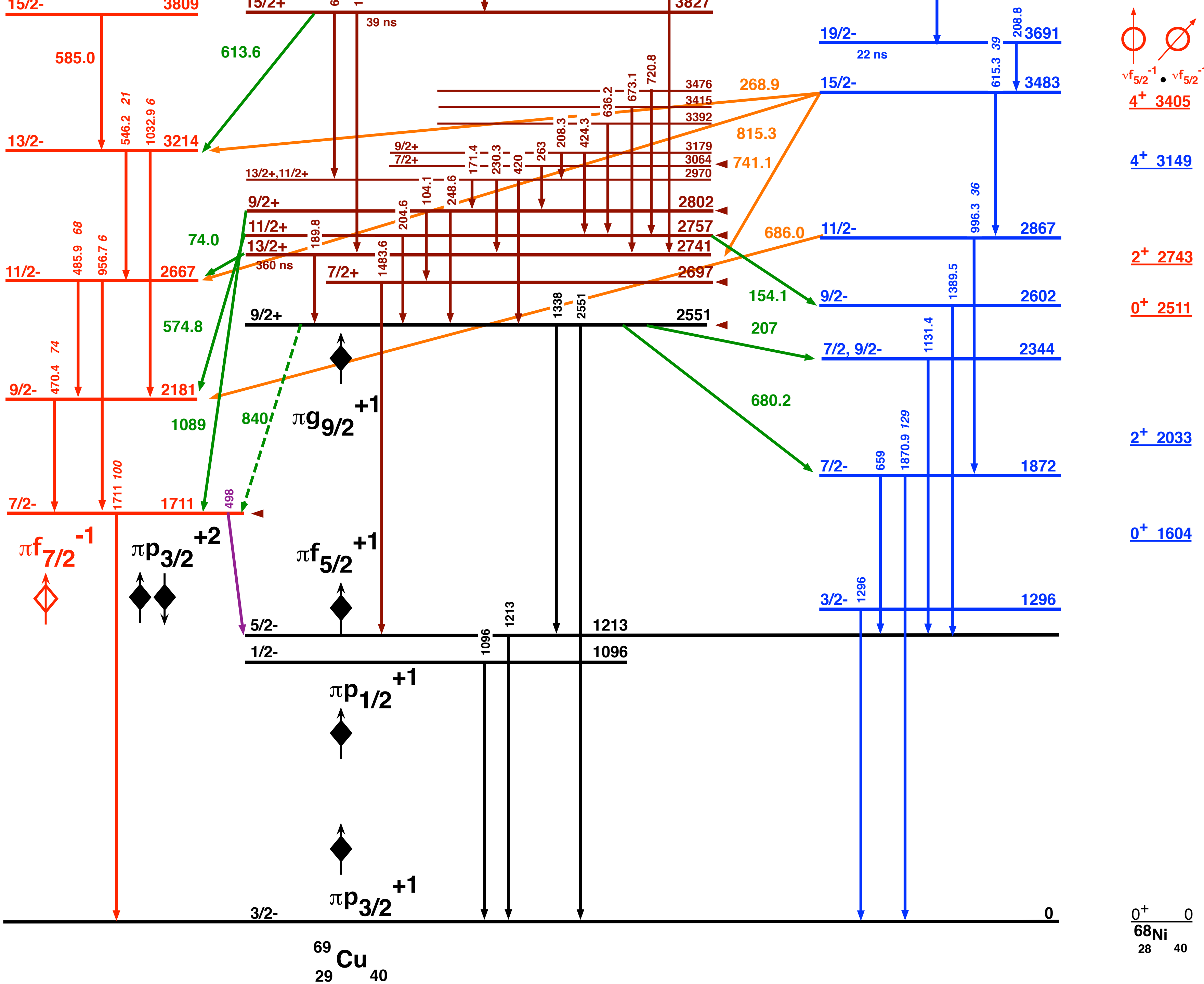
15/2- 3809
585.0
13/2- 3214
546.2 21
1032.9 6
11/2- 2667
485.9 68
956.7 6
9/2- 2181
470.4 74
7/2- 1711
1711 100
πf7/2 -1
πp3/2 +2
15/2+ 3827
39 ns
613.6
13/2+,11/2+ 2970
9/2+ 3179
7/2+ 3064
3476
3415
3392
636.2
673.1
720.8
208.3
424.3
263
420
230.3
171.4
248.6
104.1
204.6
189.8
1483.6
9/2+ 2802
11/2+ 2757
13/2+ 2741
360 ns
7/2+ 2697
74.0
574.8
1089
840
498
9/2+ 2551
πg9/2 +1
πf5/2 +1
1338
2551
5/2- 1213
1/2- 1096
1096
1213
πp1/2 +1
πp3/2 +1
3/2- 0
69 29 Cu 40
268.9
815.3
741.1
686.0
154.1
207
680.2
19/2- 3691
22 ns
208.8
39
615.3
15/2- 3483
11/2- 2867
996.3 36
9/2- 2602
1389.5
7/2, 9/2- 2344
1131.4
7/2- 1872
659
1870.9 129
3/2- 1296
1296
νf5/2 -1 • νf5/2 -1
4+ 3405
4+ 3149
2+ 2743
0+ 2511
2+ 2033
0+ 1604
0+ 0
68 28 Ni 40

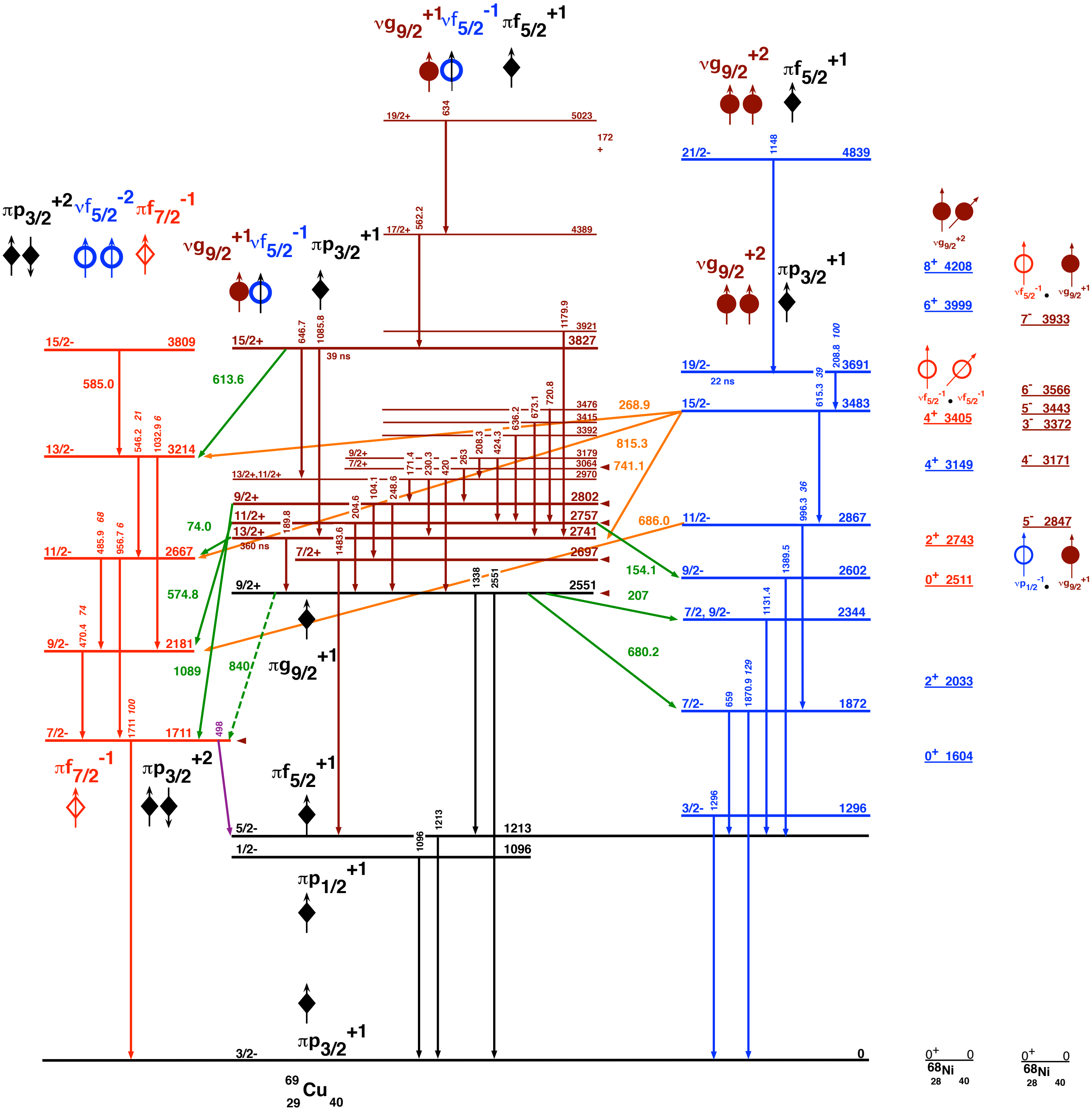

$\nu g_{9/2}^{+1} \nu f_{5/2}^{-1} \pi f_{5/2}^{+1}$
$\nu g_{9/2}^{+2} \pi f_{5/2}^{+1}$
$\pi p_{3/2}^{+2} \nu f_{5/2}^{-2} \pi f_{7/2}^{-1}$
$\nu g_{9/2}^{+1} \nu f_{5/2}^{-1} \pi p_{3/2}^{+1}$
$\nu g_{9/2}^{+2} \pi p_{3/2}^{+1}$
19/2+ 5023
634
172
17/2+ 4389
562.2
21/2- 4839
1148
3921
1179.9
15/2- 3809
15/2+ 3827
646.7
1085.8
39 ns
19/2- 3691
22 ns
208.8 100
39
585.0
613.6
3476
3415
3392
268.9
15/2- 3483
615.3
636.2
673.1
720.8
815.3
13/2- 3214
546.2 21
1032.9 6
9/2+ 3179
7/2+ 3064
741.1
13/2+,11/2+ 2970
171.4
230.3
420
263
208.3
424.3
9/2+ 2802
104.1
248.6
204.6
11/2+ 2757
13/2+ 2741
360 ns
7/2+ 2697
74.0
189.8
1483.6
686.0
11/2- 2867
996.3 36
11/2- 2667
485.9 68
956.7 6
154.1
9/2- 2602
1389.5
9/2+ 2551
1338
2551
207
574.8
7/2, 9/2- 2344
1131.4
9/2- 2181
470.4 74
840
1089
$\pi g_{9/2}^{+1}$
680.2
7/2- 1872
659
1870.9 129
7/2- 1711
1711 100
498
$\pi f_{7/2}^{-1}$
$\pi p_{3/2}^{+2}$
$\pi f_{5/2}^{+1}$
3/2- 1296
1296
5/2- 1213
1213
1096
1/2- 1096
$\pi p_{1/2}^{+1}$
$\pi p_{3/2}^{+1}$
3/2- 0
$^{69}_{29}Cu_{40}$
$\nu g_{9/2}^{+2}$
8^+ 4208
6^+ 3999
$\nu f_{5/2}^{-1} \cdot \nu g_{9/2}^{+1}$
7^- 3933
$\nu f_{5/2}^{-1} \cdot \nu f_{5/2}^{-1}$
6^- 3566
5^- 3443
4^+ 3405
3^- 3372
4^+ 3149
4^- 3171
5^- 2847
2^+ 2743
0^+ 2511
$\nu p_{1/2}^{-1} \cdot \nu g_{9/2}^{+1}$
2^+ 2033
0^+ 1604
0^+ 0
$^{68}_{28}Ni_{40}$
0^+ 0
$^{68}_{28}Ni_{40}$

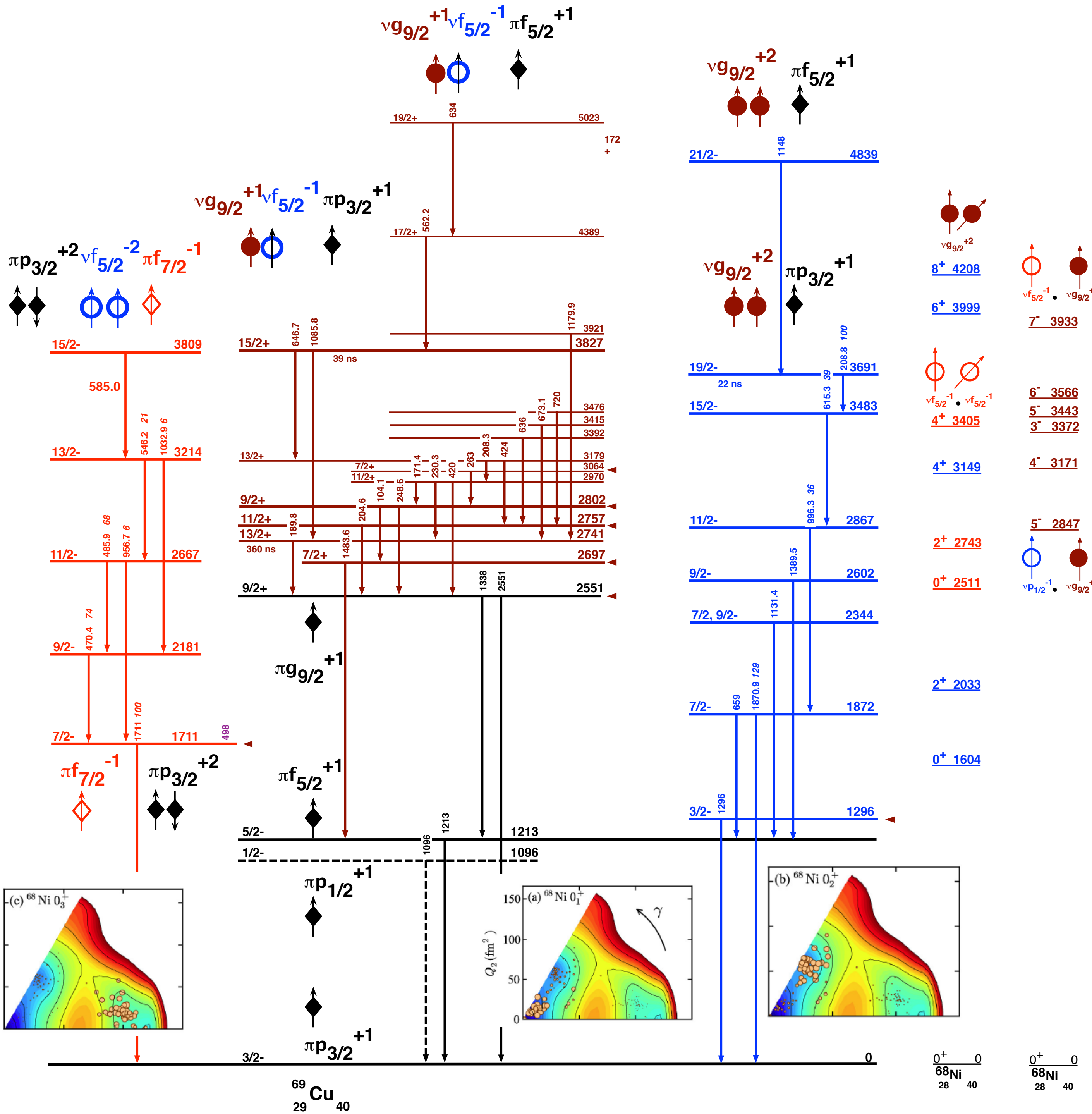

Here are the levels with crossover transitions removed showing the bands associated with the three different Tsunoda shapes.

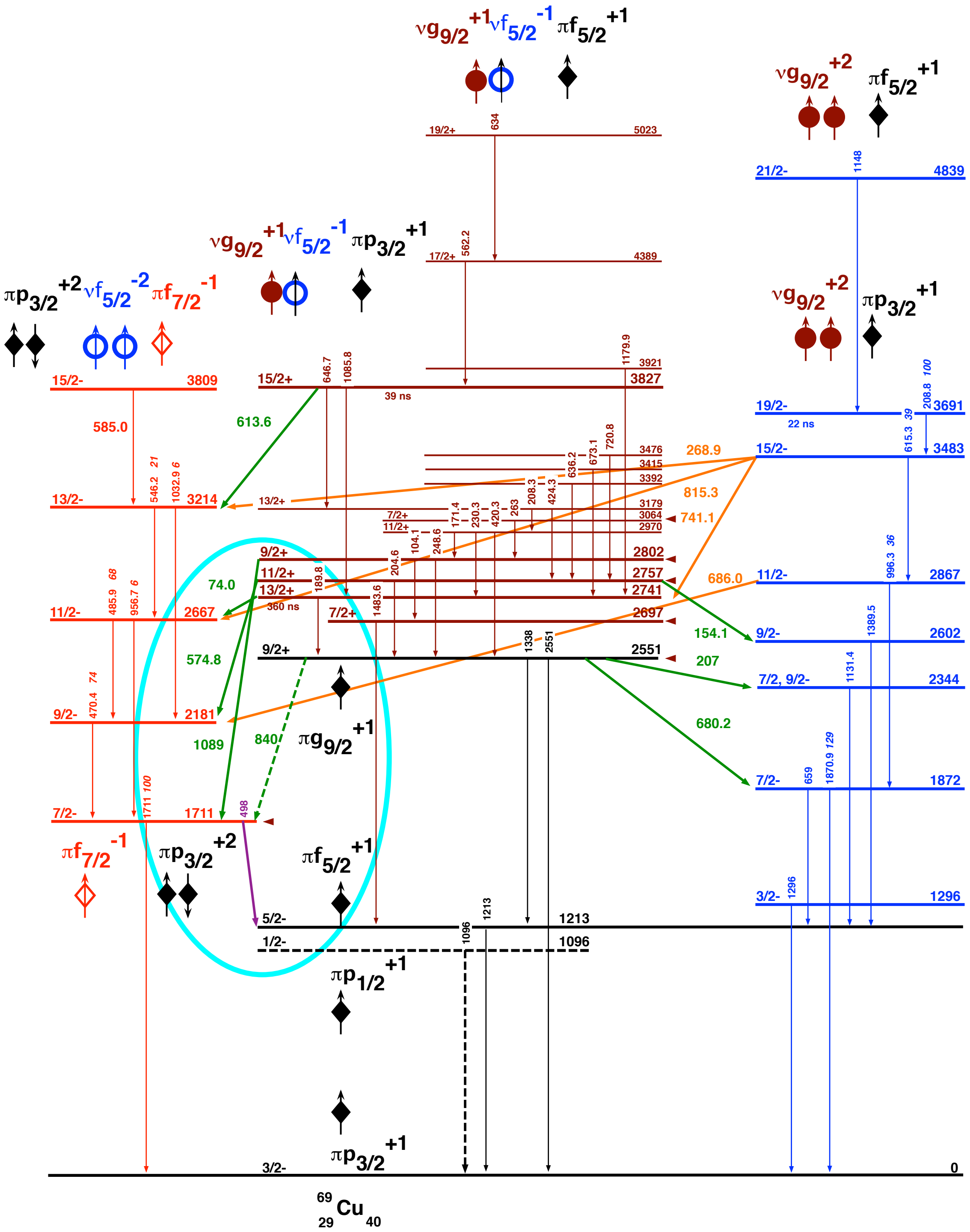

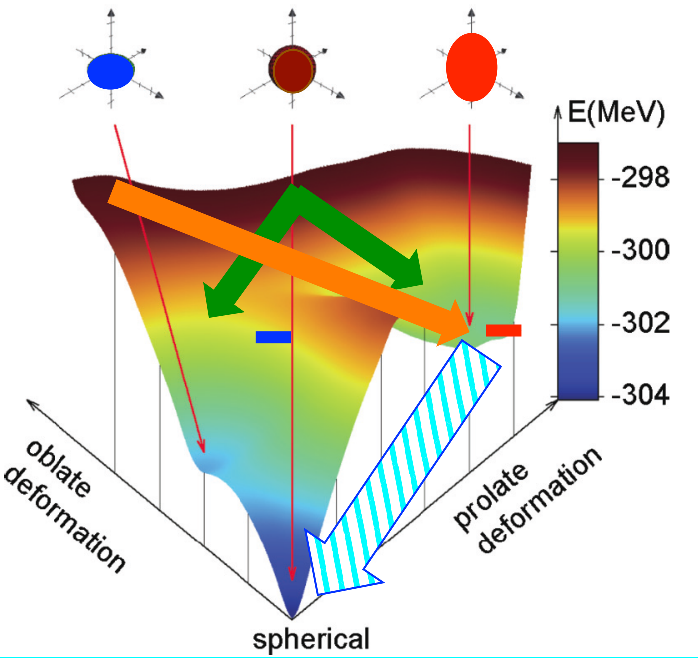

The transitions that are weak or not observed are those from the **prolate levels on the left** into the **oblate and spherical levels on the right.** **The conclusion is that the 7/2⁻ level, down in the well has not mixed with the oblate 7/2⁻ level at 1872 keV.**

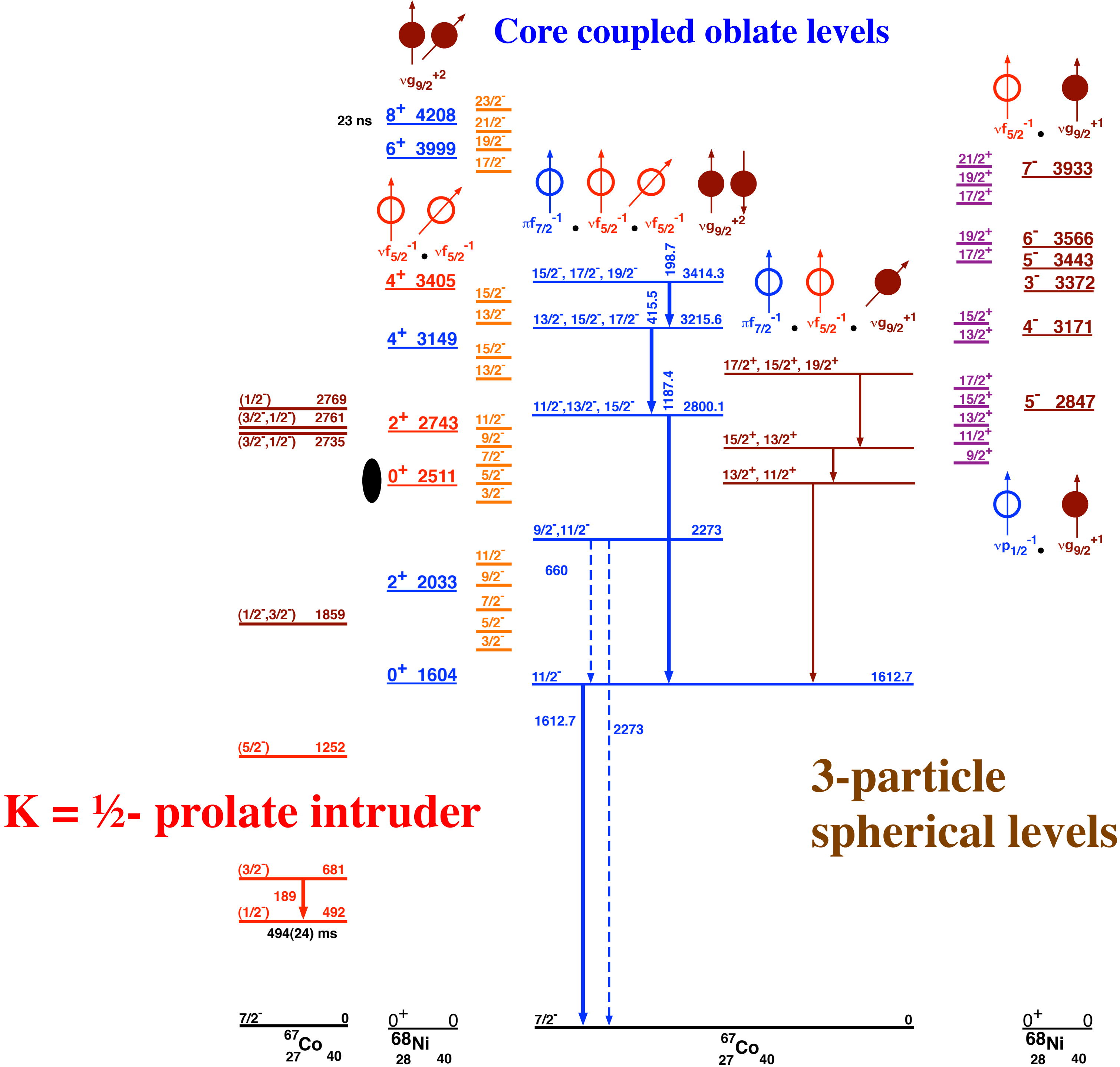

Core coupled oblate levels
K = ½- prolate intruder
3-particle spherical levels
νg9/2+2
23 ns
8+ 4208
6+ 3999
23/2-
21/2-
19/2-
17/2-
νf5/2-1 • νf5/2-1
4+ 3405
15/2-
13/2-
4+ 3149
15/2-
13/2-
2+ 2743
11/2-
9/2-
7/2-
0+ 2511
5/2-
3/2-
2+ 2033
11/2-
9/2-
7/2-
5/2-
3/2-
0+ 1604
(1/2-) 2769
(3/2-,1/2-) 2761
(3/2-,1/2-) 2735
(1/2-,3/2-) 1859
(5/2-) 1252
(3/2-) 681
189
(1/2-) 492
494(24) ms
7/2- 0
67Co 27 40
0+ 0
68Ni 28 40
πf7/2-1 • νf5/2-1 • νf5/2-1 νg9/2+2
198.7
15/2-, 17/2-, 19/2- 3414.3
415.5
13/2-, 15/2-, 17/2- 3215.6
1187.4
11/2-,13/2-, 15/2- 2800.1
9/2-,11/2- 2273
660
11/2- 1612.7
1612.7
2273
7/2- 0
67Co 27 40
πf7/2-1 • νf5/2-1 • νg9/2+1
17/2+, 15/2+, 19/2+
15/2+, 13/2+
13/2+, 11/2+
νf5/2-1 • νg9/2+1
21/2+
19/2+
17/2+
7- 3933
19/2+
17/2+
6- 3566
5- 3443
3- 3372
15/2+
13/2+
4- 3171
17/2+
15/2+
13/2+
11/2+
9/2+
5- 2847
νp1/2-1 • νg9/2+1
0+ 0
68Ni 28 40

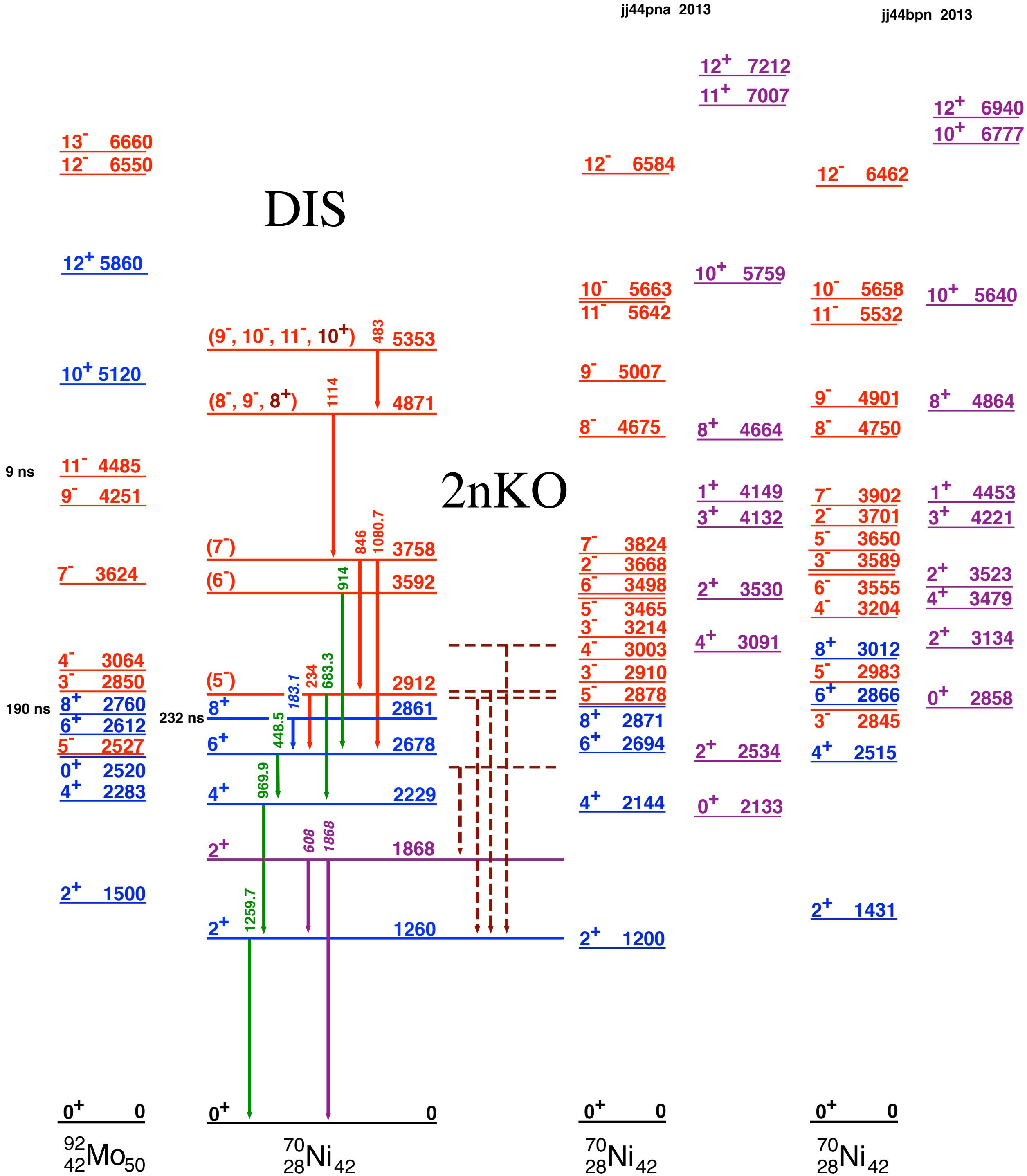

jj44pna 2013
jj44bpn 2013
DIS
2nKO
13- 6660
12- 6550
12+ 5860
10+ 5120
9 ns
11- 4485
9- 4251
7- 3624
4- 3064
3- 2850
190 ns
8+ 2760
6+ 2612
5- 2527
0+ 2520
4+ 2283
2+ 1500
0+ 0
$^{92}_{42}Mo_{50}$
(9-, 10-, 11-, 10+) 5353
483
(8-, 9-, 8+) 4871
1114
846
1080.7
(7-) 3758
(6-) 3592
914
683.3
234
183.1
(5-) 2912
232 ns
8+ 2861
448.5
6+ 2678
969.9
4+ 2229
608
1868
2+ 1868
1259.7
2+ 1260
0+ 0
$^{70}_{28}Ni_{42}$
12+ 7212
11+ 7007
12- 6584
10+ 5759
10- 5663
11- 5642
9- 5007
8- 4675
8+ 4664
1+ 4149
3+ 4132
7- 3824
2- 3668
6- 3498
5- 3465
3- 3214
4- 3003
3- 2910
5- 2878
8+ 2871
6+ 2694
2+ 3530
4+ 3091
2+ 2534
4+ 2144
0+ 2133
2+ 1200
0+ 0
$^{70}_{28}Ni_{42}$
12+ 6940
10+ 6777
12- 6462
10- 5658
11- 5532
10+ 5640
9- 4901
8- 4750
8+ 4864
7- 3902
2- 3701
5- 3650
3- 3589
6- 3555
4- 3204
1+ 4453
3+ 4221
2+ 3523
4+ 3479
2+ 3134
8+ 3012
5- 2983
6+ 2866
3- 2845
0+ 2858
4+ 2515
2+ 1431
0+ 0
$^{70}_{28}Ni_{42}$

There is a GRETINA paper due out momentarily showing the levels of ^{60}Ti. The structure shown below seems to rule out the wild notions of big-time deformations for ^{60}Ca.

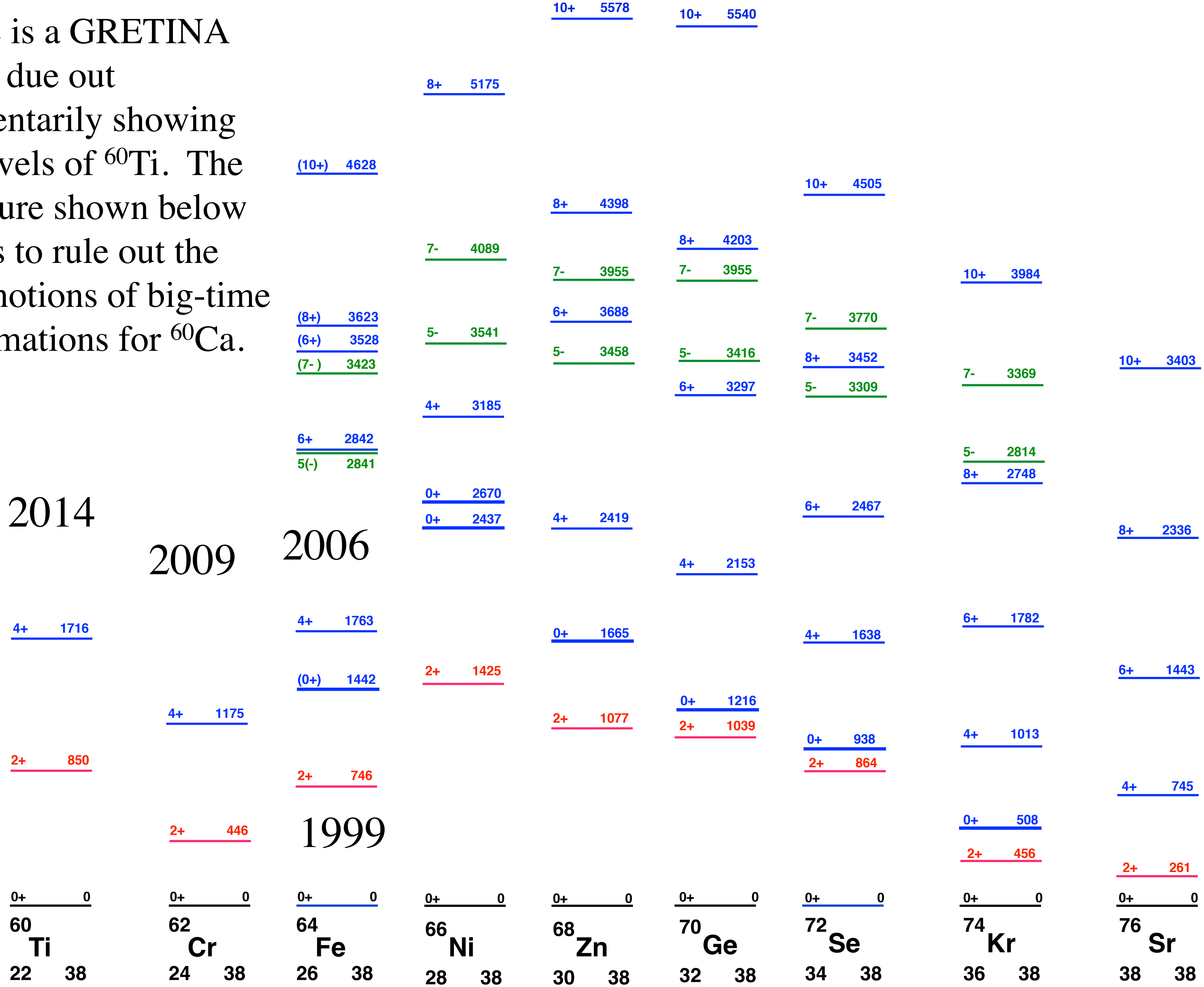

Here the three magic Ti nuclei, N = 20, 28, 32, each with two protons coupled to the Ca core. For $^{60}Ti_{38}$, it is possible to observe "some mixing" with the $g_{9/2}$ neutron broken pair from across N = 40.

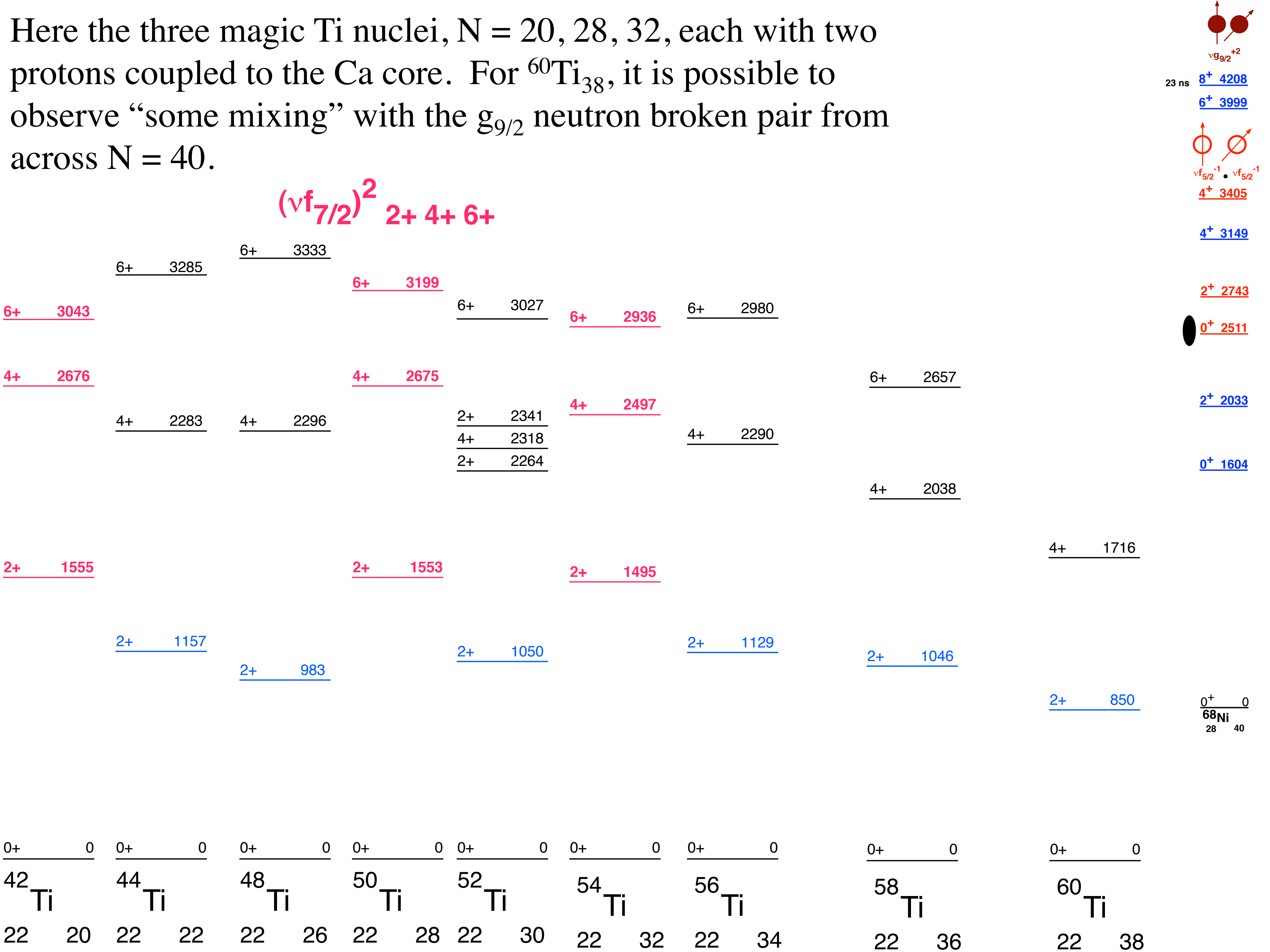

Now, I would like to return to a topic that is approaching 20 years old that is not quite yet resolved, but, at least one aspect of possible resolution seems to be at hand.

This chart was a hot topic about 18 years ago and is a composite of 2 charts shown next.

I call it “the big dip”

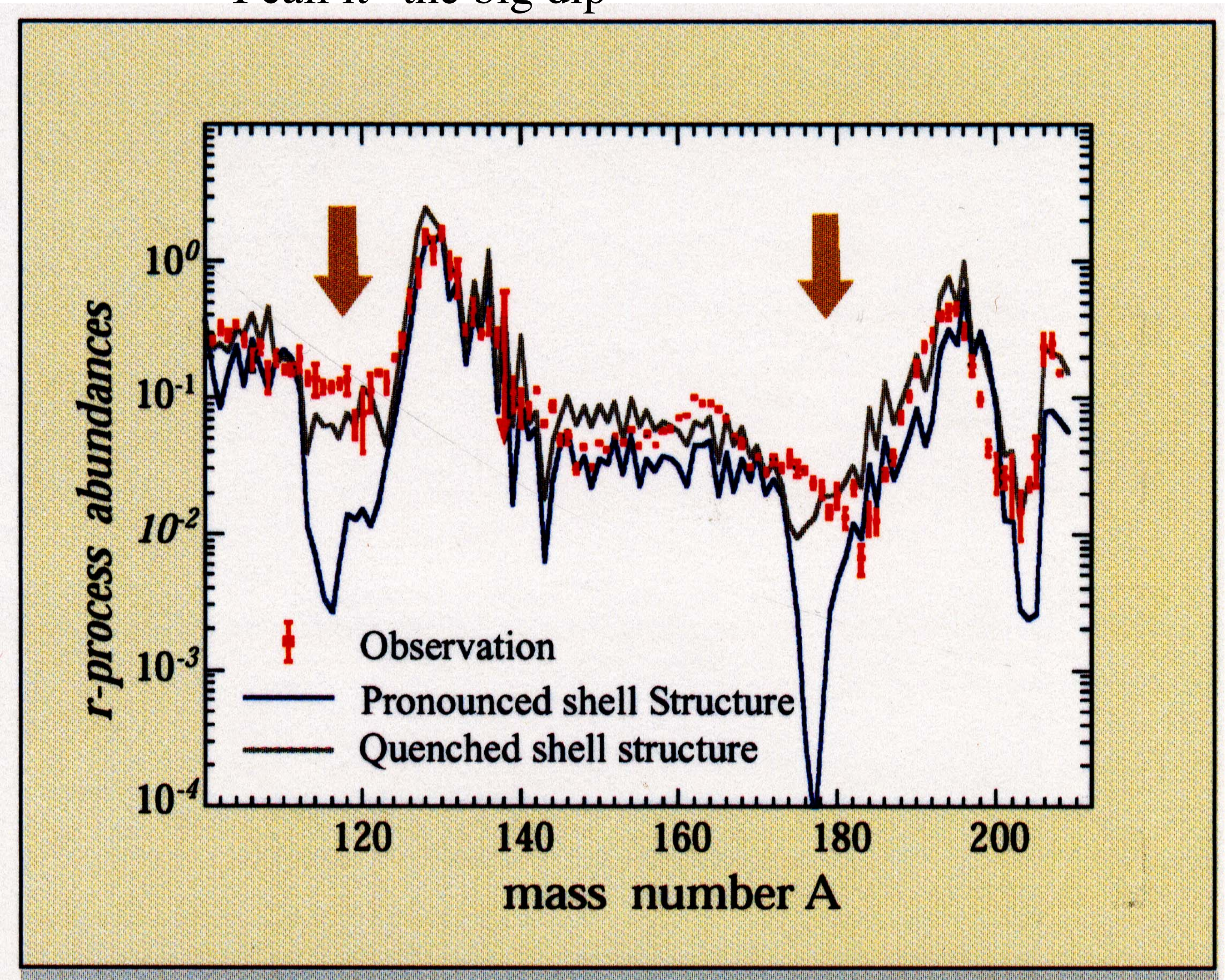

K.-L. Kratz, B. Pfeiffer et.al

Z. Phys. A 357, 235–238 (1997)

ZEITSCHRIFT
FÜR PHYSIK A
© Springer-Verlag 1997

Short note

Analysis of the solar-system r-process abundance pattern with the new ETFSI-Q mass formula

B. Pfeiffer[1], K.-L. Kratz[1], F.-K. Thielemann[2]

[1] Institut für Kernchemie, Universität Mainz, D-55099 Mainz, Germany
[2] Institut für Theoretische Physik, Universität Basel, CH-4056 Basel, Switzerland

Nuclear mass formula with Bogolyubov-enhanced shell-quenching: application to r-process ★

J.M. Pearson [a], R.C. Nayak [a], S. Goriely [b]

Physics Letters B 387 (1996) 455–459

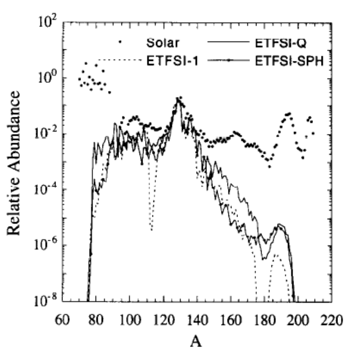

Fig. 2. Comparison between the abundances calculated with ETFSI-1 masses, ETFSI-Q masses, and ETFSI-SPH masses in the framework of the canonical model characterized by temperature $T = 1.5 \times 10^9$ K, neutron density $N_n = 10^{25}\mathrm{cm}^{-3}$, and number of neutrons captured per seed nucleus $n_{cap} = 68$. The symbols correspond to the solar-system r-process abundances [15], arbitrarily normalized to the $A = 130$ peak of the calculated curves.

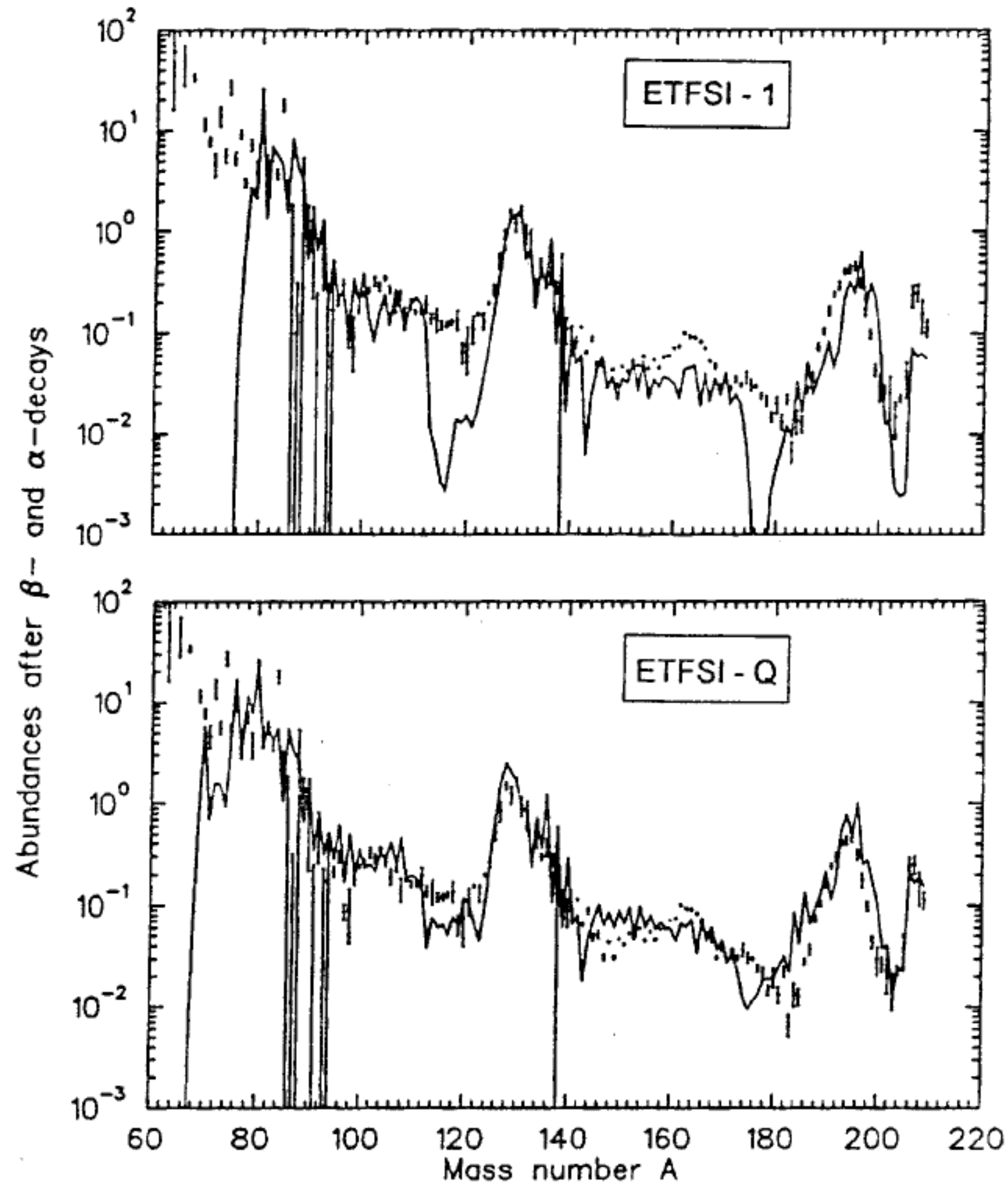

Fig. 2. Global r-abundance fits with superpositions of 16 time-dependent r-process components, calculated with the n_n–τ conditions for T_9=1.35 given in Fig. 1 of [11]. For the *upper part*, the S_n values are taken from ETFSI-1 [4], whereas for the *lower part* the new ETFSI-Q [13] mass formula was applied

The "mother paper" for the shell quenching and filling of the big dip is excerpted here. The source of the differences are shown on the next page. **Namely, the calculated overbinding of the $h_{11/2}$ neutrons for Kr, Zr, Mo, and Ru.** The net effect of "shell-quenching" has been to maintain the straight line behavior for neutron binding.

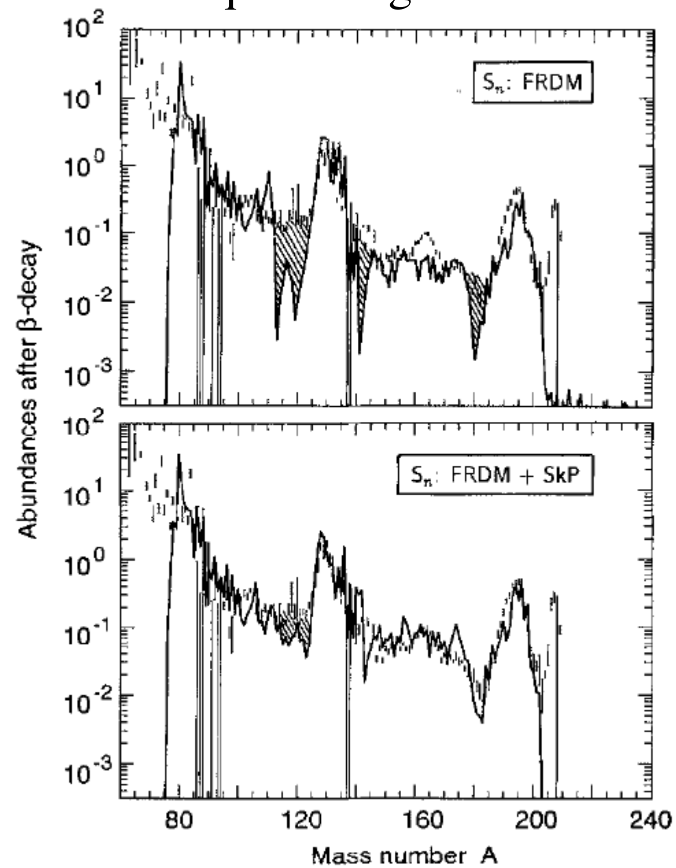

Influence of shell-quenching far from stability on the astrophysical r-process

B. Chen[a], J. Dobaczewski[b], K.-L. Kratz[c], K. Langanke[a], B. Pfeiffer[c], F.-K. Thielemann[d], P. Vogel[e]

Physics Letters B 355 (1995) 37–44

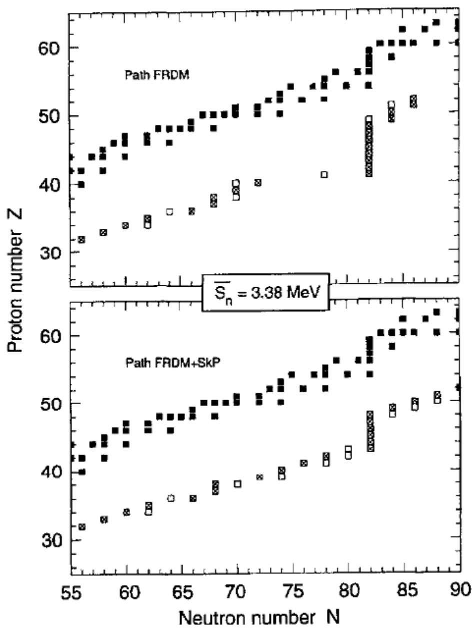

Fig. 3. r-process paths in the $80 \leq A \leq 140$ mass region. In the upper part the result is shown for the FRDM mass model. The large gap before the shell closure at $N = 82$ (also existing when using the ETFSI and SIII masses) causes the deep trough before the $N_{r,\odot}$ peak at $A = 130$ (see upper part of Fig. 2). The lower part shows the same picture, but with masses of spherical nuclei around $N = 82$ being replaced by masses from HFB calculations with the SkP force. Nuclei in the valley of stability are displayed as full squares. The population of nuclei during the r-process is shown in form of open squares (nuclei with more than 10% of the population of an isotopic chain) or open squares with a cross (nuclei with the maximum abundance in an isotopic chain).

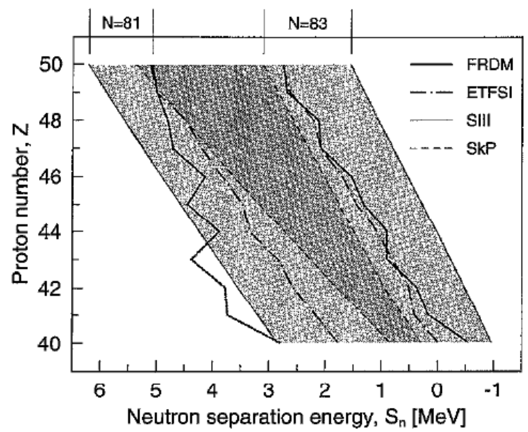

Fig. 2. r-process abundance fits obtained with ten equidistant neutron-density components from 10^{20} cm^{-3} to 3×10^{24} cm^{-3} according to Fig. 1. In the upper part, the result is presented for FRDM [10] masses with the $T_{1/2}$ and P_n values from the QRPA calculations according to Ref. [11]. In the lower part, masses of spherical nuclei around $N = 82$ have been replaced by masses from HFB calculations with the Skyrme force SkP. The quenching of the $N = 82$ shell gap (see Fig. 4) leads to a filling of the abundance troughs around $A \simeq 120$ and 140, and to a better overall reproduction of the heavy-mass region.

Neutron Separation Energies

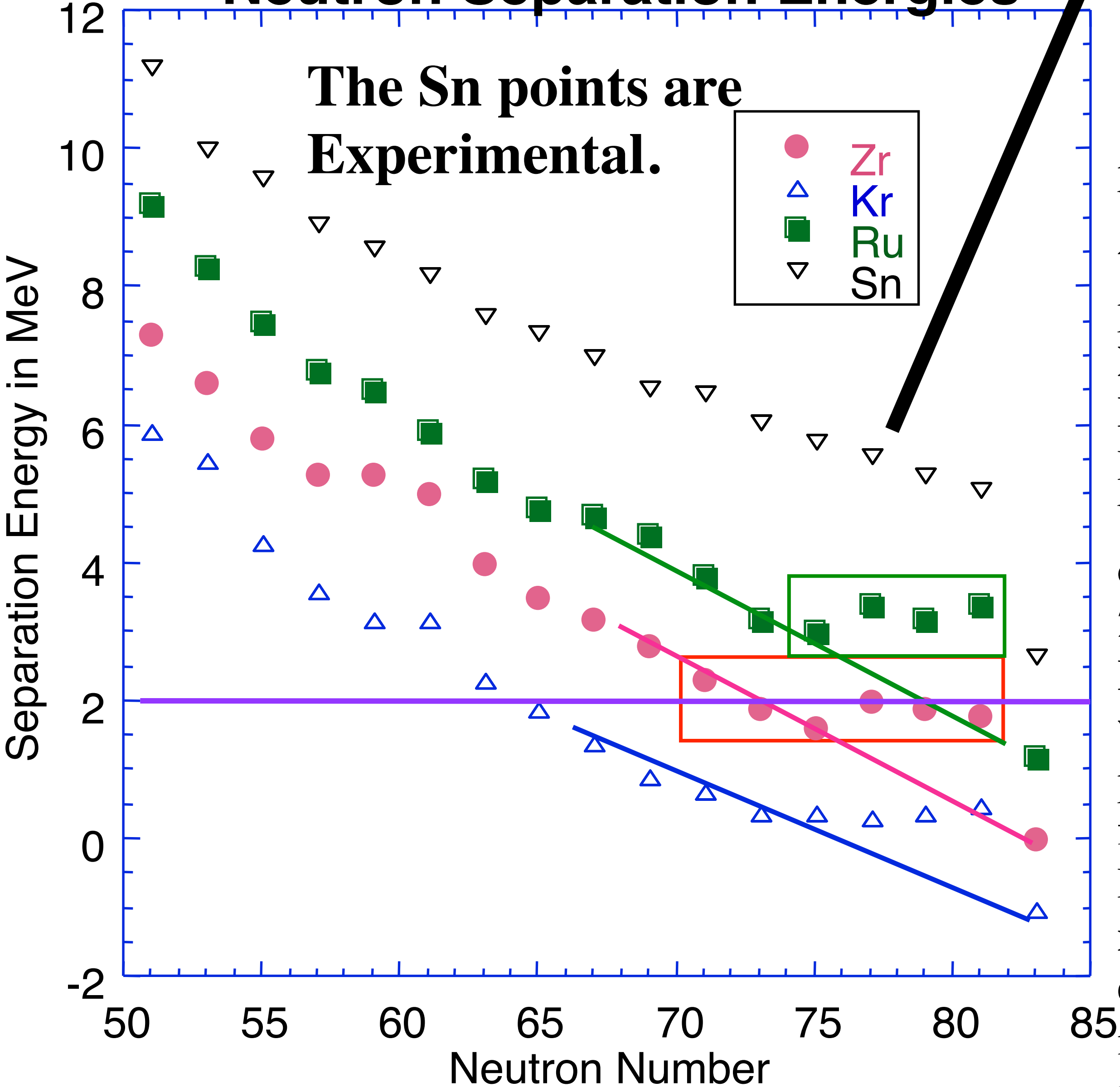

From Möller, Nix and Kratz, ANDT **66**, 131 (1997).

Observe there is NO leveling for the Sn nuclides!!!!

As ~2 MeV is the critical binding energy for many temperatures used in r-process abundances, it is **the leveling off for Sr, Zr and Mo that causes the big dip.** Ru is always tight enough bound to move to the N = 82 closed shell, and Kr reaches 2 MeV far from stability. **Hence the problem lies with Sr, Zr, and Mo**. The problem starts above N = 75 for Zr and adjacent nuclei. Note that these are **single-neutron separation energies,** those that are needed in calculations for photodisintegration in the $(\gamma,n) = (n,\gamma)$ equilibriium.

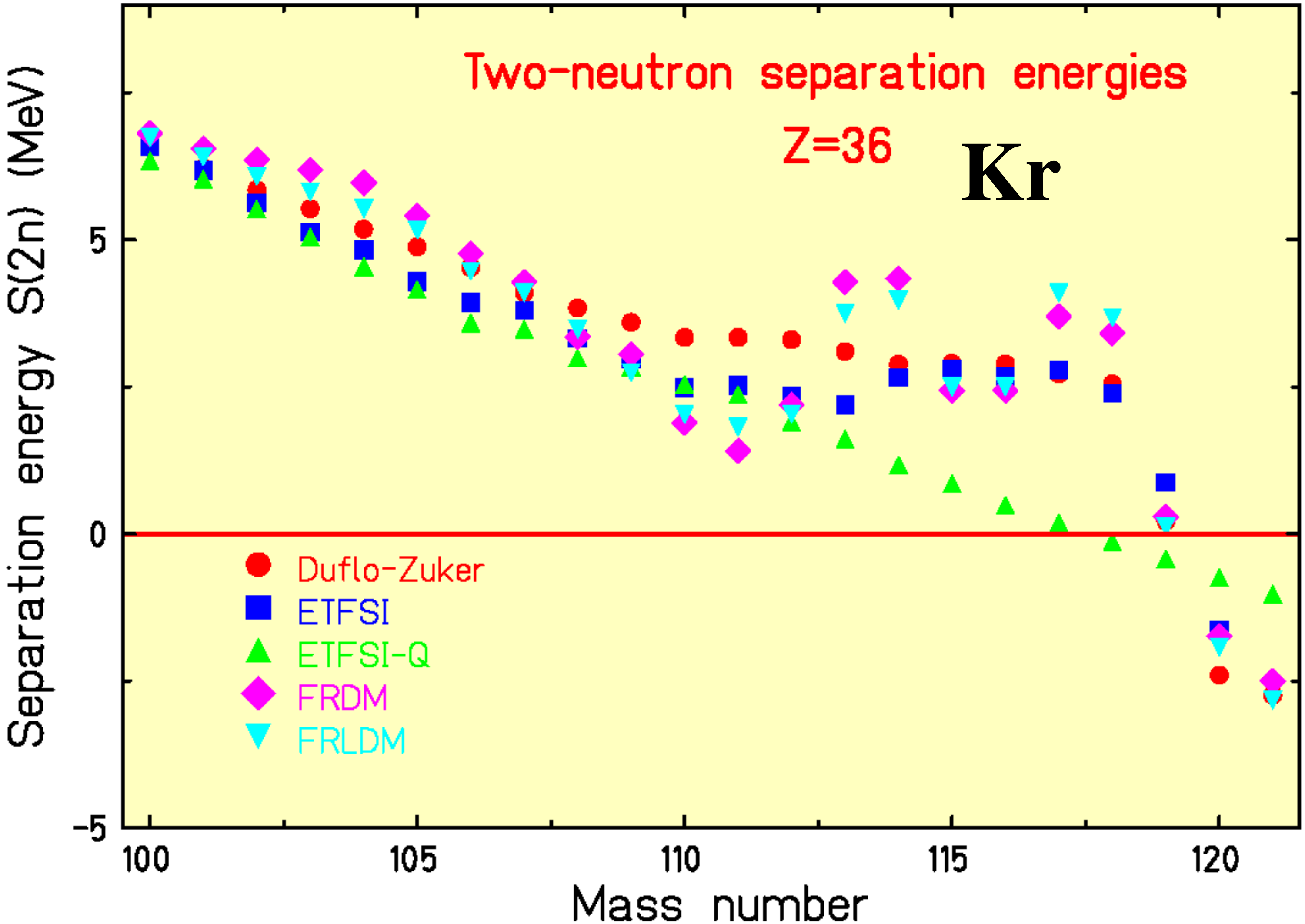

Fig. 4. *The two-neutron separation energy* S_{2n} *is plotted as a function of of the mass number* A *for krypton isotopes. The dripline is reached as soon as this quantity is negative. The different predictions are from the mass model of Duflo and Zuker, the Extended Thomas-Fermi model (ETFSI), the extended Thomas-Fermi model with shell quenching (ETFSI-Q), the finite range droplet model (FRDM), and the finite range liquid-drop model (FRLDM).*

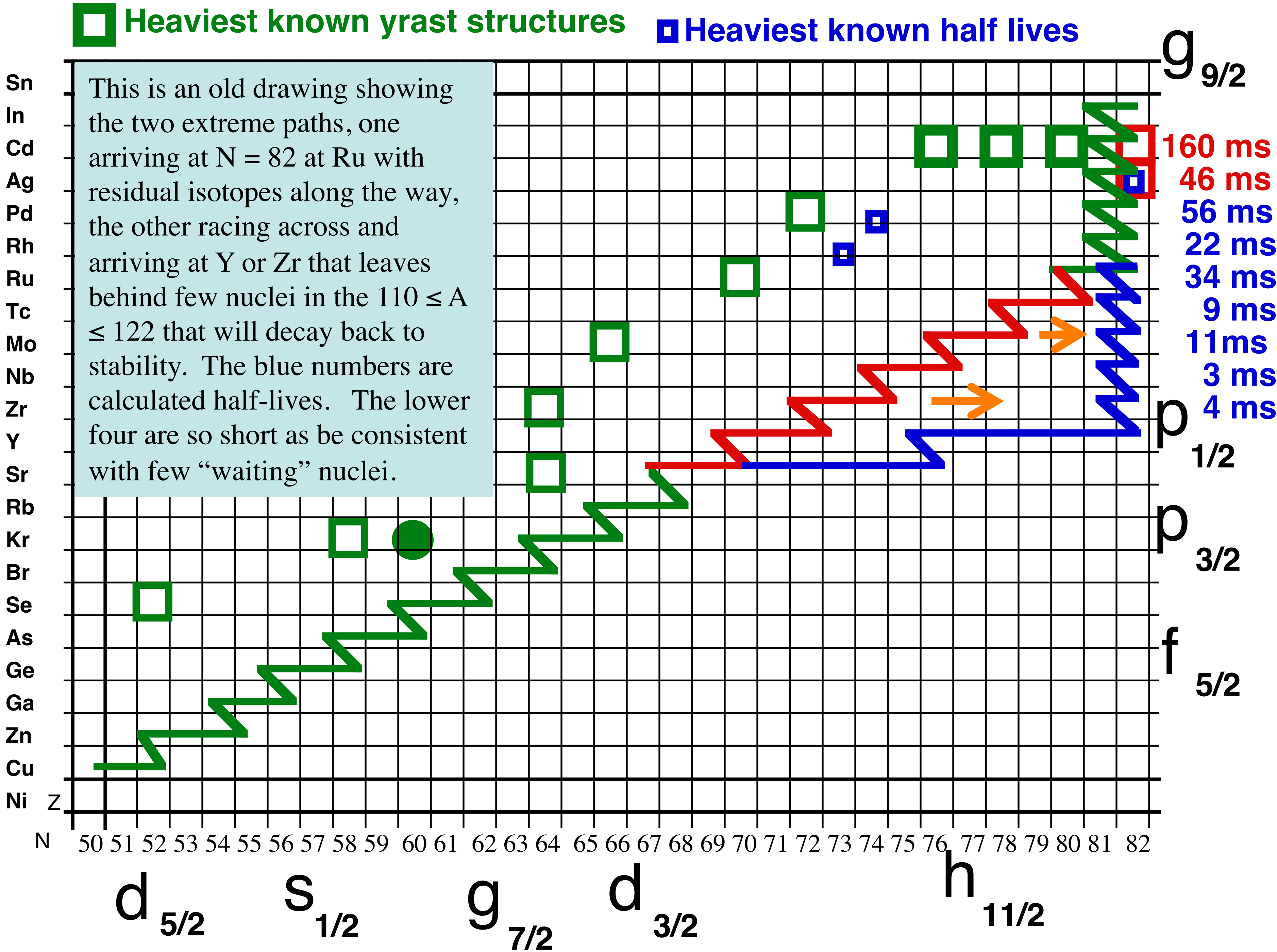
Heaviest known yrast structures
Heaviest known half lives
This is an old drawing showing the two extreme paths, one arriving at N = 82 at Ru with residual isotopes along the way, the other racing across and arriving at Y or Zr that leaves behind few nuclei in the 110 ≤ A ≤ 122 that will decay back to stability. The blue numbers are calculated half-lives. The lower four are so short as be consistent with few “waiting” nuclei.
Sn
In
Cd
Ag
Pd
Rh
Ru
Tc
Mo
Nb
Zr
Y
Sr
Rb
Kr
Br
Se
As
Ge
Ga
Zn
Cu
Ni
Z
N
50 51 52 53 54 55 56 57 58 59 60 61 62 63 64 65 66 67 68 69 70 71 72 73 74 75 76 77 78 79 80 81 82
160 ms
46 ms
56 ms
22 ms
34 ms
9 ms
11ms
3 ms
4 ms
g 9/2
p 1/2
p 3/2
f 5/2
d 5/2
s 1/2
g 7/2
d 3/2
h 11/2

N	Sn	Cd	Pd	Ru	Mo
57.000	9320.0	8437.0	7625.0	6802.0	5925.0
59.000	8632.0	7929.0	7094.0	6232.0	5398.0
61.000	8169.0	7323.0	6536.0	5910.0	5468.0
63.000	7744.0	6976.0	6153.0	5609.0	5059.0
65.000	7548.0	6539.0	5726.0	5148.0	4488.0
67.000	6943.0	6141.0	5341.0	4784.0	3981.0
69.000	6483.0	5777.0	5007.0	4310.0	3460.0
71.000	6170.0	5350.0	4664.0	4150.0	
73.000	5946.0	5188.0	4091.0		
75.000	5733.0	4873.0	3973.0		
77.000	5527.0	4718.0			
79.000	5316.0	4305.0			
81.000	5211.0				
83.000	2402.0				
85.000	2271.0				

Chinese Physics **36**, 1157 (2012).

These are the current 1-neutron separation energies in keV from the new AME paper. So far, only Sn has moved close to the 2-MeV level.

104					−65731.5	9.8	103.929434	1.1E−05	1.013E−07	**Adopted**
105	660(65) ms		**Zr**	JYFLTRAP	−61469	12	104.934010	1.3E−05	1.228E−07	06HA03§
106	260(38) ms			IMS	−58380	300	105.93733	3.2E−04	3.040E−06	04MAXZ§
110					−64549	24	109.930704	2.6E−05	2.333E−07	**Adopted**
111	200(39) ms		**Mo**	IMS	−59940	260	110.93565	2.8E−04	2.516E−06	04MAXZ
111				JYFLTRAP	−59933	13	110.935659	1.4E−05	1.258E−07	11HA48
111				JYFLTRAP	−59936	12	110.935656	1.3E−05	1.161E−07	11KU16
111					−59934.6	8.8	110.9356575	9.5E−06	8.528E−08	**Adopted**
114					−70220.4	3.8	113.9246153	4.1E−06	3.602E−08	**Adopted**
115	740(80) ms				−66430	130	114.92869	1.4E−04	1.214E−06	03AU02
115				JYFLTRAP	−66071	8	114.9290699	8.6E−06	7.473E−08	07HA20
115				β decay	−66430	128	114.92869	1.4E−04	1.196E−06	08KLXZ
115					−66073.7	8.0	114.9290669	8.6E−06	7.444E−08	**Adopted**
116	204^{+32}_{-29} ms	0^+	**Ru**	JYFLTRAP	−64069	4	115.9312191	4.3E−06	3.704E−08	11HA48§
117	142.6(175) ms			IMS	−59526	390	116.93610	4.2E−04	3.580E−06	04MAXZ§

Atomic Data and Nuclear Data Tables 100 (2014) 403–535

Contents lists available at ScienceDirect

Atomic Data and Nuclear Data Tables

journal homepage: www.elsevier.com/locate/adt

Atomic mass compilation 2012

B. Pfeiffer[a,b,*], K. Venkataramaniah[c], U. Czok[a], C. Scheidenberger[b,a]

[a] II. Physikalisches Institut, Justus-Liebig-Universität Gießen, Gießen, Germany
[b] GSI Helmholtzzentrum für Schwerionenforschung, Darmstadt, Germany
[c] Sri Sathya Sai Institute of Higher Learning, Prasanthinilayam, India

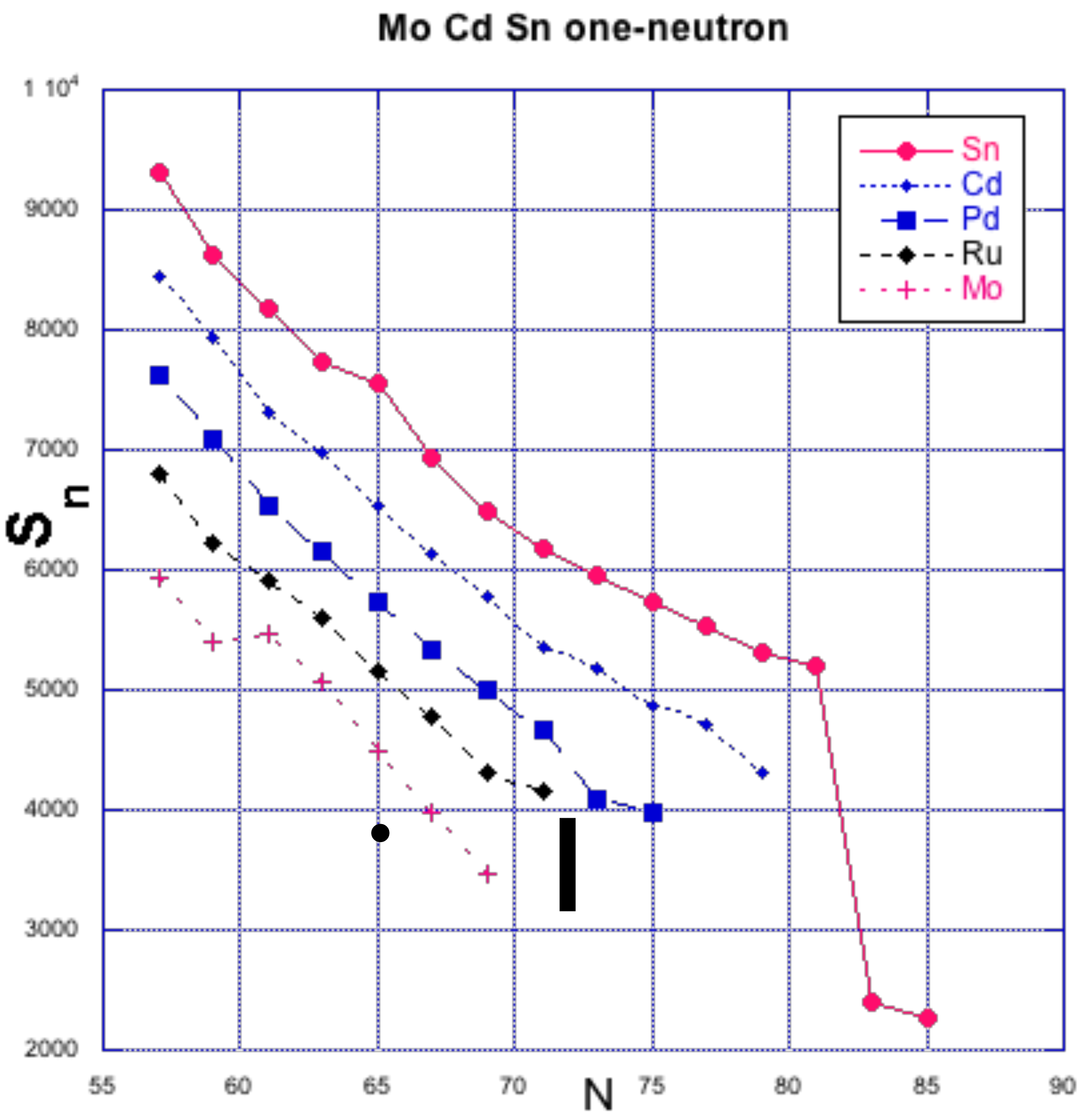

This is a clean plot of the data on the previous page.

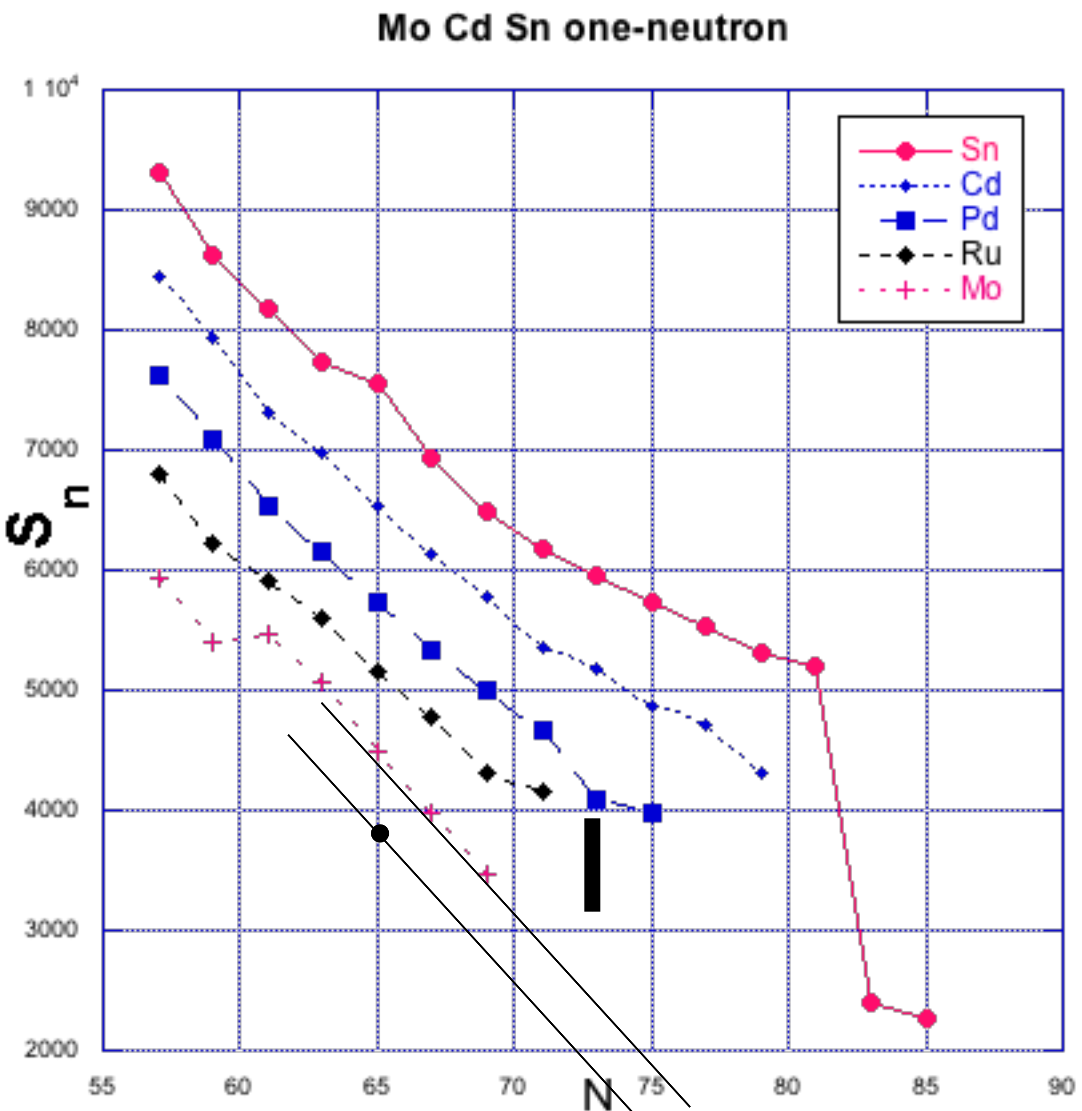

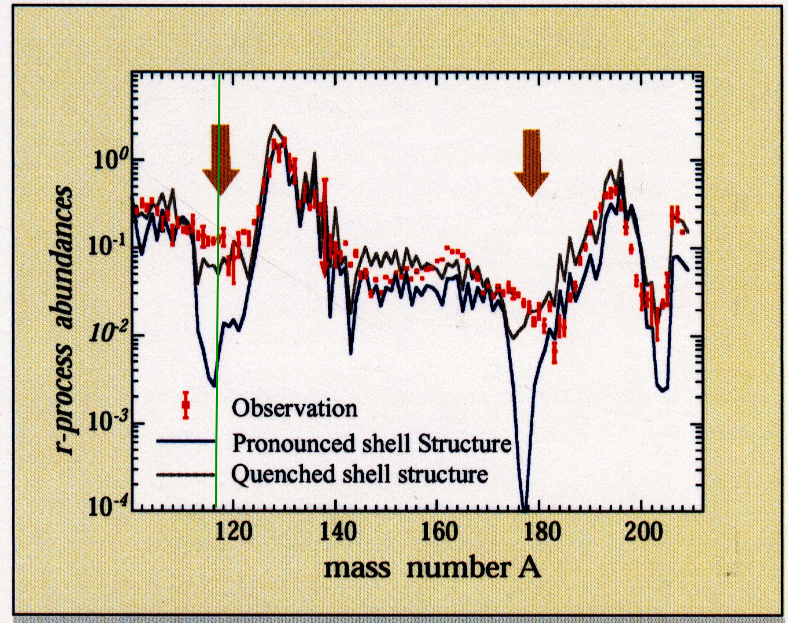

This is a plot showing the extrapolation of the 1-neutron separation energies. What is seen is that for $^{117}Mo_{75}$, the 2-MeV separation energy at N = 75 would fall in the middle of the "big dip" and……. completely destroy the calculated "big dip? However, misbehavior can be seen for Ru and Pd as N increases, so there may be no justification for a straight line.

There could be isomers in both Ru and Pd. These 1-neutron separation energies are never going to play a role in the big dip as they never reach 2 MeV before the N = 82 closed shell. But, if there is "enhanced binding" in those N = 70 to 78 nuclei, then, indeed, the straight line for Mo may not be supported, EVEN if it is difficult to measure the Mo masses, new data for Ru and Pd would be helpful.

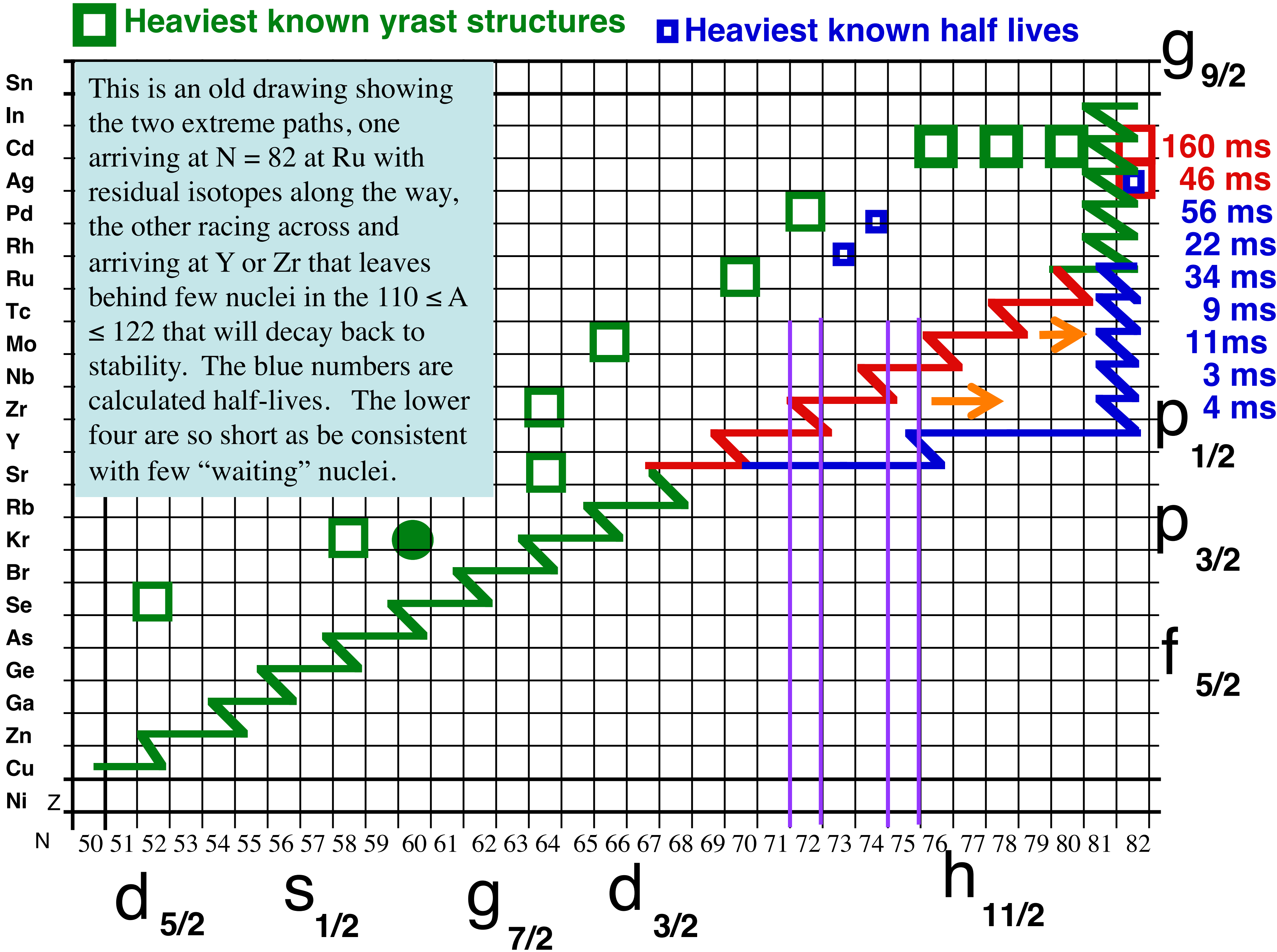
Heaviest known yrast structures
Heaviest known half lives
This is an old drawing showing the two extreme paths, one arriving at N = 82 at Ru with residual isotopes along the way, the other racing across and arriving at Y or Zr that leaves behind few nuclei in the 110 ≤ A ≤ 122 that will decay back to stability. The blue numbers are calculated half-lives. The lower four are so short as be consistent with few “waiting” nuclei.
Sn
In
Cd
Ag
Pd
Rh
Ru
Tc
Mo
Nb
Zr
Y
Sr
Rb
Kr
Br
Se
As
Ge
Ga
Zn
Cu
Ni
Z
N
50 51 52 53 54 55 56 57 58 59 60 61 62 63 64 65 66 67 68 69 70 71 72 73 74 75 76 77 78 79 80 81 82
160 ms
46 ms
56 ms
22 ms
34 ms
9 ms
11ms
3 ms
4 ms
g 9/2
p 1/2
p 3/2
f 5/2
d 5/2
s 1/2
g 7/2
d 3/2
h 11/2

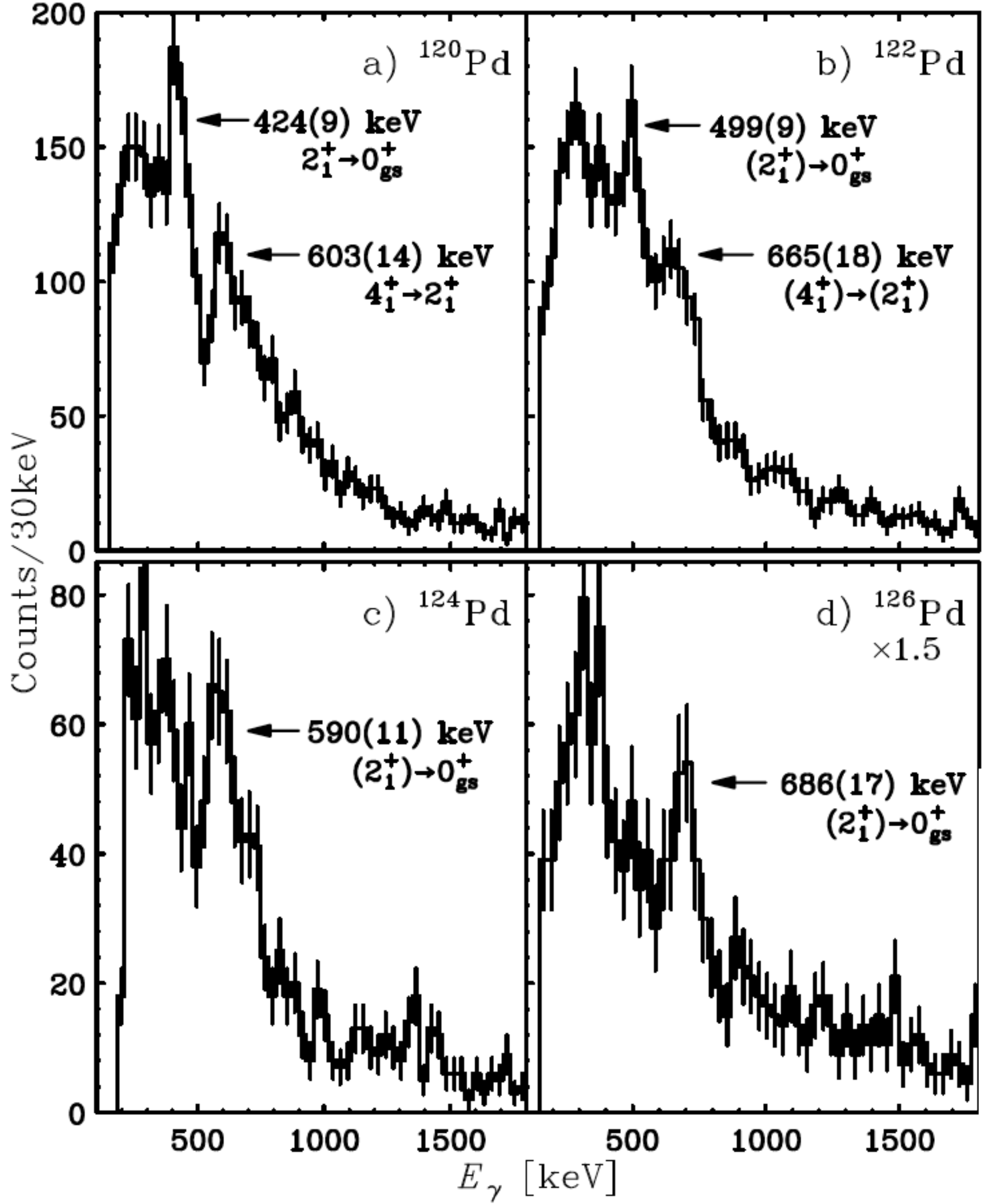

686 on left

693.3 below

RIKEN DATA

So, 506 and 674 for ^{122}Pd and 597 for ^{124}Pd maybe guess 720 for 4^+ to 2^+ in ^{124}Pd?

	E_x (keV)	$T_{1/2}$	E_γ (keV)	I_γ (%)	$J_i^\pi \rightarrow J_f^\pi$
^{128}Pd	1311.4		1311.4	100(29)	$(2^+) \rightarrow 0^+$
	1815.8		504.4	88(24)	$(4^+) \rightarrow (2^+)$
	2075.9		260.1	74(20)	$(6^+) \rightarrow (4^+)$
	2151.0	5.8(8) μs	75.1	28(10)	$(8^+) \rightarrow (6^+)$
^{126}Pd	693.3		693.3	100(5)	$(2^+) \rightarrow 0^+$
	1481.0		787.7	57(4)	$(4^+) \rightarrow (2^+)$
	2023.4	0.33(4) μs	542.4	52(3)	$(5^-) \rightarrow (4^+)$
			1330.2	40(3)	$(5^-) \rightarrow (2^+)$
	2109.7	0.44(3) μs	86.2	21(2)	$(7^-) \rightarrow (5^-)$

PRL **111,** 152501 (2013) PHYSICAL RE

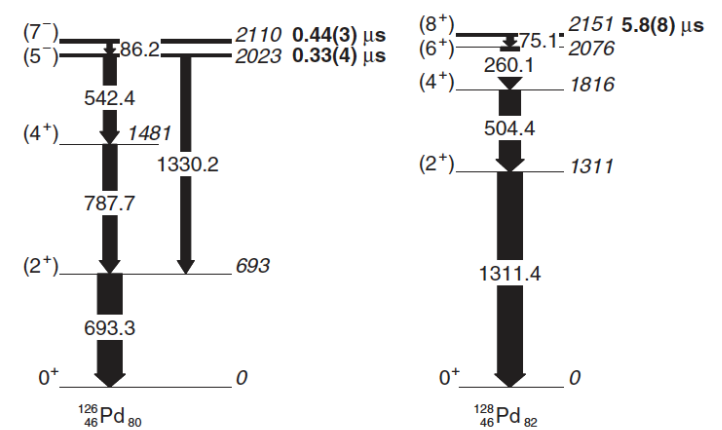

One point is that if it has been possible to accumulate enough atoms or Pd and Rh to obtain these data, then there should be enough atoms of Ru, Tc, and Mo to obtain masses much nearer to N = 82. It has taken 10 years since we reported the structure of ^{120}Pd to move on to the shell. It is possible to see the broken $g_{9/2}$ pair in both $^{96}Pd_{50}$ and $^{128}Pd_{82}$ and the changes brought about by adding 32 neutrons to the nucleus.

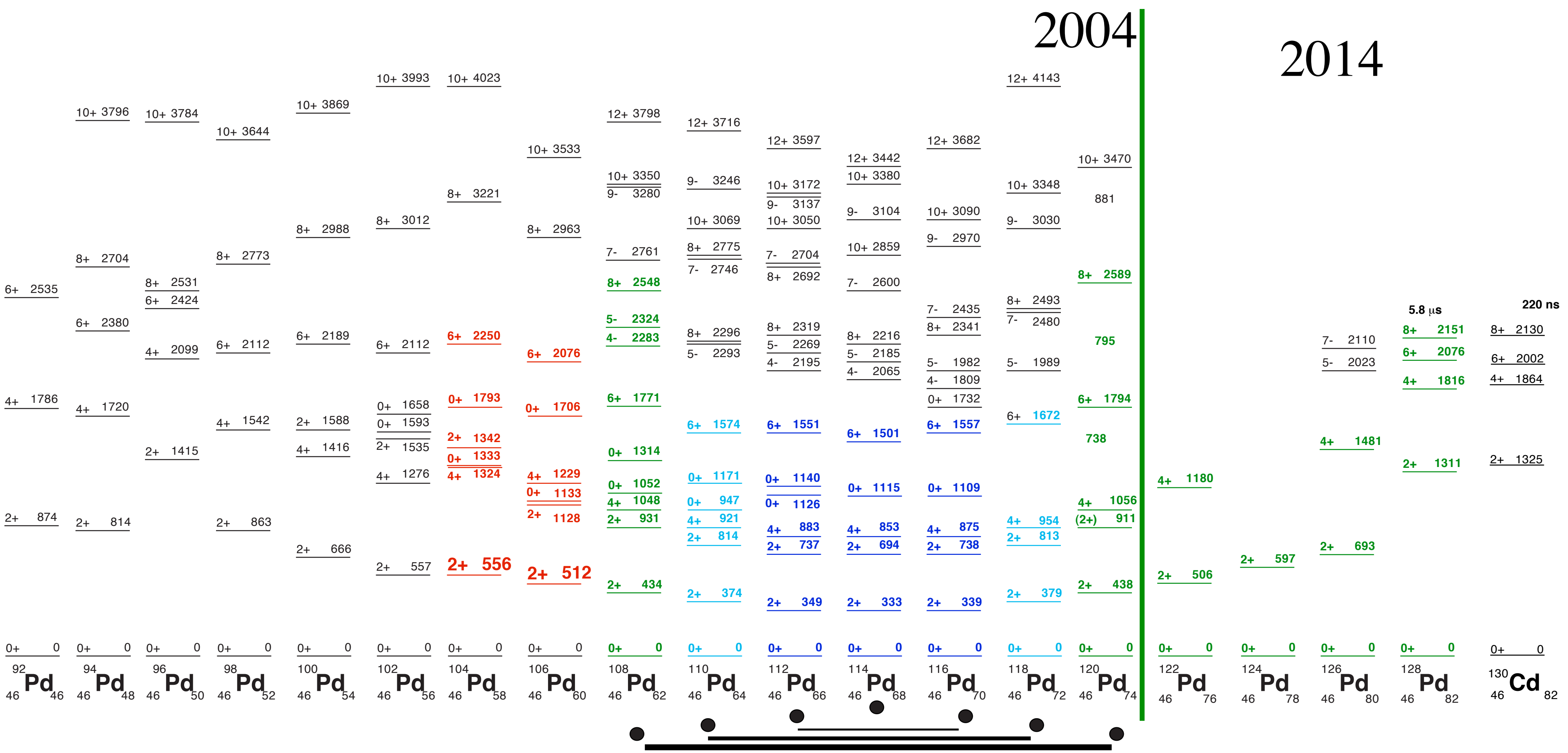

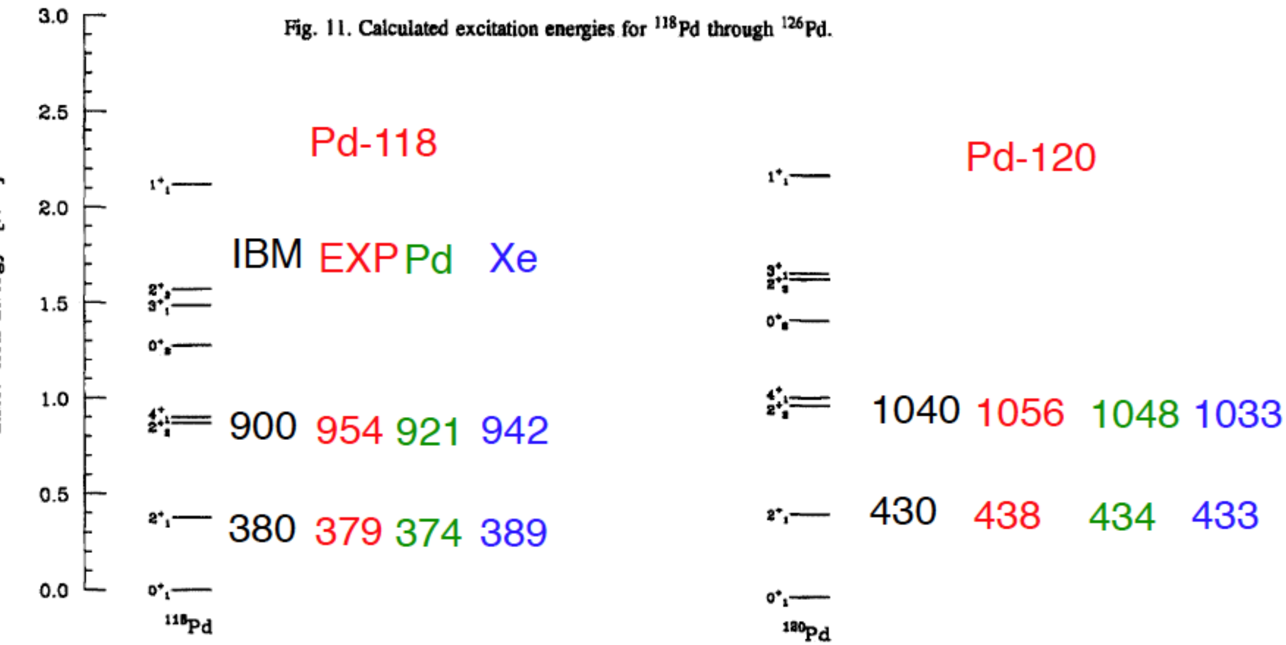

Mark Stoyer and I did some work trying to see if their alpha-induced mass-gated fission data could be extended beyond ^{120}Pd. The observed numbers suggest more collectivity than found in isotonic Xe or symmetric Pd for ^{122,124,126}Pd, in spite of the nearly identical structures for ^{126}Pd and ^{128}Cd.

ELSEVIER Nuclear Physics A 787 (2007) 455c–462c

Spectroscopy of neutron-rich Pd and Cd isotopes near A=120

M.A. Stoyer[a*], W.B. Walters[a], C.Y. Wu[b†] D. Cline[b], H. Hua[b], A.B. Hayes[b], R. Teng[b], R.M. Clark[c], P. Fallon[c], A. Goergen[c], A.O. Macchiavelli[c], K. Vetter[c‡], P. Mantica[d], and B. Tomlin[d]

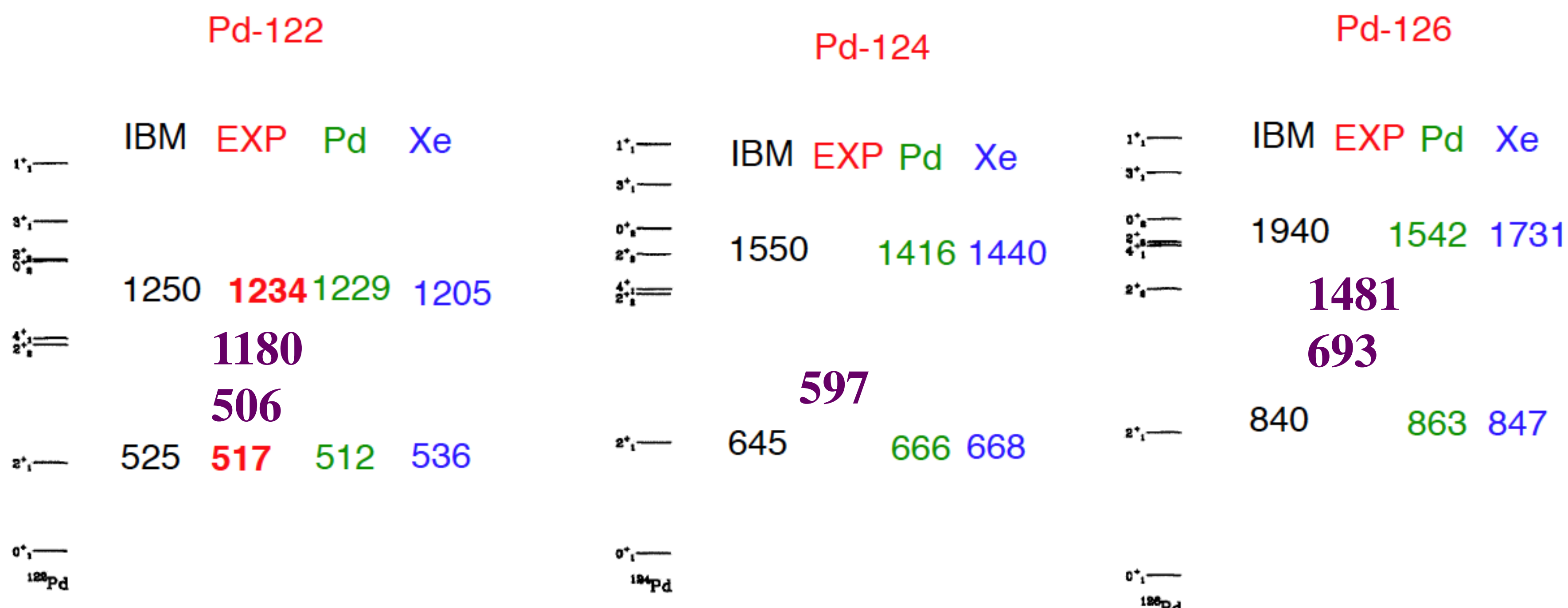

PHYSICAL REVIEW C **88**, 054318 (2013)

PHYSICAL REVIEW C **70**, 034314 (2004)

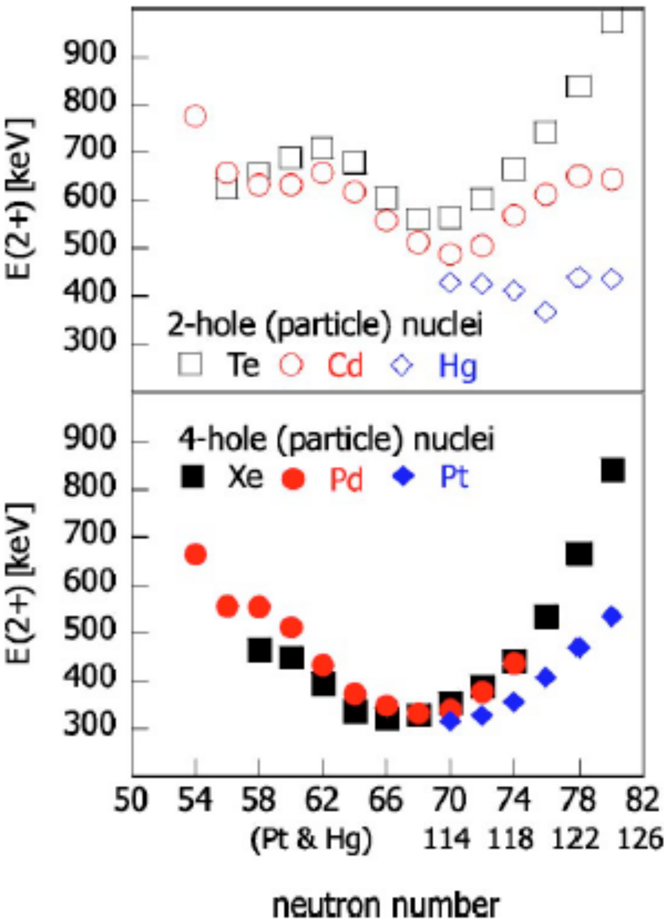

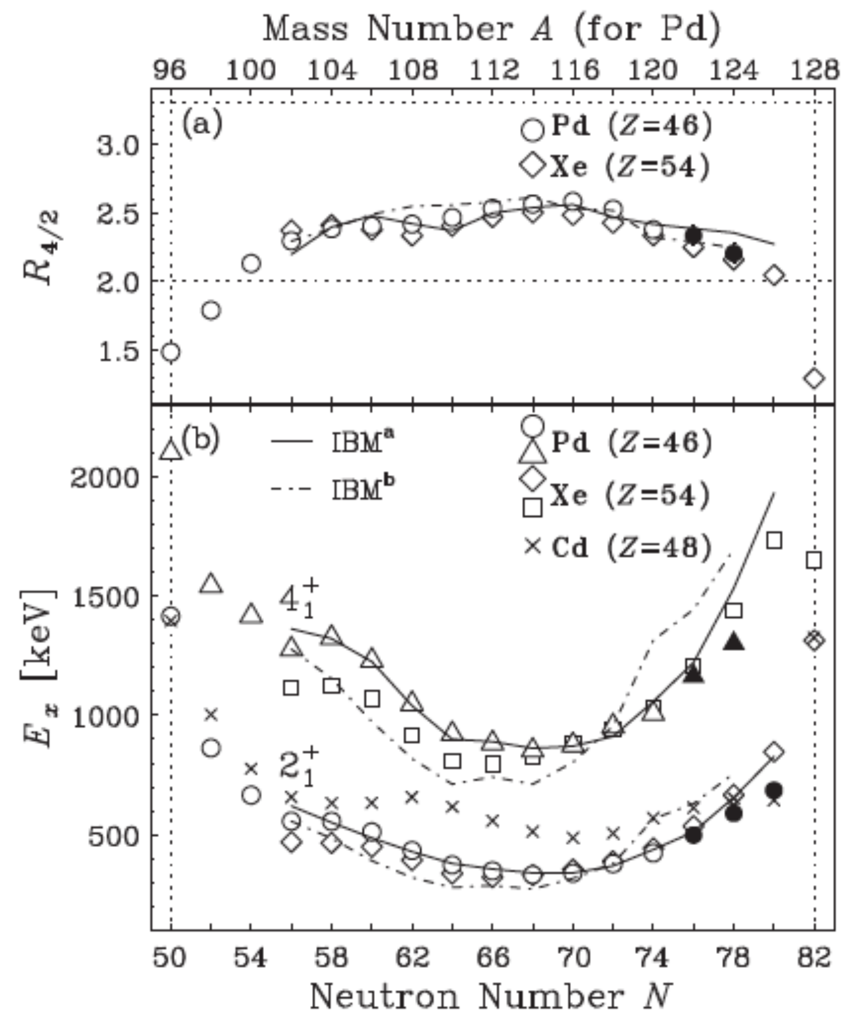

One point is that if it has been possible to accumulate enough atoms or Pd and Rh to obtain these data, then there should be enough atoms of Ru, Tc, and Mo to obtain masses much nearer to N = 82. It has taken 10 years since we reported the structure of ^{120}Pd to move on to the shell. It is possible to see the broken $g_{9/2}$ pair in both $^{96}Pd_{50}$ and $^{128}Pd_{82}$ and the changes brought about by adding 32 neutrons to the nucleus.

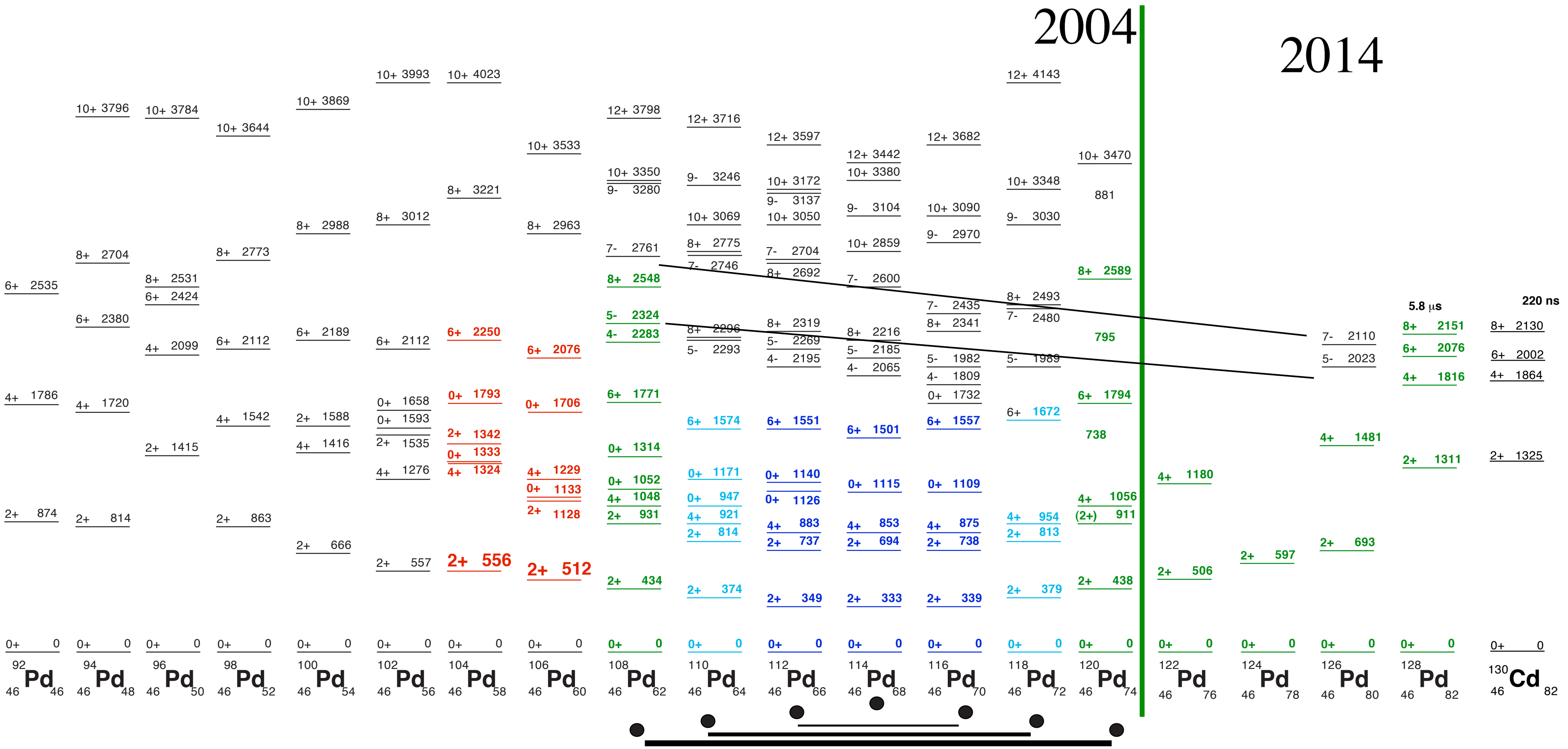

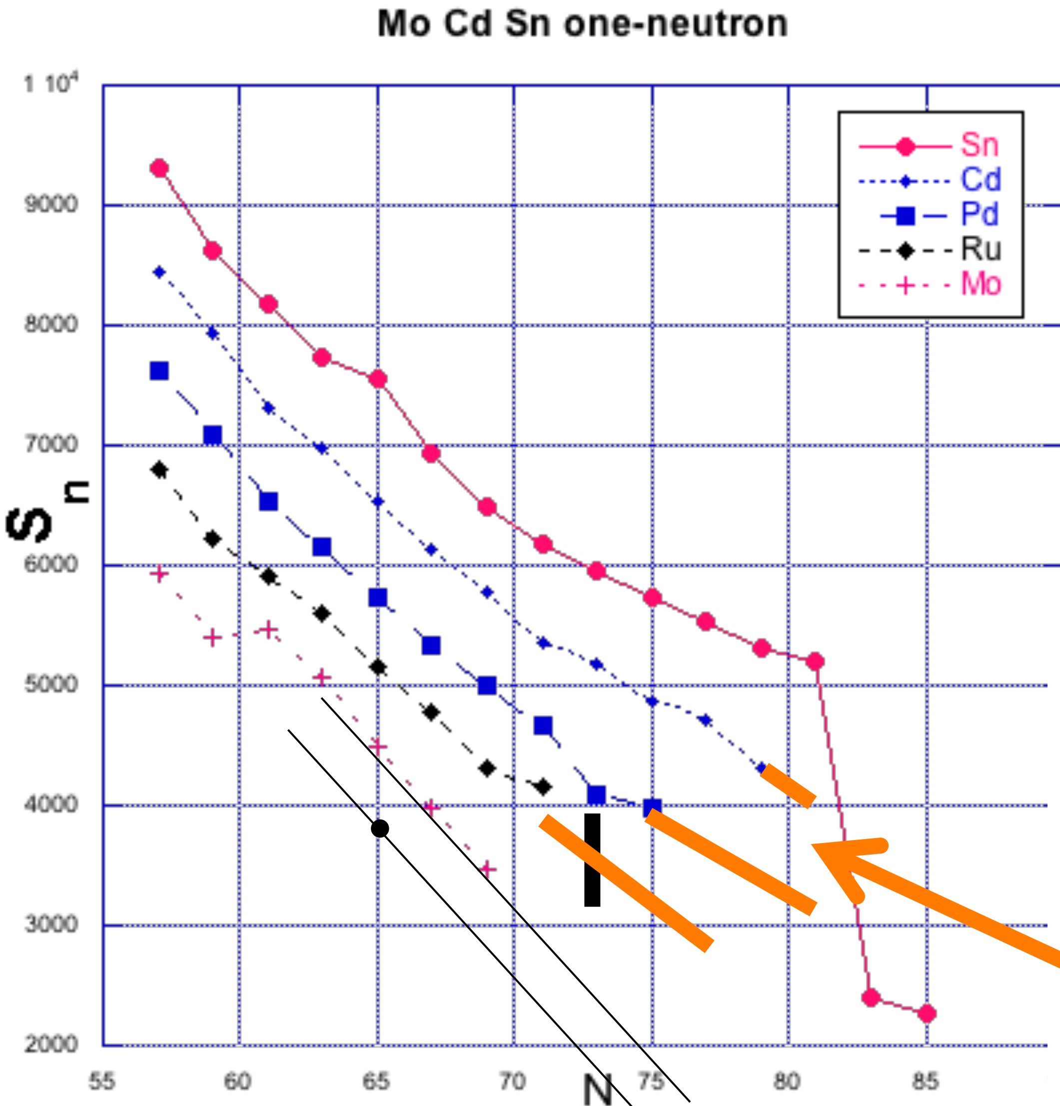

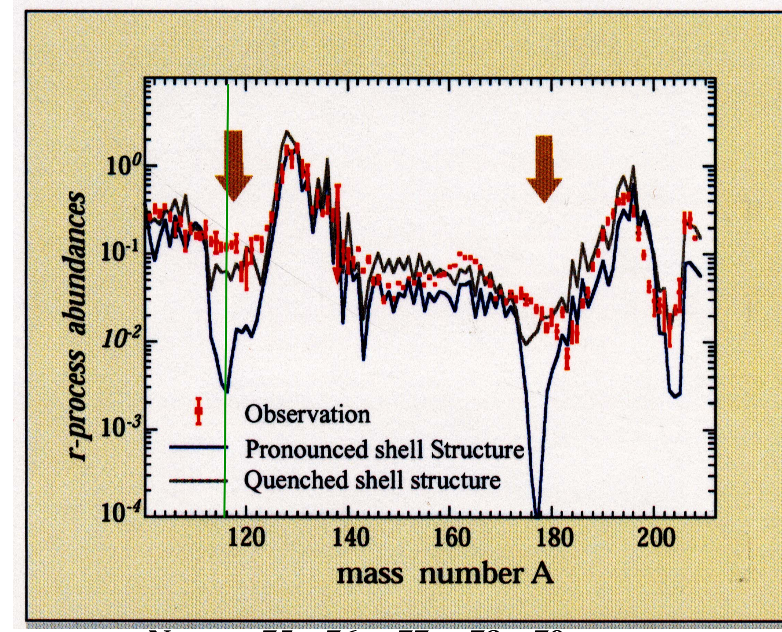

N = 75 76 77 78 79

PHYSICAL REVIEW C **88**, 054318 (201

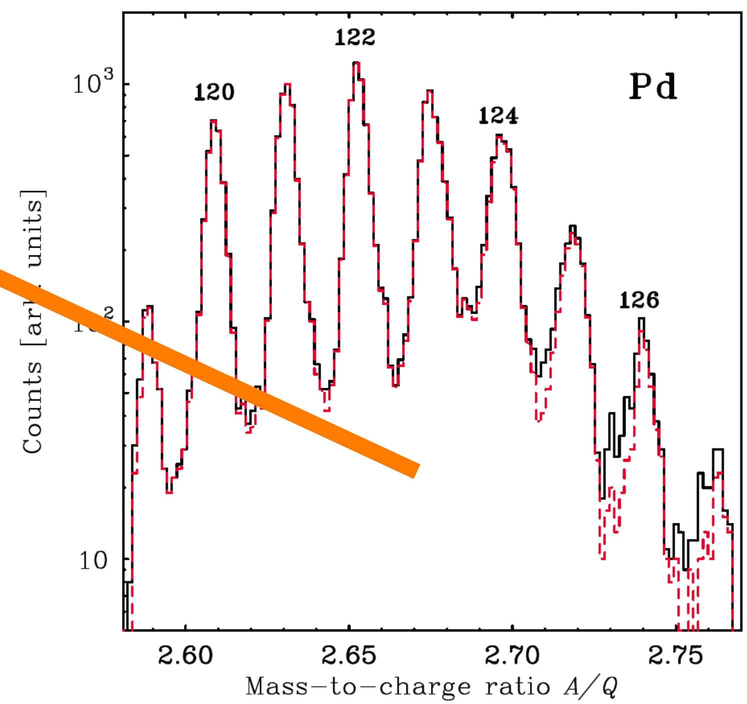

My point is that if enough Pd can be made at RIKEN to reach ^{128}Pd, surely it will soon be possible measure Cd, and Pd masses out to N = 82. And most likely, enough to go out to ^{121}Ru$_{77}$, far enough to see if the "bump" has any chance to exist for Mo and Zr.

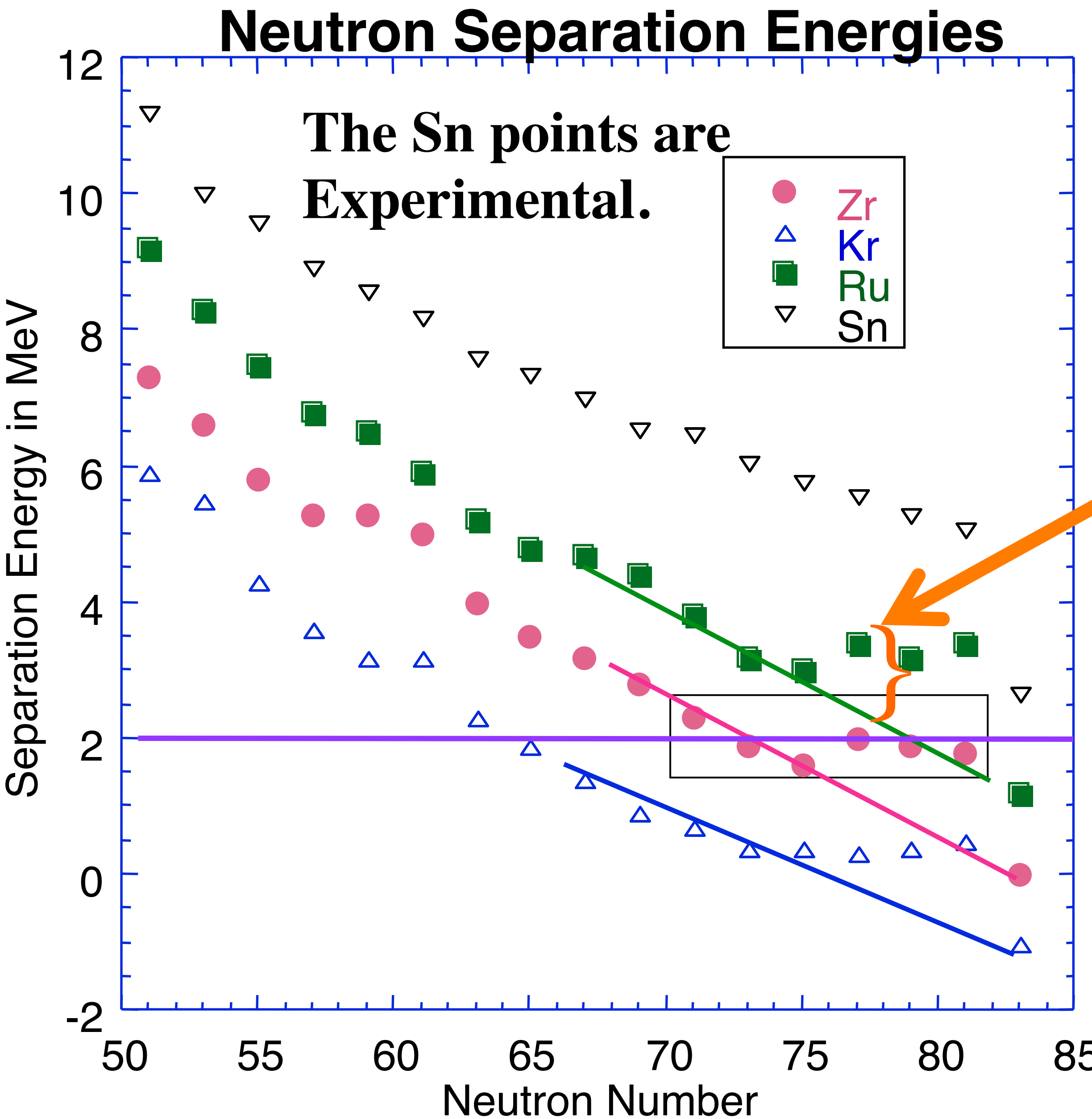

Here, it can be seen that N = 77 is the critical point where the “bump” is present for Ru, meaning $^{121}Ru_{77}$.

From Möller, Nix and Kratz, ANDT **66**, 131 (1997).

Now I would like to make a few comments about some occasional exaggerations about the importance of nuclear data for r-process abundance calculations.

Consider the claim that uncertainty in the values for the neutron capture of ^{130}Sn will have huge effects on the calculated yields of Pb region nuclei!!!
The neutron density when Pb is being made is probably ~10^{26} n/cm^3.
Where is the r-process at that density?

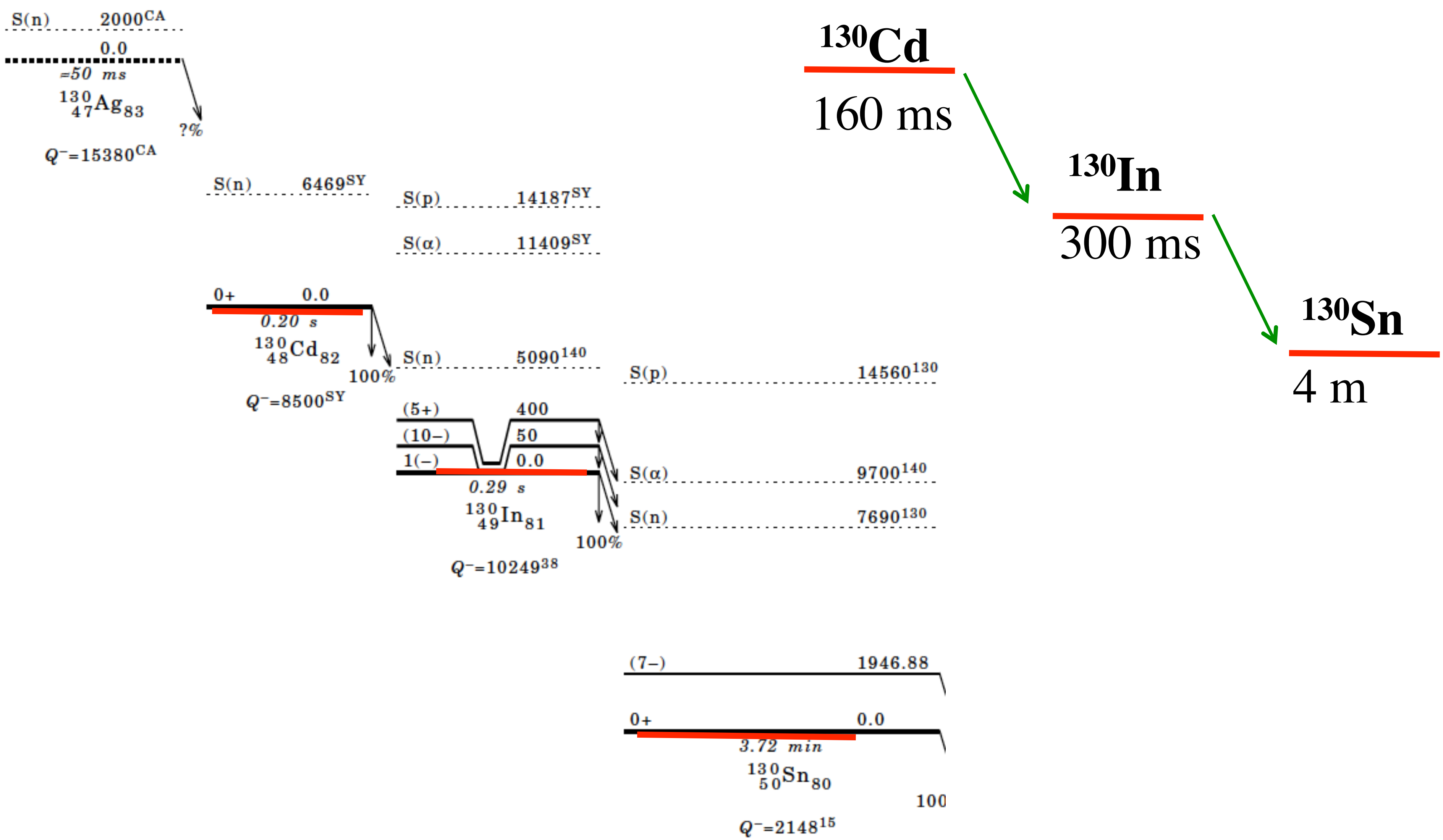

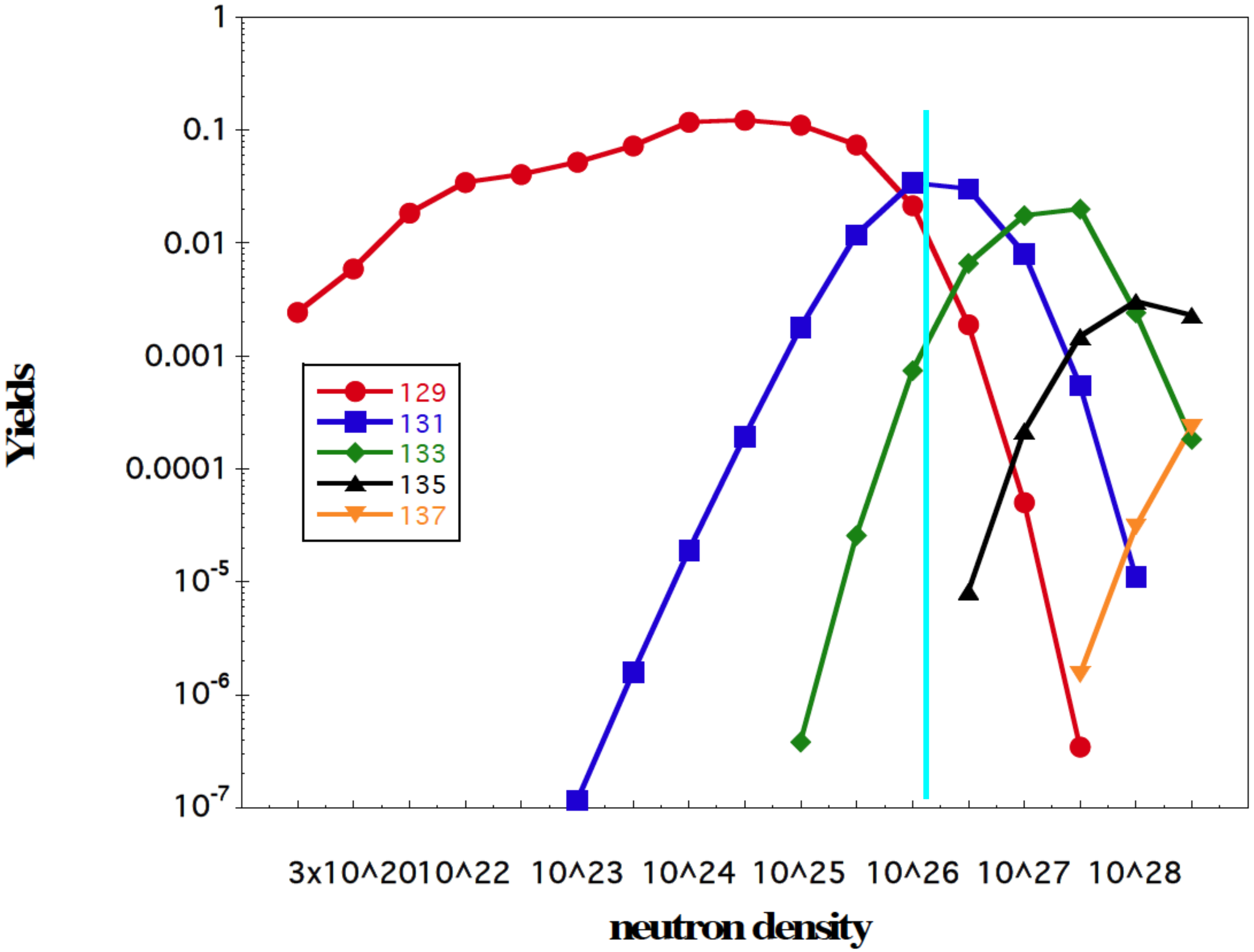

At 10^{26}, Ag is around A = 131

At 10^{26}, Cd is around A = 134. At what neutron density is ^{130}Cd dominant, down around 10^{24}? But when the flux is THAT low, very few Pb region nuclei will be produced.

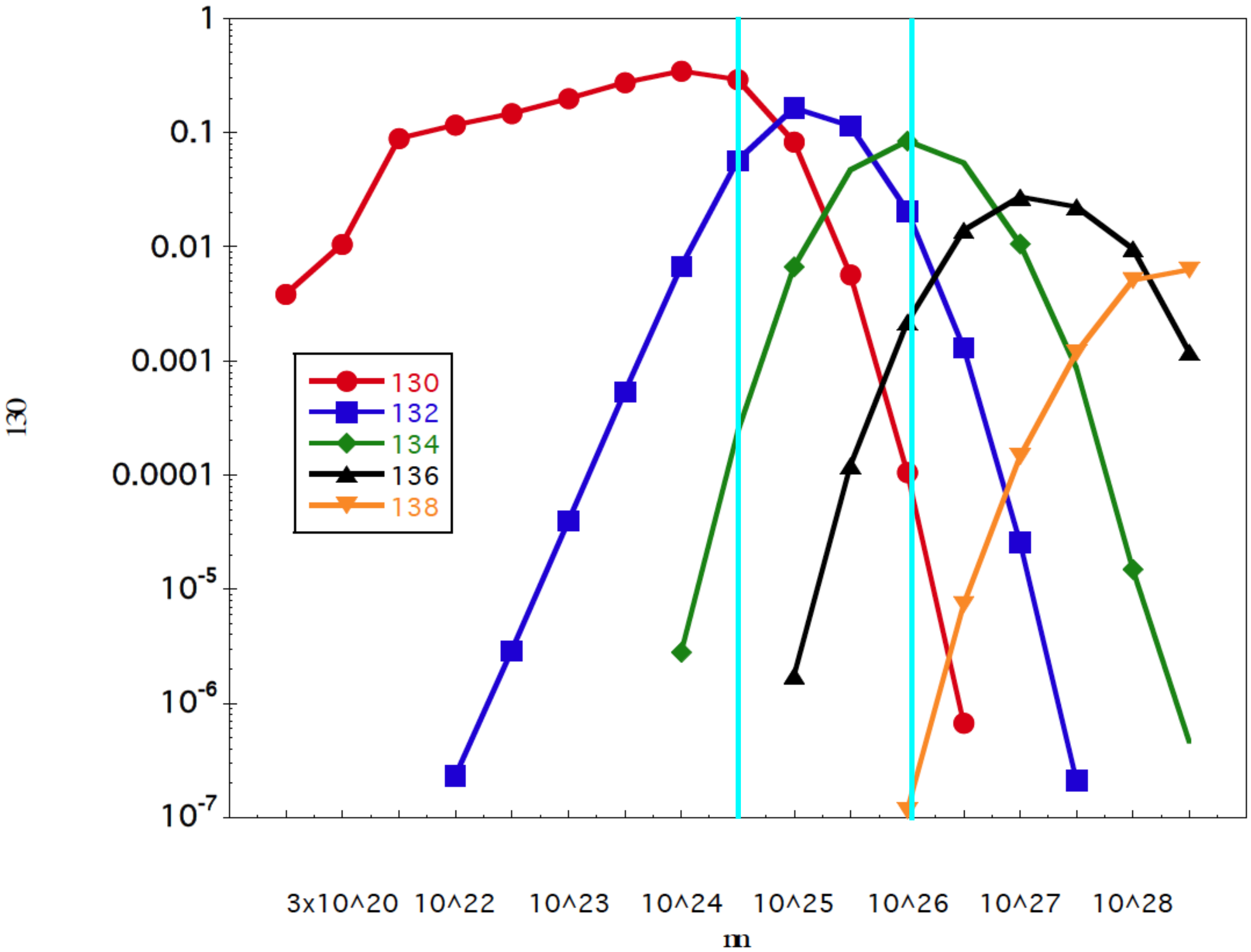

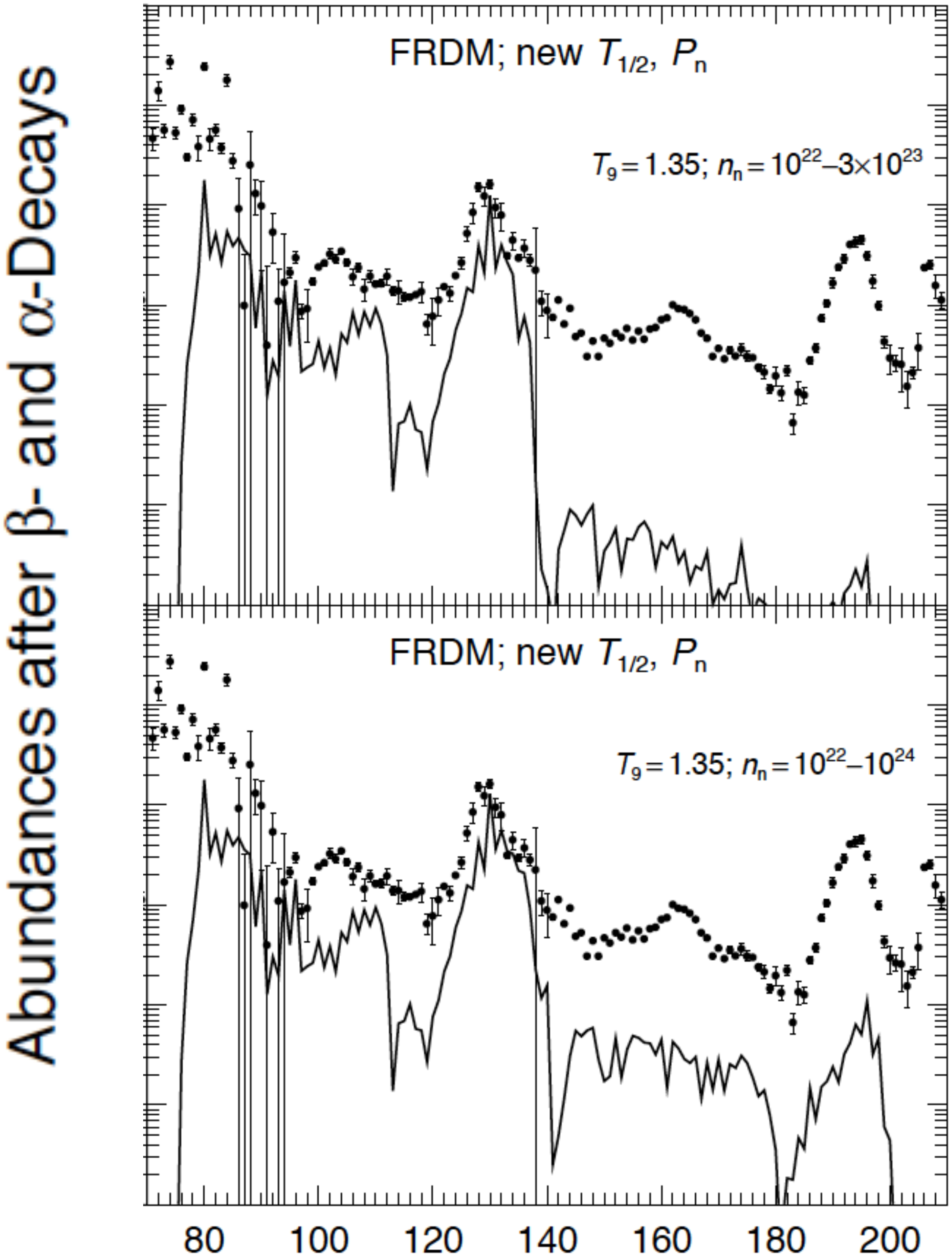
Abundances after β- and α-Decays
FRDM; new $T_{1/2}$, P_n
$T_9 = 1.35$; $n_n = 10^{22}$–3×10^{23}
FRDM; new $T_{1/2}$, P_n
$T_9 = 1.35$; $n_n = 10^{22}$–10^{24}
80
100
120
140
160
180
200

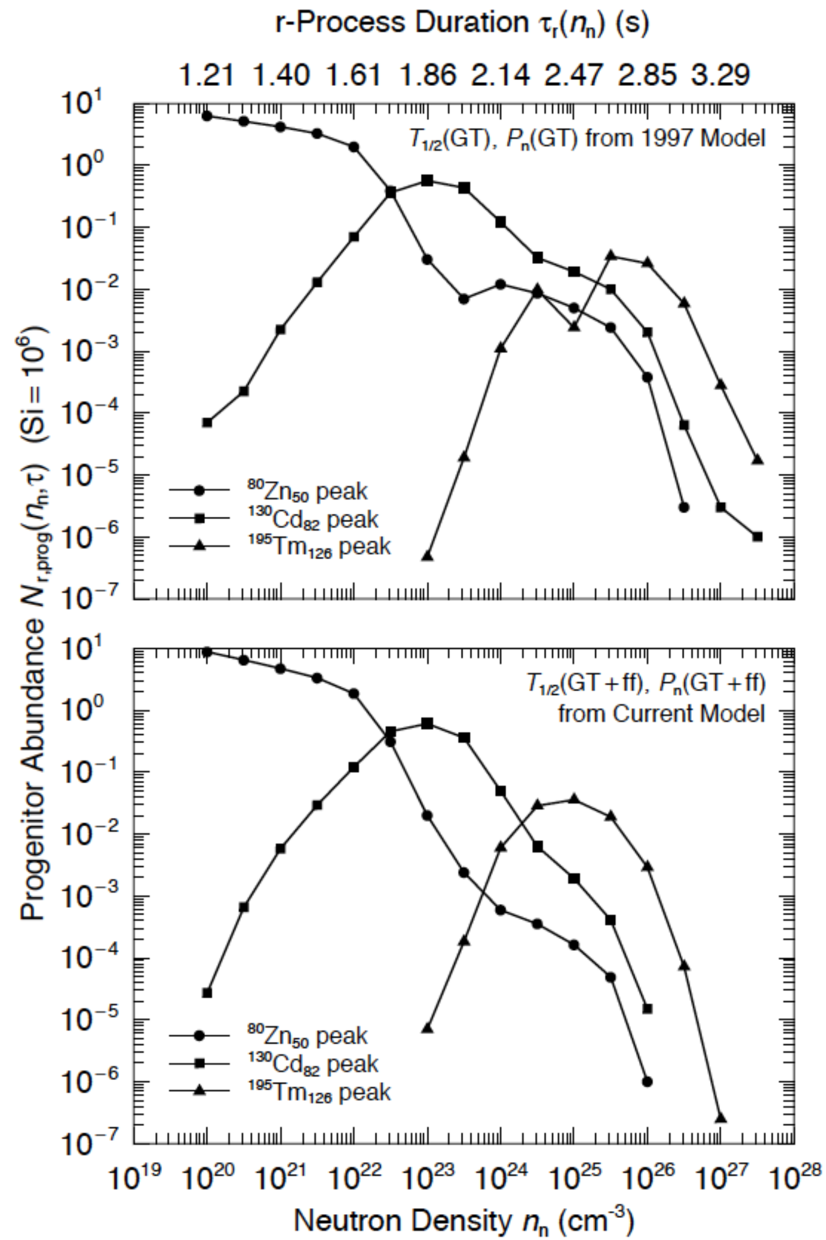
r-Process Duration $\tau_r(n_n)$ (s)
1.21 1.40 1.61 1.86 2.14 2.47 2.85 3.29
$T_{1/2}$(GT), P_n(GT) from 1997 Model
$T_{1/2}$(GT+ff), P_n(GT+ff) from Current Model
$^{80}Zn_{50}$ peak
$^{130}Cd_{82}$ peak
$^{195}Tm_{126}$ peak
Progenitor Abundance $N_{r,prog}(n_n,\tau)$ (Si = 10^6)
Neutron Density n_n (cm^{-3})

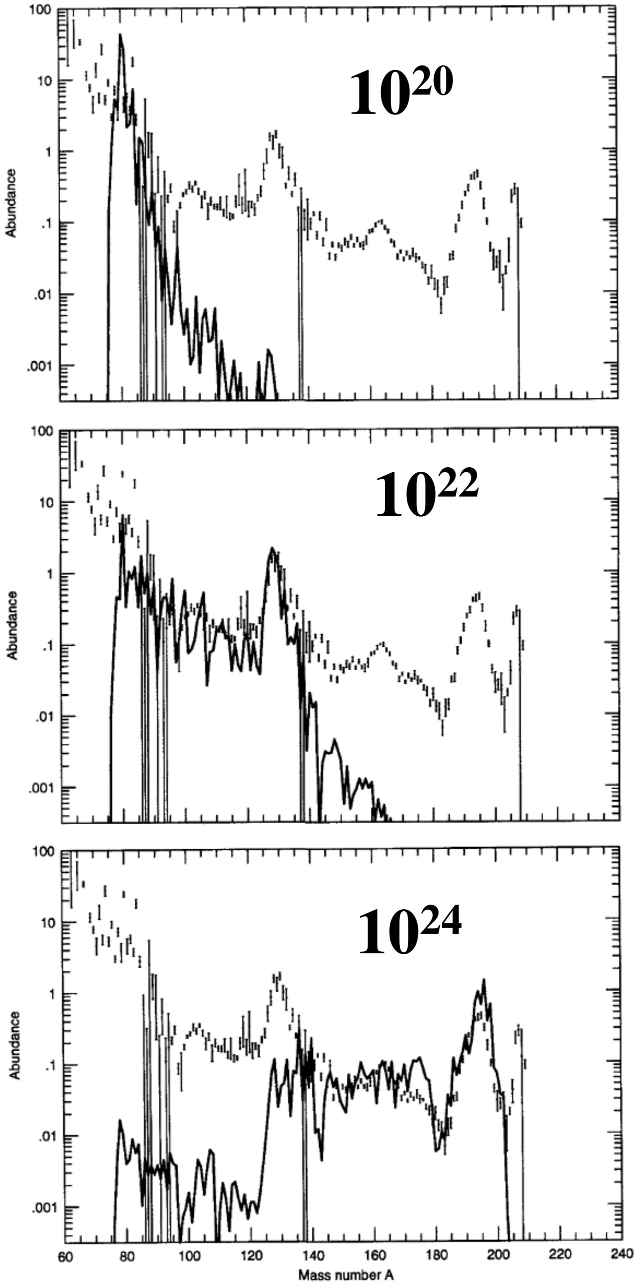

Fig. 2. Results of time-dependent r-process calculations with $n_n = 10^{20}$, 10^{22}, and 10^{24} g cm^{-3} at $T = 1.35 \times 10^9$ K for duration times τ of 1.2 (upper part), 1.7 (middle), and 2.1 s (lower part), respectively, in comparison with solar r-process abundances [34].

N·H
ELSEVIER
Nuclear Physics A 693 (2001) 282–324
NUCLEAR PHYSICS A
www.elsevier.com/locate/npe

Nuclear structure studies for the astrophysical r-process

B. Pfeiffer [a,*], K.-L. Kratz [a], F.-K. Thielemann [b], W.B. Walters [c]

[a] *Institut für Kernchemie, Universität Mainz, D-55128 Mainz, Germany*
[b] *Departement für Physik und Astronomie, Universität Basel, Switzerland*
[c] *Department of Chemistry, University of Maryland, USA*

Received 3 April 2001; revised 1 June 2001; accepted 5 June 2001

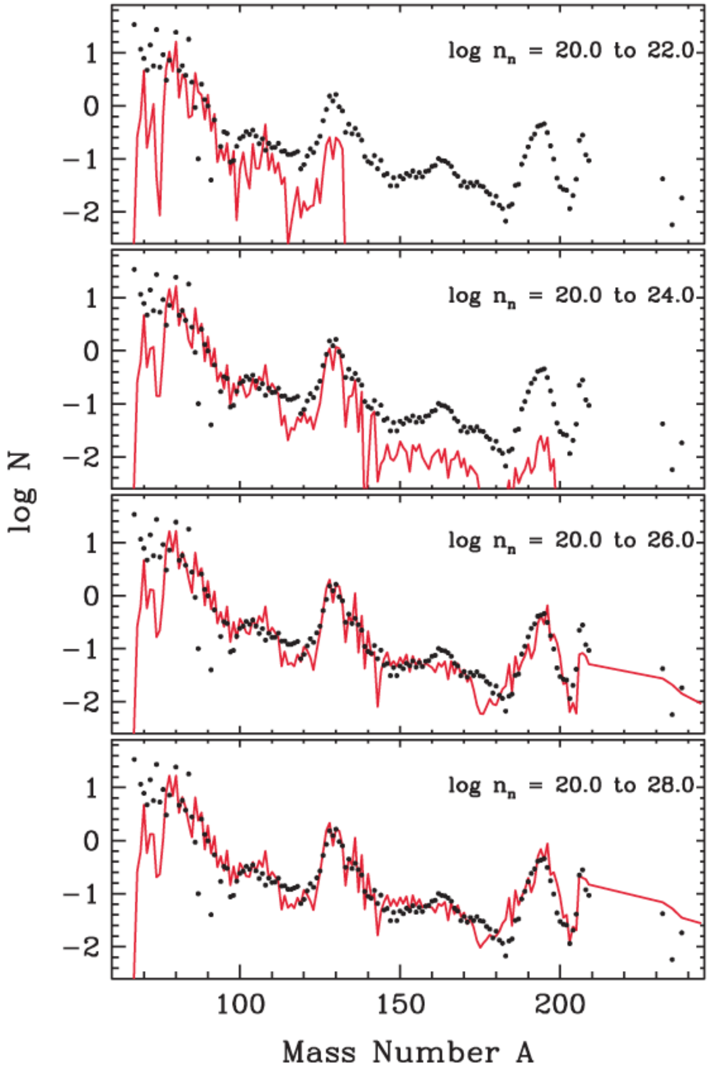

FIG. 5.—Comparison of meteoritic SS *r*-process–only isotopic abundances to weighted sums of *r*-process computations for different neutron densities ranges. The SS abundances (*black points*; Käppeler et al. 1989; Wisshak et al. 1998; O'Brien et al. 2003; see listing in Cowan et al. 2006) are on the standard meteoritic scale in which $\log N_{\rm Si} = 6$. The four panels show from top to bottom the effect of incorporating progressively higher ranges of n_n. The top panel predictions span $20.0 \le \log n_n \le 22.0$, adequate only for matching the lightest isotopes. The bottom three panels successively add more neutron density components weighted to simultaneously match the greatest mass range of nuclei. The values displayed here are ones taking into account α- and β-decays of nuclei back to stability.

THE ASTROPHYSICAL JOURNAL, 662:39–52, 2007 June 10
© 2007. The American Astronomical Society. All rights reserved. Printed in U.S.A.

EXPLORATIONS OF THE *r*-PROCESSES: COMPARISONS BETWEEN CALCULATIONS AND OBSERVATIONS OF LOW-METALLICITY STARS

KARL-LUDWIG KRATZ,[1,2] KHALIL FAROUQI,[2] BERND PFEIFFER,[2] JAMES W. TRURAN,[3]
CHRISTOPHER SNEDEN,[4] AND JOHN J. COWAN[5]
Received 2006 August 24; accepted 2007 March 1

The point is that by the time any significant quantity of ^{130}Sn is produced, the neutron density is far to low to carry those nuclei toward Pt. The sum of the mean lives for ^{130}Cd and ^{130}In is ~600 ms. If the speeding up argument is sound, the r-process is over before there is any significant quantity of ^{130}Sn. Stated another way, when the neutron density is high, there are few ^{130}Sn nuclei, by the time there are a lot of ^{130}Sn nuclei, there are few neutrons.

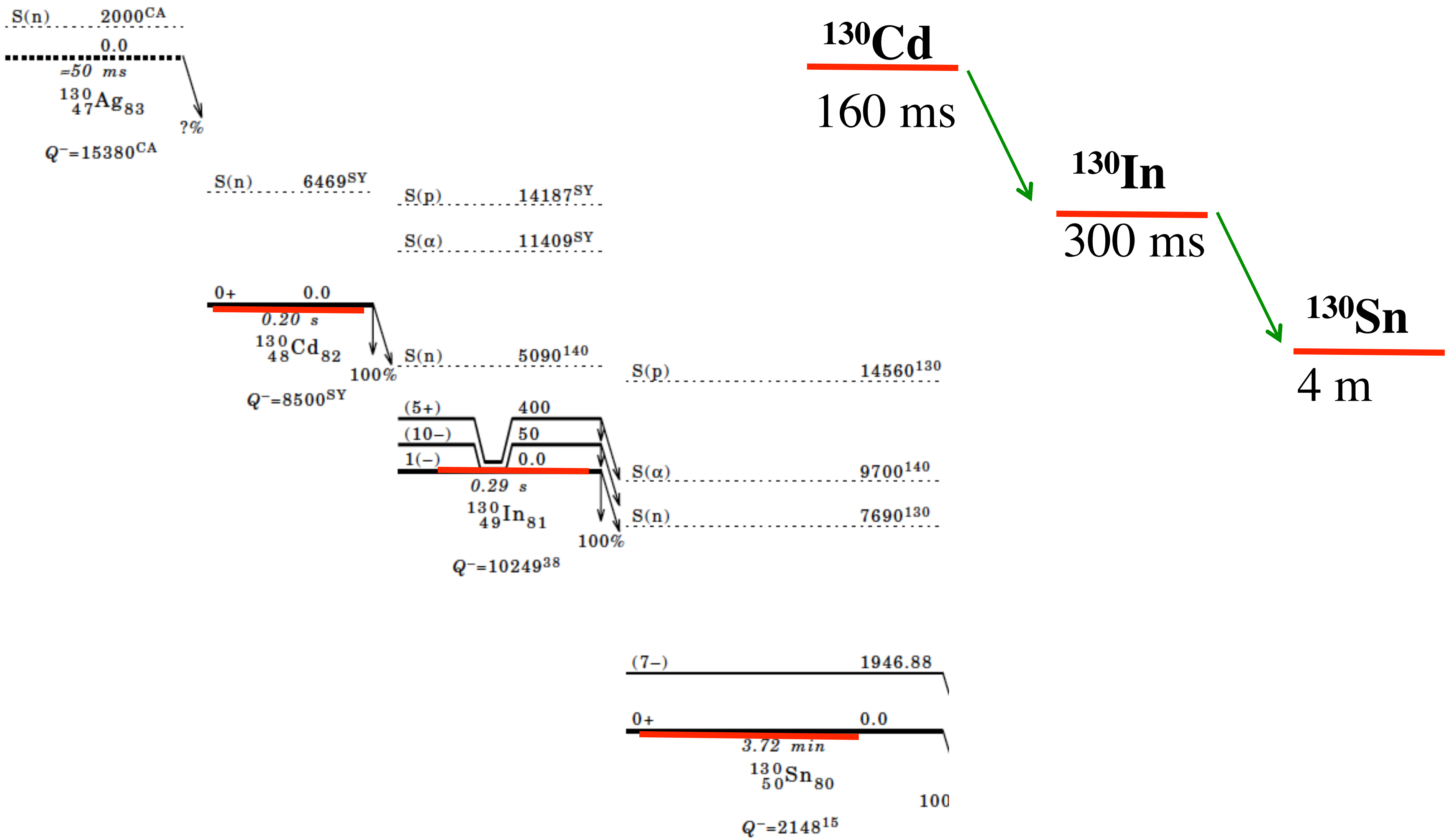

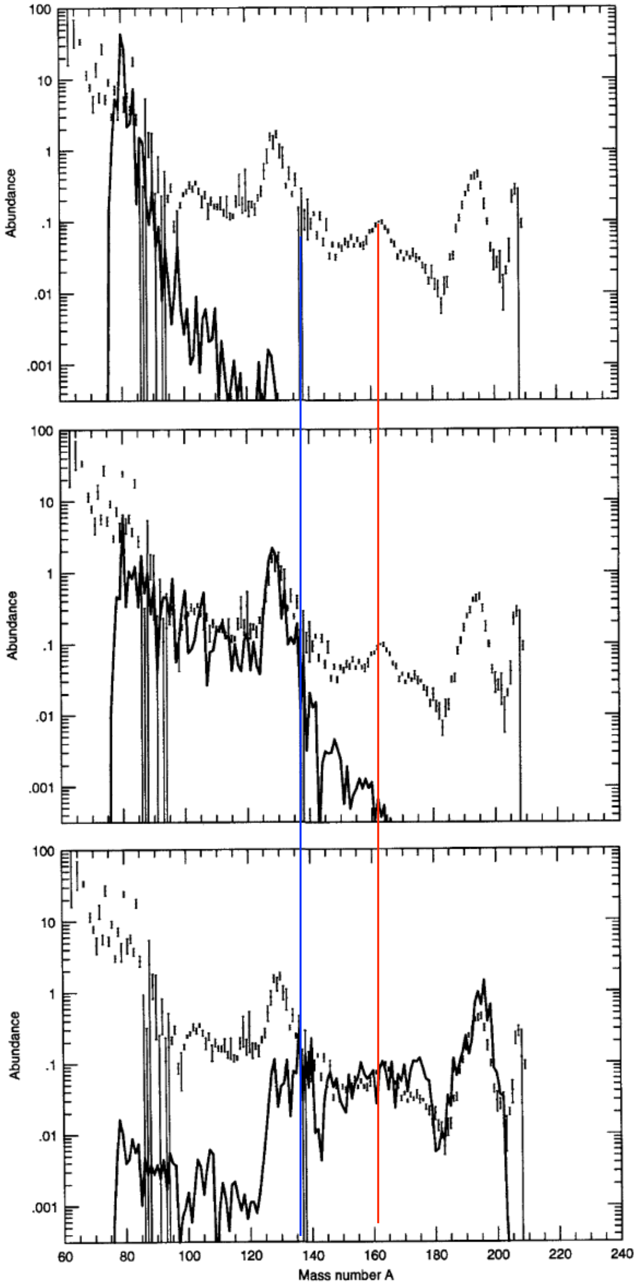

Fig. 2. Results of time-dependent r-process calculations with $n_n = 10^{20}$, 10^{22}, and 10^{24} g cm^{-3} at $T = 1.35 \times 10^9$ K for duration times τ of 1.2 (upper part), 1.7 (middle), and 2.1 s (lower part), respectively, in comparison with solar r-process abundances [34].

PHYSICAL REVIEW C VOLUME 5, NUMBER 5 MAY 1972

Distribution of Mass in the Spontaneous Fission of ^{256}Fm†

K. F. Flynn, E. P. Horwitz, C. A. A. Bloomquist, R. F. Barnes, R. K. Sjoblom, P. R. Fields, and L. E. Glendenin
Chemistry Division, Argonne National Laboratory, Argonne, Illinois 60439
(Received 20 December 1971)

Now I want to comment on the "rare-earth bump and fission recycling". The left graph is selected because is shows so clearly t**hat the bump centers at A = 160**, and the graph below shows that the **heavy fission mass bump would center at A = 139**. Maybe the "fuzz" on the heavy side of the A = 132 peak could come from fission, most likely from slow beta decay.

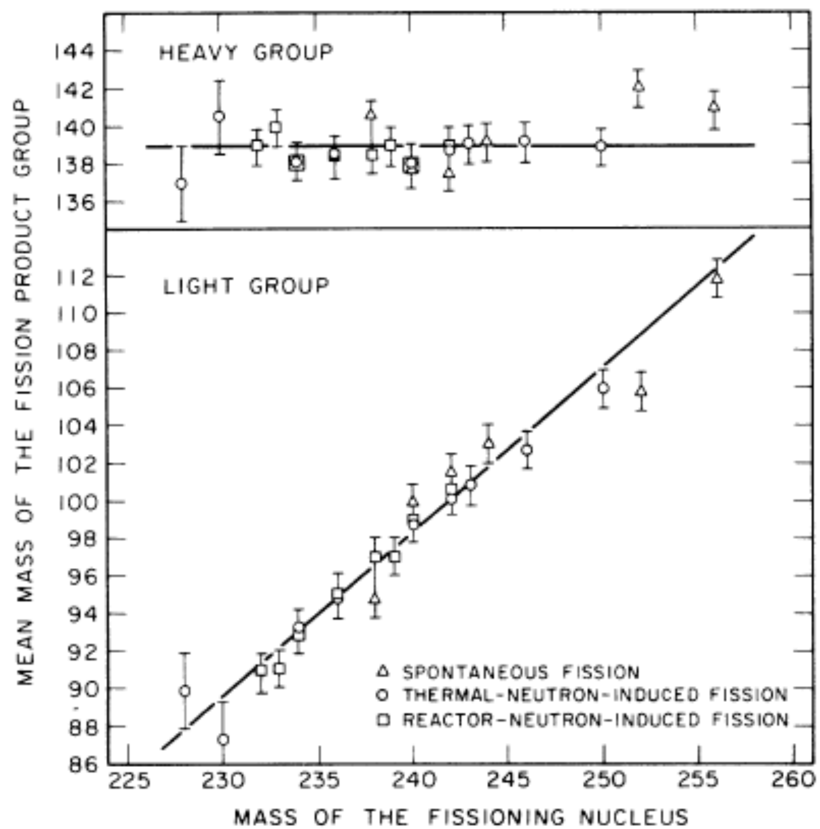

FIG. 4. Average masses of light and heavy groups as a function of the masses of the fissioning nucleus.

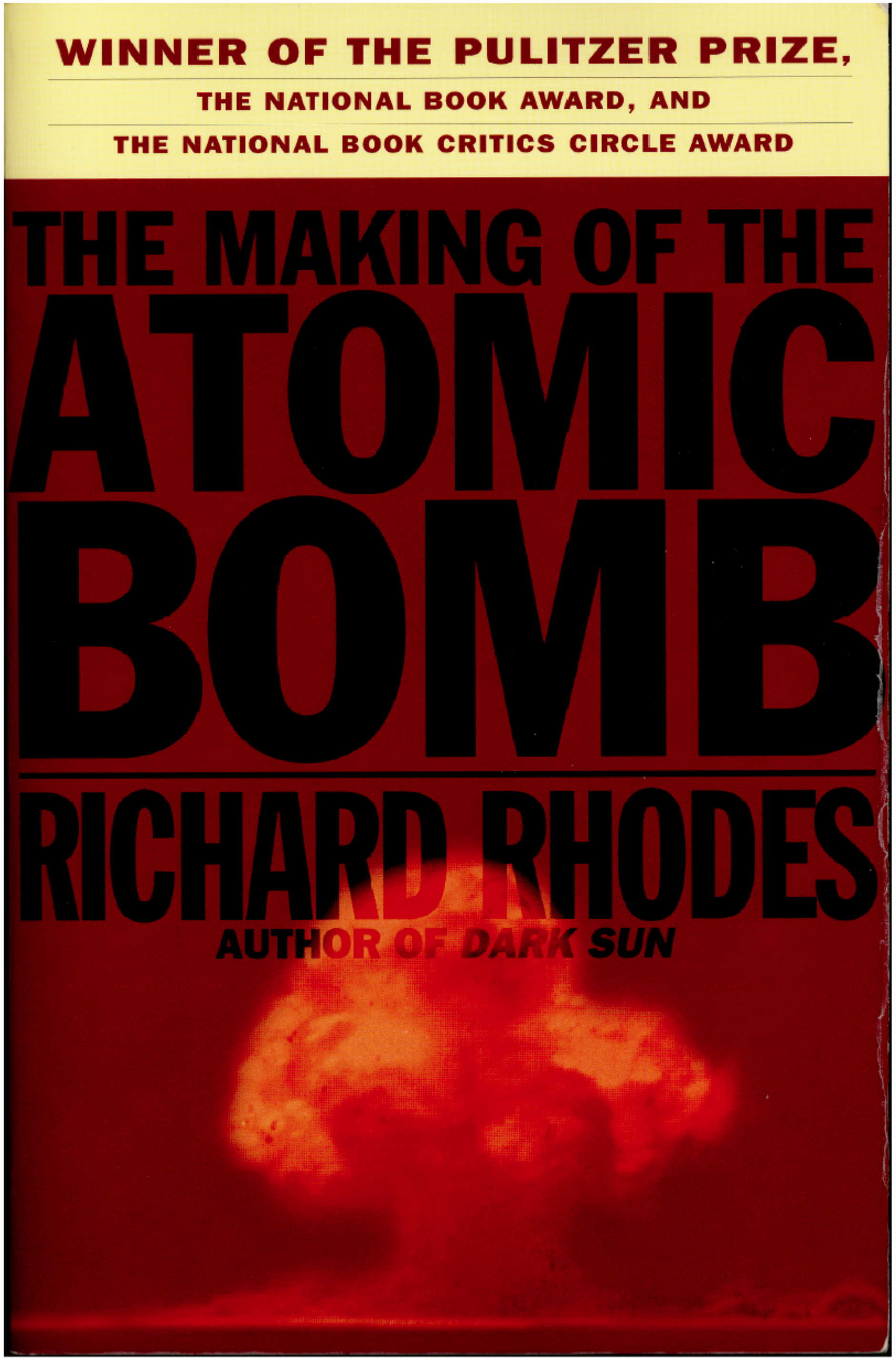

Delayed neutrons for control

Wigner, **John Wheeler**, ^{135}Xe and the Hanford Pu production reactors 1500 + corner 500   December 1944

Henry Stimson, Sec. of War.

The first 9 chapters are an excellent description of the history of nuclear science in the early 20th century that led to the discovery of fission.

The last 9 chapters are devoted to describing the human, scientific, and engineering activities that actually produced and delivered the bomb.

Delayed neutrons and the r-process

I checked with Karl-Ludwig and he confirmed the notion that the neutron to see ratio varies downward from100 when making U and Th to around 30 when making A = 130.

As with the control of a reactor, delayed neutrons reflect nuclei produced slightly earlier.

So, even if every irradiated "seed" nucleus was spraying out 1 delayed neutron each, the net increase might only be 5%. In other words, 3% of the nuclei have been irradiated, and the delayed neutrons come from a time slightly earlier. Not a big deal????

Wigner designed Pu reactors, Wheeler built them. Wheeler was cautions and "worried" about a fission product "poison". He drilled in large unoccupied corners. When the ^{135}Xe poison shut the reactor down, it was possible to fill out the corners and stuff them with U and get going again. The delay was about 3 months for the drilling. By December 1944, fuel rods were being sent to Seaborg's robotic separators at full speed.

Now, I want to ask about the low value for Rh and Ag in old halo stars? Fermi used Rh as his flux monitor in the Rome experiments of 1936/7.

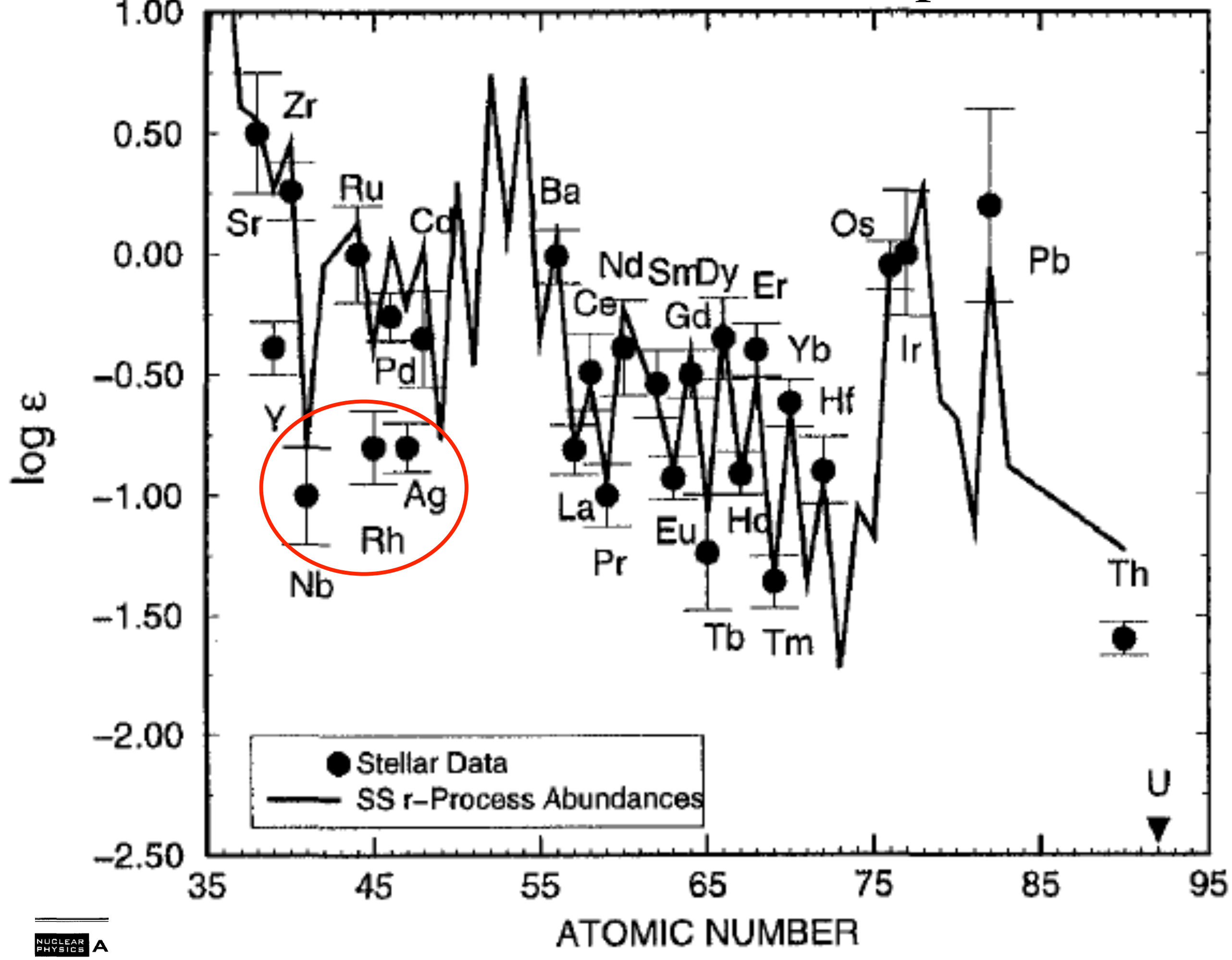

ELSEVIER

Nuclear Physics A688 (2001) 330c–339c

NUCLEAR PHYSICS A

www.elsevier.nl/locate/npe

Halo Star Abundances and r-Process Synthesis

James W. Truran[a], John J. Cowan[b], and Brian D. Fields[c]

Figure 1. The heavy element abundance patterns for CS 22892-052 compared with the solar system r-process abundance distribution (solid line) [7]

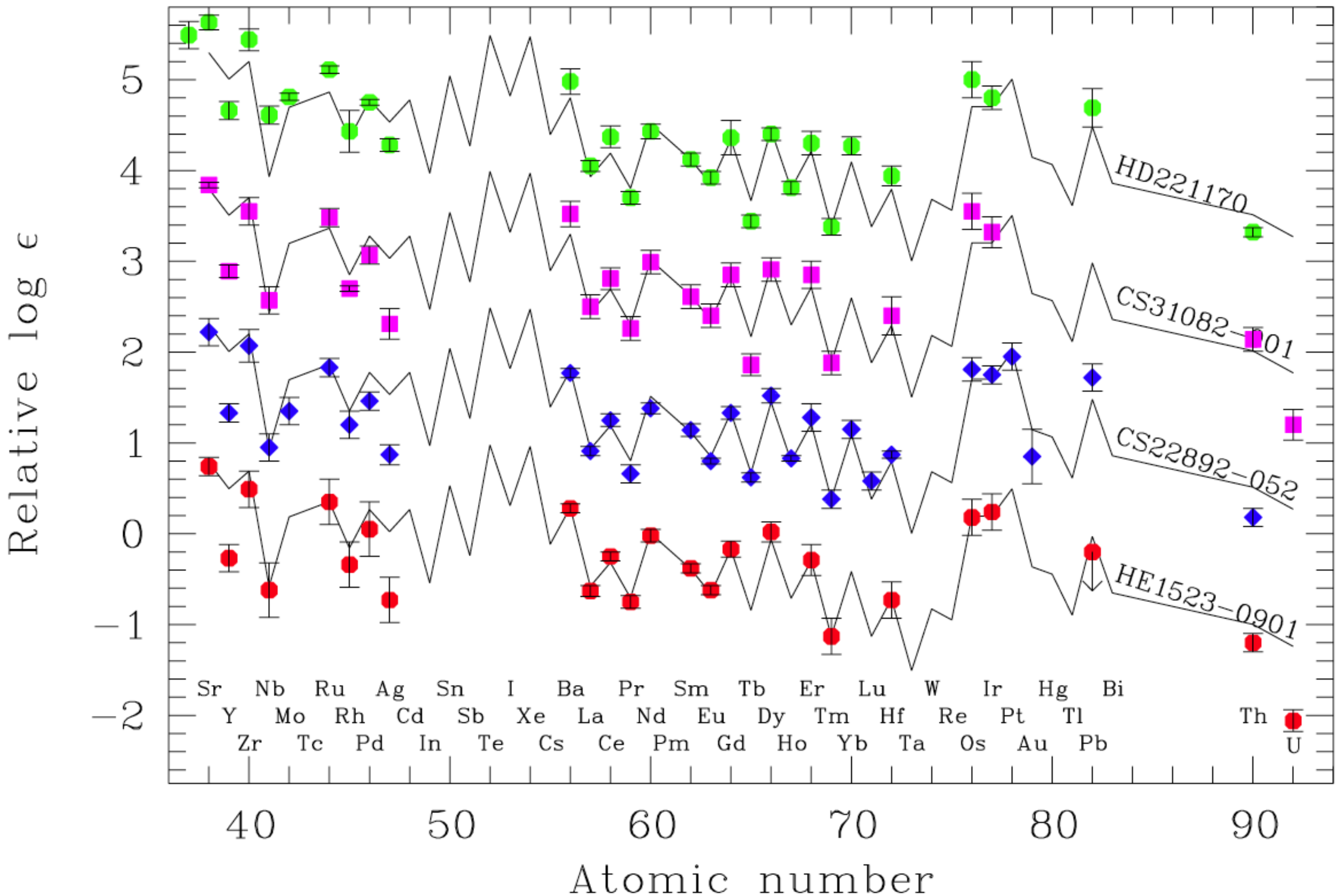

Figure 5. Element abundance patterns of a sample of r-process element enriched stars (points), with the solar r-process pattern scaled to each star's Eu abundance (solid lines). The agreement between the solar pattern and the stellar abundances is excellent for elements $Z \approx 56 - 72$. However, the agreement with the solar pattern of the lighter elements ($Z \approx$ 38–40) is not as good. References for the abundances: HD 221170—Ivans *et al* (2006); CS 31082-001—Hill *et al* (2002); CS 22892-052—Sneden *et al* (1996); HE 1523−0901—Frebel *et al* (2007). (Figure adapted from Frebel and Norris 2013.)

These are usually seen in a log plot where they all look equal. Even in a linear plot, these abundances are, more or less equal, varying in this plot by a factor of 3.

If Rh is large in Solar, does this mean the main source is the s-process?

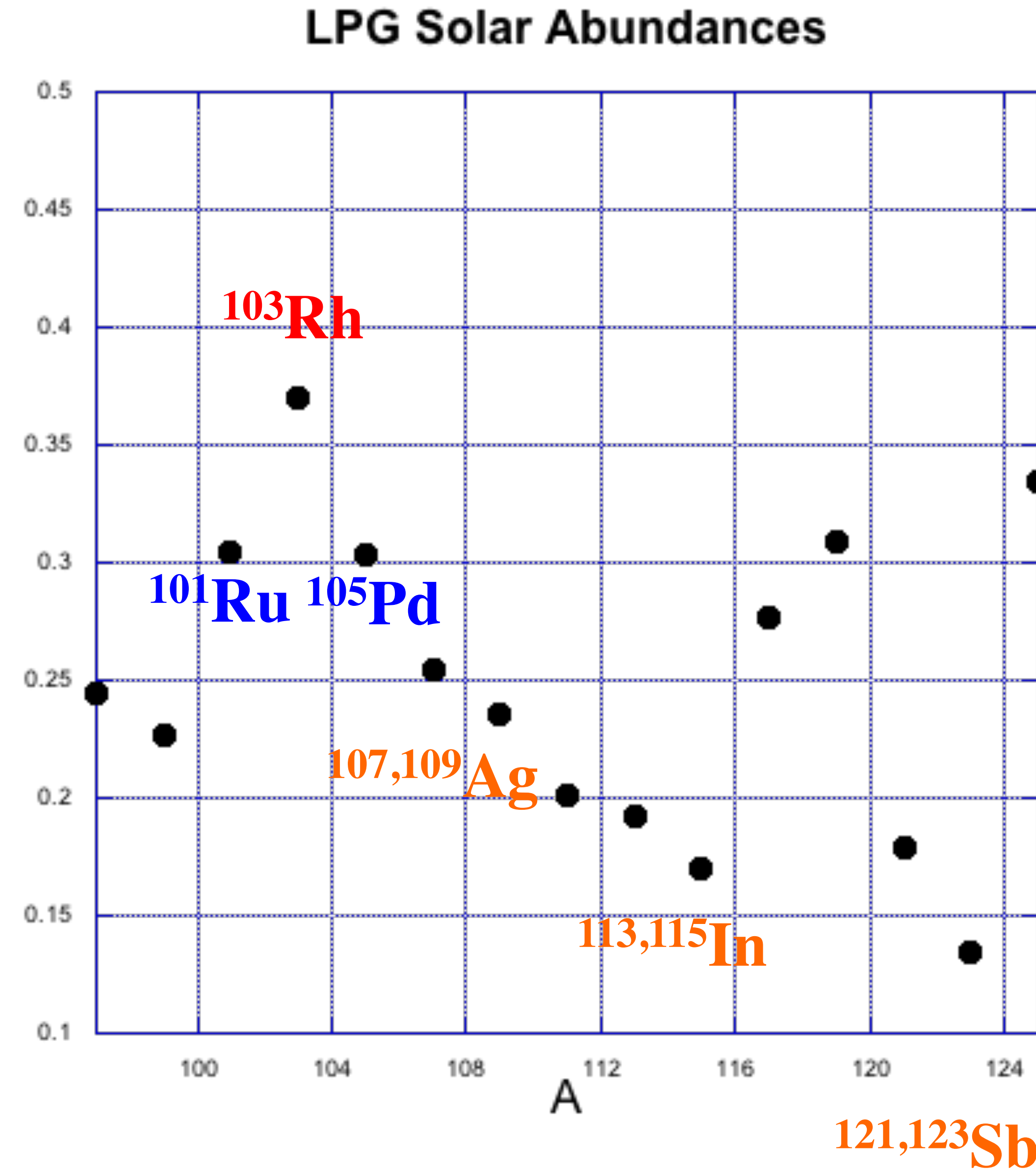

December 2008
submitted to:
Landolt-Börnstein, New Series, Astronomy and Astrophysics,
Springer Verlag, Berlin, 2009
K. Lodders
Department of Earth and Planetary Sciences,
Washington University, St. Louis, Missouri 63130, USA
H. Palme
Sektion Meteoritenforschung
Forschungsinstitut und Naturmuseum Senckenberg
Senckenberganlage 25, D-60325 Frankfurt am Main, Germany
H.-P. Gail
Center for Astronomy, Institute of Theoretical Astrophysics,
University of Heidelberg, Albert-Überle-Str. 2, 69120 Heidelberg, Germany

Monthly Notices of the Royal Astronomical Society
Mon. Not. R. Astron. Soc. 418, 284–319 (2011) doi:10.1111/j.1365-2966.2011.19484.x

S. Bisterzo et al.

The s-process in low-metallicity stars – II. Interpretation of high-resolution spectroscopic observations with asymptotic giant branch models

S. Bisterzo,[1★] R. Gallino,[1,2] O. Straniero,[2] S. Cristallo[3] and F. Käppeler[4]

Table 5 – *continued*

Isotope (1)	Solar Abb. AG89 (2)	Solar Abb. L09 (3)	N_s A99 (4)	s (per cent) A99 (5)	N_s Updated (6)	s (per cent) Updated[(a)] (7)	r (per cent) Updated (8)
^{99}Ru	2.36E−01	2.27E-01	6.69E−02	28.3	7.52E−02	33.1	
^{100}Ru	2.34E−01	2.24E-01	2.23E−01	95.3	–	+9.9 per cent[(b)]	
^{101}Ru	3.16E−01	3.04E-01	4.83E−02	15.3	5.38E−02	17.7	
^{102}Ru	5.88E−01	5.62E-01	2.53E−01	43.0	2.81E−01	50.0	
^{104}Ru	3.48E−01	3.32E-01	9.52E−03	2.7	8.17E−03	2.5	
Ru				32.0		37.3 ± 2.2	
^{103}Rh	3.44E−01	3.70E-01	4.67E−02	13.6	5.64E−02	15.2	
Rh				14.0		15.2 ± 1.5	
^{104}Pd	1.55E−01	1.51E-01	–	+5.7 per cent[(b)]	–	+21.6 per cent[(b)]	
^{105}Pd	3.10E−01	3.03E-01	4.27E−02	13.8	4.75E−02	15.7	
^{106}Pd	3.80E−01	3.71E-01	1.95E−01	51.3	2.17E−01	58.4	
^{108}Pd	3.68E−01	3.59E-01	2.40E−01	65.2	2.68E−01	74.6	
^{110}Pd	1.63E−01	1.59E-01	5.93E−03	3.6	4.73E−03	3.0	
Pd				46.0		53.1 ± 2.7	
^{107}Ag	2.52E−01	2.54E-01	3.77E−02	15.0	4.21E−02	16.6	
^{109}Ag	2.34E−01	2.36E-01	5.86E−02	25.0	6.64E−02	28.1	
Ag				20.0		22.1 ± 1.1	
^{108}Cd	1.43E−02	1.40E-02	1.61E−05	0.1	5.34E−05	0.4	
^{110}Cd	2.01E−01	1.97E-01	1.95E−01	97.0	–	+15.1 per cent[(b)]	
^{111}Cd	2.06E−01	2.01E-01	4.87E−02	23.6	7.65E−02	38.0	
^{112}Cd	3.88E−01	3.80E-01	2.05E−01	52.8	2.84E−01	74.8	
^{113}Cd	1.97E−01	1.92E-01	6.85E−02	34.8	8.30E−02	43.2	
^{114}Cd	4.63E−01	4.52E-01	2.95E−01	63.7	4.06E−01	89.8	
^{116}Cd	1.21E−01	1.18E-01	2.13E−02	17.6	2.00E−02	17.0	
Cd				52.0		69.6 ± 4.9	
^{113}In	7.90E−03	8.00E-03	5.59E−08	0.0	5.96E−08	0.0	
^{115}In	1.76E−01	1.70E-01	6.43E−02	36.5	7.53E−02	44.3	
In				35.0		42.4 ± 3.0	
^{93}Nb	6.98E−01	7.80E-01	5.96E−01	85.4	6.68E−01	85.6	
Nb				85.0		85.6 ± 8.6	

Where do Solar Nb, Rh and Ag come from, given that they eat neutrons strongly, including those beta-delayed neutrons, at the end of the r-process?

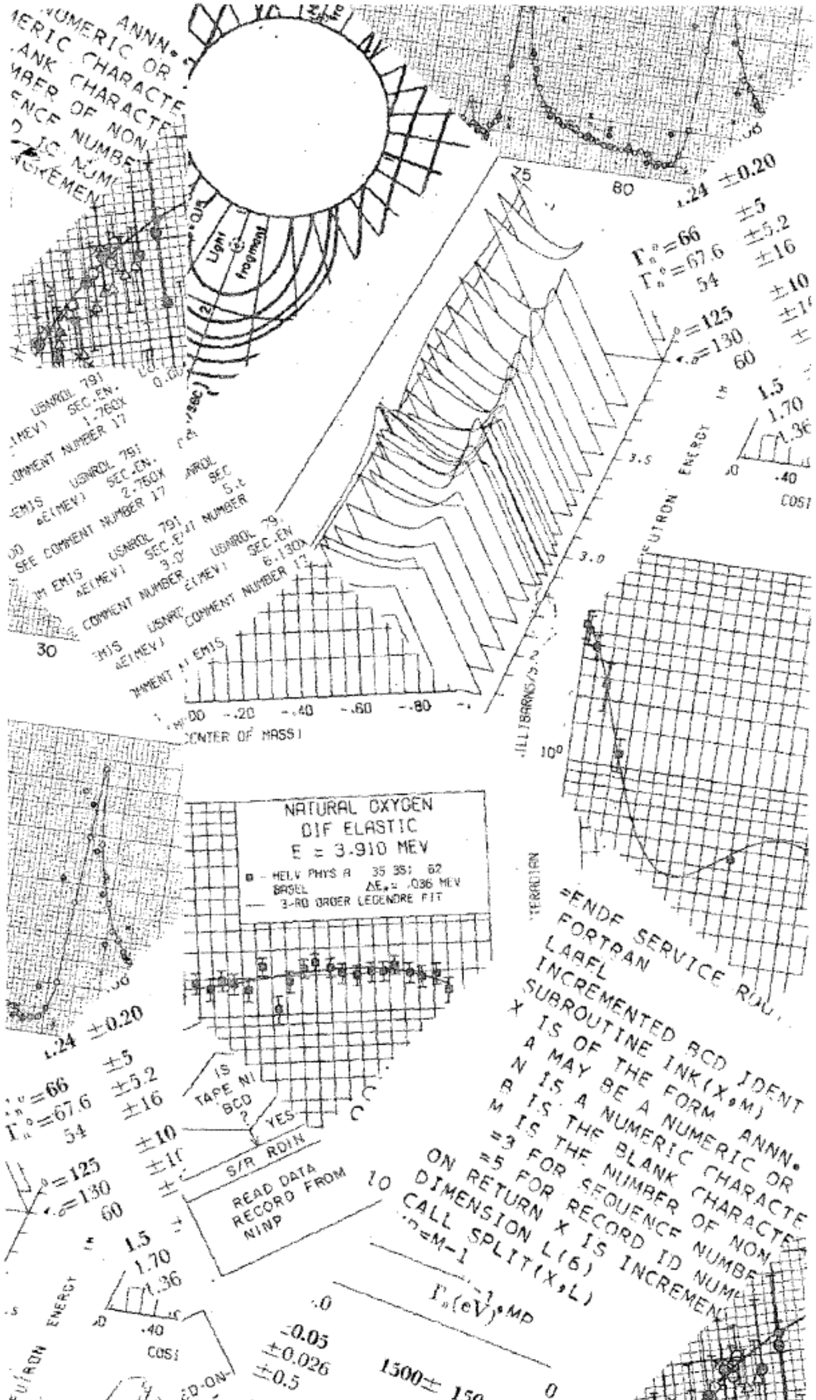

BNL 325
Third Edition, Volume II
(Physics, Nuclear - TID-4500)
[EANDC(US)-183]
[INDC(USA)-58]

NEUTRON CROSS SECTIONS
VOLUME II, CURVES

D.I. GARBER AND R.R. KINSEY

January 1976

INFORMATION ANALYSIS CENTER REPORT

NATIONAL NEUTRON CROSS SECTION CENTER
BROOKHAVEN NATIONAL LABORATORY
UPTON, NEW YORK 11973

$^{103}_{45}Rh$

σ_{tot}

[1125]

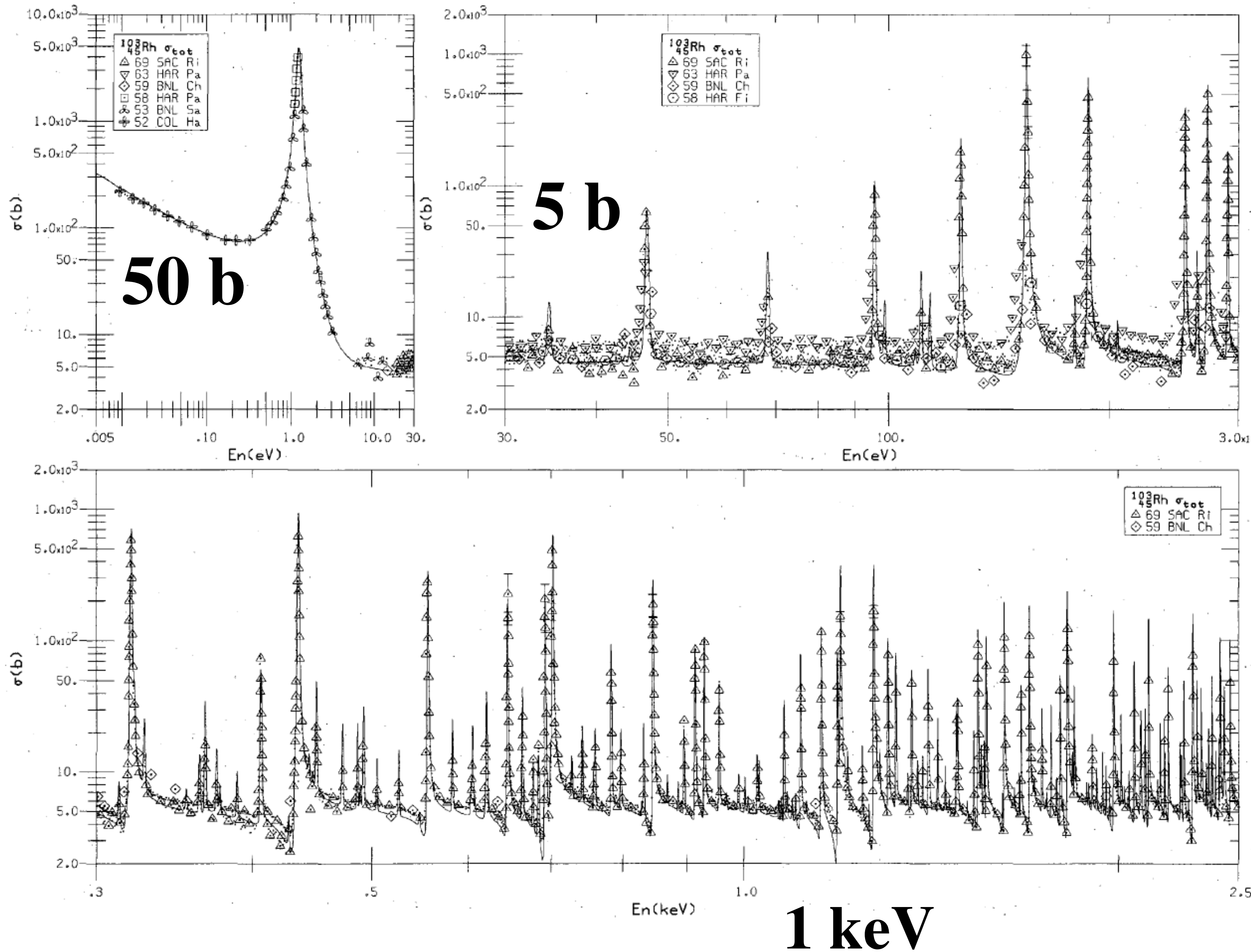

The point is that the capture cross sections for Rh are HIGH!!!

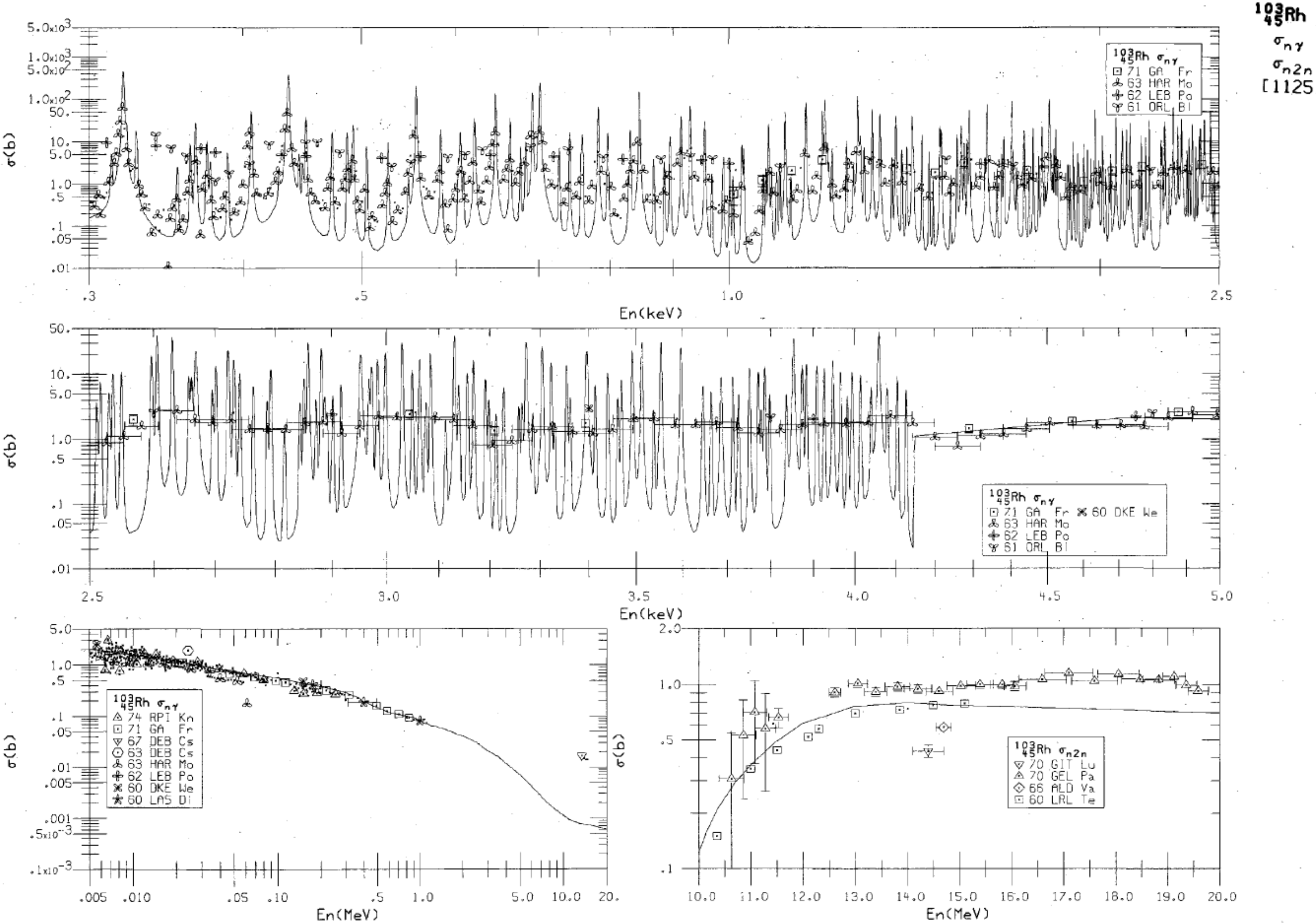

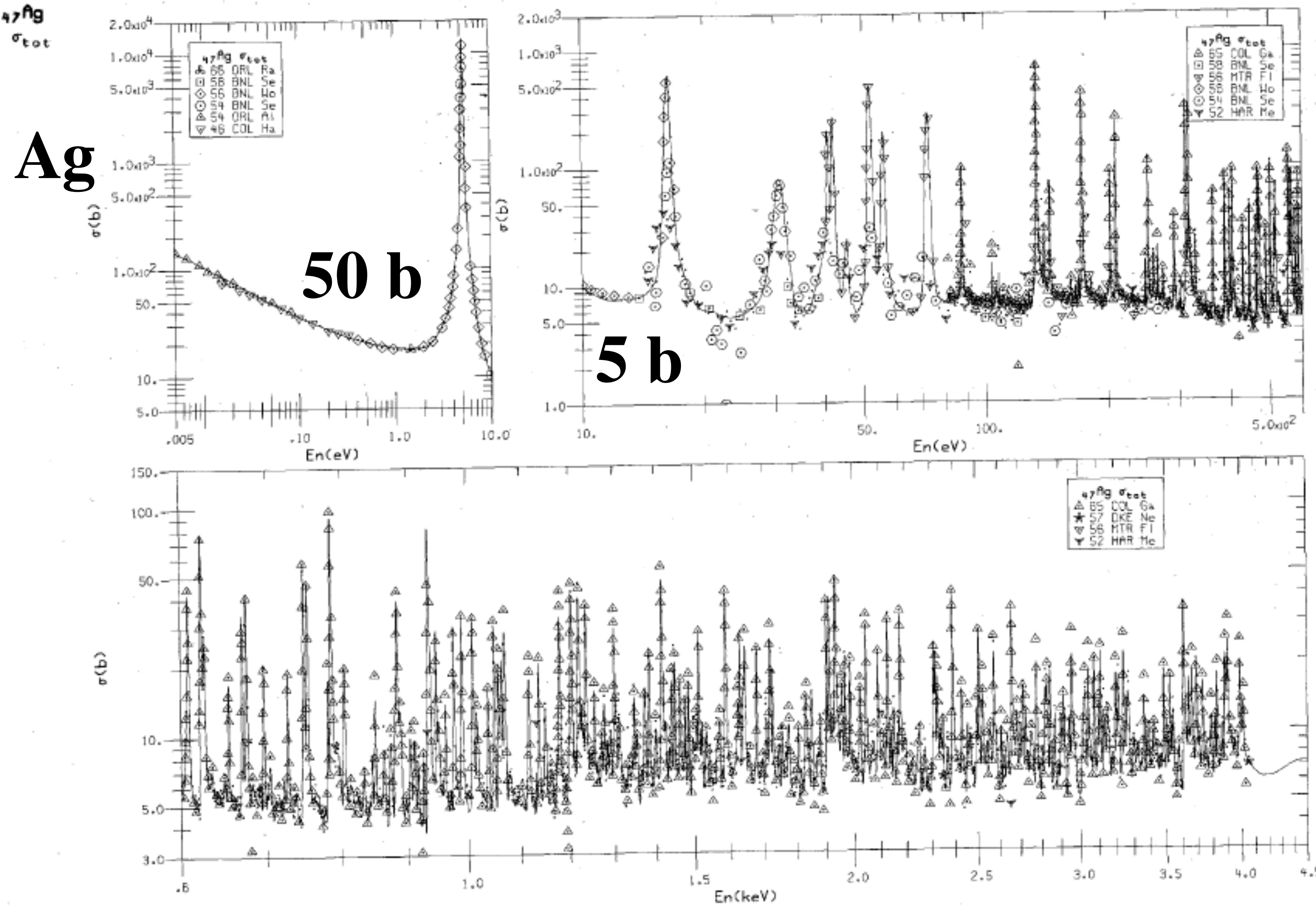
47Ag
σtot
Ag
50 b
5 b
47Ag σtot
66 ORL Ra
58 BNL Se
56 BNL Wo
54 BNL Se
54 ORL Al
46 COL Ha
47Ag σtot
65 COL Ga
58 BNL Se
56 MTR Fi
56 BNL Wo
54 BNL Se
52 HAR Me
47Ag σtot
65 COL Ga
57 DKE Ne
56 MTR Fi
52 HAR Me
σ(b)
En(eV)
En(keV)

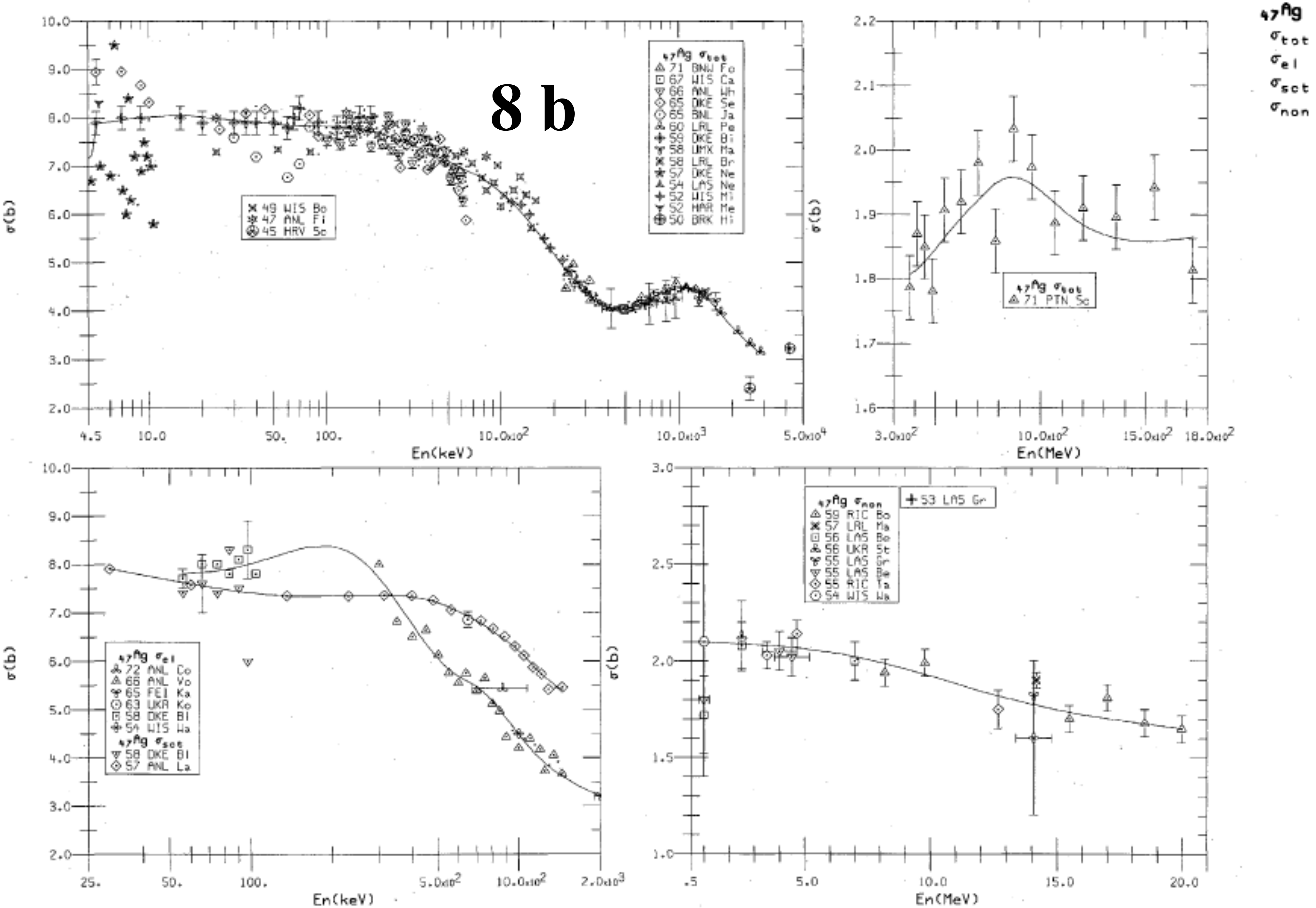
8 b
47Ag σtot
71 BNW Fo
67 WIS Ca
66 ANL Wh
65 DKE Se
65 BNL Ja
60 LRL Pe
59 DKE Bi
58 UMX Ma
58 LRL Br
57 DKE Ne
54 LAS Ne
52 WIS Mi
52 HAR Me
50 BRK Hi
49 WIS Bo
47 ANL Fi
45 HRV Sc
σ(b)
En(keV)
47Ag σtot
71 PTN Sc
En(MeV)
47Ag σel
72 ANL Co
66 ANL Vo
65 FEI Ka
63 UKR Ko
58 DKE Bi
54 WIS Wa
47Ag σsct
58 DKE Bi
57 ANL La
En(keV)
47Ag σnon
59 RIC Bo
57 LRL Ma
56 LAS Be
56 UKR St
55 LAS Gr
55 LAS Be
55 RIC Ta
54 WIS Wa
53 LAS Gr
En(MeV)
47Ag
σtot
σel
σsct
σnon

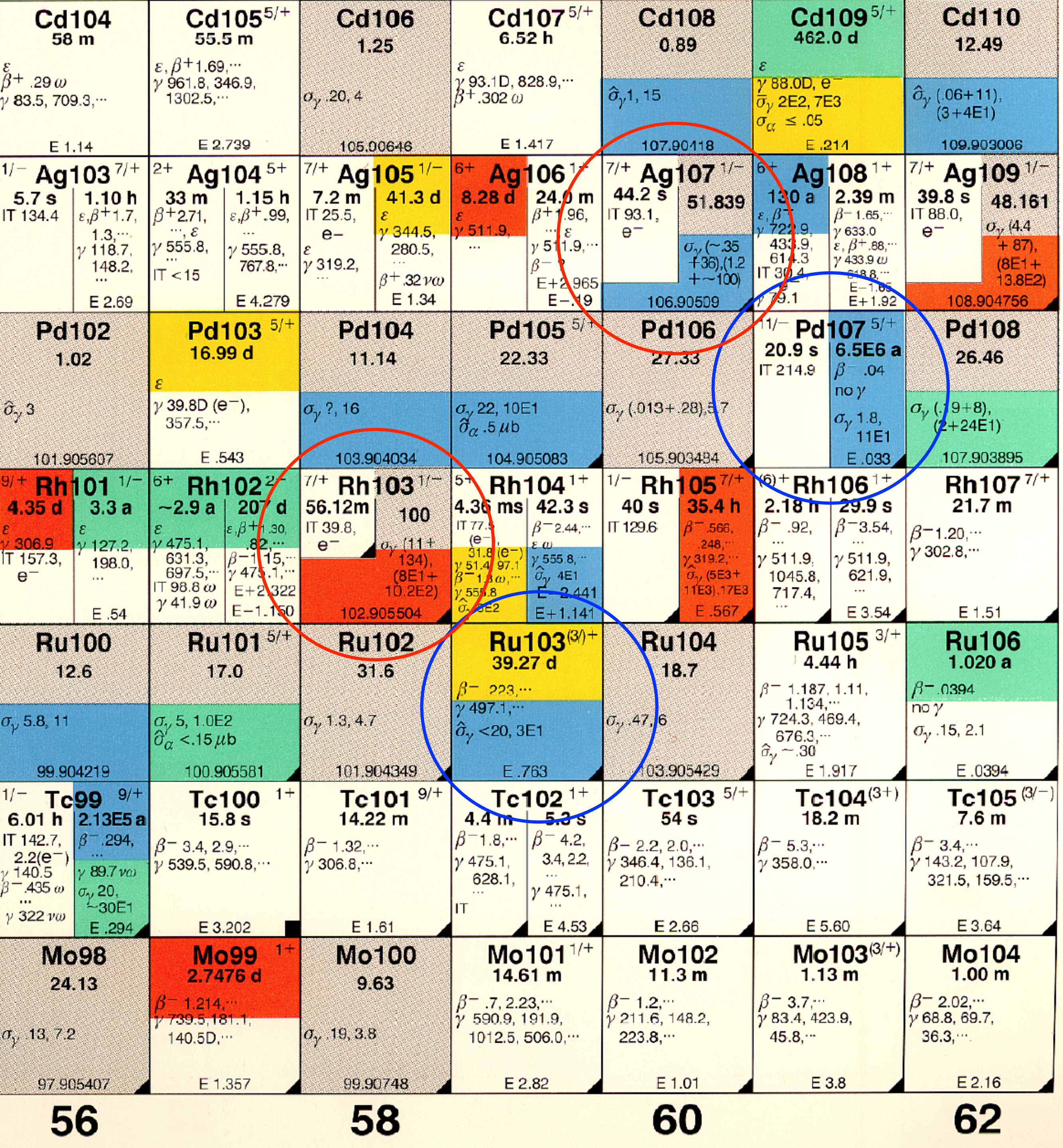

Here, it is possible to see that ^{103}Rh is "protected" in the r-process by 40-day ^{103}Ru, so any neutrons from late beta-delayed processes will have little effect. Moreover, ^{107}Ag is well protected by six million-year ^{107}Pd.

My question is "how are the ^{103}Rh and Ag being eaten in the old halo stars?"

The large cross section for ^{103}Rh and short daughter half life made ^{104}Rh an excellent flux monitor for Fermi in his Rome experiments when he was irradiating "everything" with neutrons.